Flanking sound transmission in coupled panels of cross-laminated-timber

Zur Erlangung des akademischen Grades eines
Doktors der technischen Wissenschaften
ausgeführte Dissertation

eingereicht an der
Fakultät für Bauingenieurwissenachaften
der Technischen Universität Graz

von

Blasius Buchegger

Berichter:

Univ.-Prof. Dr.-Ing. Michael Möser
Univ.-Prof. Dr.-Ing. Gerhard Müller
Univ.-Prof. Dr.-Ing. Martin Schanz

Graz, März 2019

AFFIDAVIT

I declare that I have authored this thesis independently, that I have not used other than the declared sources/resources, and that I have explicitly indicated all material which has been quoted either literally or by content from the sources used. The text document uploaded to TUGRAZonline is identical to the present doctoral thesis.

20.03.2019
Date

Signature

Abstract

This thesis deals with numerical and experimental investigations on the flanking sound transmission of airborne- and impact sound insulation in coupled panels of cross-laminated timber. The focus is on calculations of the structure-borne sound transmission in the junction with respect to the used fastener systems. Furthermore, relevant physical effects are investigated which have an essential influence on flanking sound transmission.

Cross-laminated timber is an aspiring construction method that allows ecological, fast and cheap building. The usage, especially, for building multi-storey dwellings is internationally increasing. However, in a technical point of view, the competitiveness of cross-laminated timber compared to other building materials is reduced in many cases caused by the limited applicability of current available standardized measurement- and prediction methods. On the one hand, this often leads to an oversizing of the constructions that results in additional financial effort. On the other hand, developments of new innovative products require a high effort because, currently, sensitivity analyses have to be performed based on measurement investigations on mock-ups of almost building size. In this thesis, alternative prediction methods for flanking sound transmission based on numerical calculations (finite element method) are developed that can be used, especially, for pre-dimensioning or optimizing of junctions. Step by step, the complexity of the investigations is increased. First, free vibrating panels of cross-laminated timber are investigated to determine suitable calculation methods of the acoustic behaviour of single panels. Second, single panels are connected to form junctions using different fastener systems. The flanking sound reduction index is evaluated to get input parameters for subsequent standardized calculations. Third, these standardized calculations are used to predict the total sound transmission for a selected real building situation. Every step is validated using measurement data from suitable practical constructions. The aim is to reduce the need for expensive measurement procedures by the use of a numerical pre-development process to allow more efficient advancements of innovative new products.

Furthermore, essential physical effects have been investigated that can have a significant influence on the flanking sound transmission in constructions of cross-laminated timber. An effect called “modal (de-)coupling” shows a high potential for an improvement of the designs at low and very low frequencies, where other measures like the use of additional linings have insufficient effect. Here, the aim is to supress the coupling of “local” modes of a single panel

or a cavity to “global” modes of two panels and a cavity. The latter results in a vibration of the entire system, and as a consequence, a high flanking sound transmission. Furthermore, an effect called “wave transformation” is investigated that leads to a conversion of out-of-plane wave components into in-plane wave components at a junction. The effect shows a high optimization potential for flanking sound transmission in the mid frequency range, where the effect of coincidence also occurs in panels of cross-laminated timber. The aim is to evoke the transformation of out-of-plane wave components to in-plane components in the junction. The induced out-of-plane components in the first room do not lead to a sound radiation in the adjacent room and, as a consequence, the flanking sound transmission can be reduced.

Zusammenfassung

Diese Dissertation beinhaltet numerische und experimentelle Untersuchungen der Flankenschalldämmung von Brettsperrholz. Hierbei liegt der Fokus auf Berechnungen der Körperschallübertragung in der Stoßstelle. Des Weiteren werden spezielle physikalische Effekte untersucht, welche ein hohes Potential für die Nutzung als Optimierungsmaßnahme zeigen.

Die Verwendung von Massivholzkonstruktionen im mehrgeschossigen Wohnbau gewinnt international immer mehr an Bedeutung, da diese Bauweise enorme Vorteile, wie z.B. einen hohen Vorfertigungsgrad, geringes Gewicht und somit reduzierte Baukosten und Bauzeit, oder ein hohes Niveau an Nachhaltigkeit mit sich bringt. Um den umfangreichen bautechnischen Anforderungen insbesondere im Bereich der Flankenschalldämmung gerecht zu werden, ist eine kontinuierliche Optimierung der Konstruktionssysteme erforderlich. Dies ermöglicht es u.a., die Wettbewerbsfähigkeit von Brettsperrholz zu erhalten bzw. zu steigern. Für die Entwicklung innovativer Konstruktionen müssen zumeist messtechnische Untersuchungen an Prototypen realer Bauteilgröße durchgeführt werden. In Kombination mit der hohen Anzahl an möglichen Stoßstellenausbildungen im Massivholzbau mit Brettsperrholz führt dies zu einem enormen zeitlichen und finanziellen Aufwand. Unter Verwendung eines numerischen Vorentwicklungsprozesses kann diese hohe Anzahl an Variationen auf die vielversprechendsten Varianten reduziert werden. Des Weiteren können Struktur und Aufbau der Verbindungsmittel und Stoßstellen vor den Messungen auf deren Wirksamkeit untersucht werden, wodurch frühzeitig Sensitivitäten und Tendenzen erkennbar sind. Anhand dessen können Modifikationen gezielt angesetzt werden. In dieser Dissertation werden verschiedenste numerische Berechnungsansätze auf Basis der Finiten Elemente Methode diskutiert. Die Komplexität der Entwicklung der Modelle wird Schritt für Schritt erhöht, um die Einflussparameter präzise und nachvollziehbar untersuchen zu können. Zunächst wird das akustische Verhalten frei schwingender Brettsperrholzplatten charakterisiert um passende Berechnungsparameter für das einzelne Element zu ermitteln. Im nächsten Schritt werden die einzelnen Elemente unter Verwendung geeigneter Verbindungsmittel zu Stoßstellen verbunden. Normative Messungen des Stoßstellendämm-Maßes werden mit experimentellen Mess- und Berechnungsmethoden erweitert. Abschließend werden die so ermittelten Werte einem normgemäßen Berechnungsmodell zugeführt, um eine Berechnung der Schalldämmung einer realen Bausituation zu ermöglichen. Die numerischen

Berechnungen aller dieser Projektphasen werden mit Daten aus passenden messtechnischen Untersuchungen validiert.

Um einen qualitativ hochwertigen Holzbau auch für die Zukunft sicherzustellen, gilt es, neue Wege und Methoden zu beschreiten. Dabei ist eine gute Schalldämmung besonders in kritischen Frequenzbereichen sicherzustellen um den Holzbau auch für sensitive Nutzer attraktiv zu machen. Hierzu werden in dieser Dissertation spezielle physikalische Effekte untersucht, welche ein hohes Potential zur Verbesserung der Flankenschallübertragung in diesen kritischen Frequenzbereichen zeigen. Zunächst wird der Effekt der modalen (Ent)-Kopplung umfassend analysiert, welcher ein hohes Optimierungspotential besonders in tieffrequenten Bereichen zeigt. Des Weiteren wird der Effekt der Wellentransformation untersucht, der die Umwandlung von schallabstrahlenden Normalkomponenten der schwingenden Fläche in nicht-schallabstrahlende Parallelkomponenten der Wände im Bereich der Stoßstelle beschreibt. Dieser Effekt tritt im mittelfrequenten Bereich auf, somit im selben Frequenzbereich wie auch der Effekt der Koinzidenz, welcher negative Auswirkungen auf die Schalldämmung hat. Hierbei ist das Ziel, die Auswirkungen der Koinzidenz durch eine geschickte Nutzung der Wellentransformation zu kompensieren.

CONTENTS

ACKNOWLEDGEMENTS

The research presented in this thesis was performed during my work at the Laboratory of Building Sciences, in collaboration with the Department of Applied Mechanics of the University of Technology in Graz.

I want to thank my scientific supervisor, Prof. Dr.-Ing. Martin Schanz and my supervisor in building science, Dipl.-Ing. Heinz Ferk for the excellent guidance through the research project and the competent support.

Furthermore, I gratefully acknowledge the funding by the Austrian Federal Ministry of Science, Research and Economy, as well as the Austrian trade association for timber within the framework of the PhD initiative “DokIn’Holz”.

I also want to thank the company “KLH-Massivholz GmbH” for providing specimen used during experimental investigations.

Finally, I want to express my gratitude to my family, especially, to my mother Katharina and my father Blasius, for their patience and support during the course of the work. This thesis is dedicated to them.

Graz, March 2019

Blasius Buchegger

LIST OF ABBREVIATIONS

CLT	Cross-Laminated Timber
K_{ij}	Vibration Reduction Index
FEM	Finite Element Method
SEA	Statistical Energy Analysis
EMA	Experimental Modal Analysis
OMA	Operational Modal Analysis
ESEA	Experimental Statistical Energy Analysis
BEM	Boundary Element Analysis
PIM	Power Injection Method
EFA	Energy Flow Analysis
STI	Structural Intensity
LMS	Least Mean Square
RMS	Root Mean Square
FRF	Frequency Response Functions
SDOF	Single Degree Of Freedom
MAC	Modal Assurance Criterion
DOF	Degree Of Freedom
PIM	Power Injection Method
BIM	Building Information Modelling

NOTATION

Symbol	Unit	Description
m	kg	mass
m''	kg/m^2	mass per unit area
$\psi_{(r)}$	-	eigenfunction
$\underline{\xi}$	m	complex-valued displacement
$\underline{n}_{dyn}(\omega)$	m/N	complex-valued receptance
$\underline{F}(\omega)$	N	complex-valued force
$\mathcal{L}\{f(t)\}$		Laplace transformation
m	kg	mass
k	N/m^2	stiffness
c	-	damping constant
$\underline{Y}(\omega)$	(m/Ns)	complex-valued admittance or mobility
$\underline{A}(\omega)$	m/Ns^2	complex-valued inertance or accelerance
δ	-	modal damping
ω	Hz	angular frequency
$\underline{H}(\omega)$	$Variable$	complex-valued frequency response function
Δ	-	Laplace operator
ζ	m	displacement perpendicular to the surface

E	N/m^2	Young's modulus
v	-	Poisson's ratio
k	$1/m$	wave number
B	Nm^2	bending stiffness
h	m	thickness of a plate
c	m/s	speed of sound
ω_0	Hz	eigenfrequency
p	Pa	sound pressure
η	-	damping constant
$\boldsymbol{M}$	-	mass matrix
$\boldsymbol{K}$	-	stiffness matrix
α	-	mass damping
β	-	stiffness damping
ξ	-	proportional damping
f_D	-	hysteretic damping
sgn		signum
R'_w	dB	weighted apparent sound reduction index
$R_{Dd,W}$ / R	dB	weighted sound reduction index
K_{ij}	dB	vibration reduction index
$D_{v,ij}$	dB	velocity level differences between element i and element j
a_i / a_j	m	absorption length of panel i or panel j
S_i / S_j	m^2	surface area of panel i or panel j
$\eta_{tot,i}$/ $\eta_{tot,j}$	-	total loss factor of panel i or panel j
X_i	-	number of the experimental mode shape
A_j	-	correlation points from the numerical data

Δf	*Hz*	difference of measured and calculated eigenfrequencies
$f_{m,i}$	*Hz*	measured eigenfrequency
$f_{s,i}$	*Hz*	calculated eigenfrequency
η_{ges}	-	total loss factor
T_S	*s*	structure-borne reverberation time
f	*Hz*	frequency
k_A	*N/m/m²*	spring constant per unit area
F	*N*	force
p	*Pa*	sound pressure
l	*m*	length of a tension rod
K	*N/m*	spring stiffness
U	*m*	deformation
A	*m²*	area of a cross-section
Δl	*m*	change of length
σ	*N/m²*	stress
ε	-	strain
ε_q	-	transversal contraction
G	*N/m²*	shear modulus
$\bar{p}$	*Pa*	Spatial averaged sound pressure

1 INTRODUCTION

This thesis describes possible advancements of the numerical prediction, as well as several optimization approaches of the flanking sound insulation in panels of cross-laminated timber.

In section 1.1, the motivation and the background of the scientific investigations in this topic is described comprehensively.

In section 1.2, the current state-of-the-art is described. Previous and current international projects and their outcomes are discussed, as well as different numerical and experimental prediction methods concerning the topic.

Section 1.3 provides an outline of the content of this thesis and a summary of the corresponding chapters of this thesis.

1.1 Motivation

At the present time, the number of new timber-based multi-storey dwellings is growing in several countries in Europe. Therefore, the usage of cross-laminated-timber is increasing caused by several ecological and economical reasons, as well as by the advanced performance of the building material. On the one hand, the total construction costs of a building can be significantly decreased due to the high level of prefabrication of CLT. On the other hand, the renewable building material timber allows an ecological, fast and sustainable building practice. Especially, the importance of sustainability is increasing due to the current energy transition.

Cross-laminated timber is a – more or less – young construction method compared to massive constructions like concrete or masonry. Major steps for its development to a suitable building material occurred, especially, in the 1990s. Caused by its easy handling and versatile applicability, the construction method was able to take root in markets that were dominated by mineral-based solid construction materials for more than 100 years. Especially, in the last 20 years, the worldwide production of CLT has been highly increasing. The worldwide production increased from the year 2000 from about 50 000 m³ to about 550 000 m³ in the year 2013. [1]

Although the fabrication of CLT and the number of new buildings is growing, two major challenges still reduce the competitiveness of cross-laminated timber compared to massive construction methods like concrete or masonry: moisture sensitivity and sound insulation.

The performance in sound insulation is based on a combination of the performance of direct- and flanking sound insulation. In Austria, the legal requirements concerning sound insulation are very high and it is expected that they still will be increasing in the future. To fulfil these requirements, the development of innovative constructions is necessary. With regard to the acoustic performance of the products, flanking sound insulation plays a decisive role. The Development of new innovative products is effortful, because standardized measurement investigations have to be performed on mock-ups of nearly building size currently. These measurements require a lot of effort and time resources and developments and optimizations of timber constructions are highly limited. Hence, sensitivity analyses of the main influencing parameters may lead to a high time and financial effort because of the high number of possible designs of cross-laminated timber, as well as near uncountable variations of the junctions by the numerous available fastener systems. Therefore, the research and development of flanking sound insulation results in a big challenge at the present time. Substituting this measurement procedure by numerical calculations allows a more efficient development process and an increased competitiveness of timber constructions in the future.

As an alternative, the use of numerical calculations can reduce the considerable time and financial effort of experimental investigations. The large number of possible combinations of constructions can be outsourced to a computational environment. Such a pre-development process allows very extensive sensitivity and parameter studies in advance of normative measurements. The studies can be used for the optimization of existing systems as well as for the pre-development of new connection systems and types of joints and can encourage the

development of innovative master details for solid wood based constructions to facilitate the application in building practice.

Furthermore, the fundamentals of the standardized prediction methods are widely based on former investigations on homogenous isotropic materials like concrete. Timber constructions show deviations in acoustic behaviour, especially, in the junctions, which should be taken into account in calculation procedures. Validated numerical calculations of the acoustic behaviour across the junctions allow a deep insight into the underlying physical processes. The obtained knowledge can expand the calculation models. Furthermore, such numerical calculations enable a development of novel approaches for a reduction of the flanking sound transmission, based on the special acoustic characteristics of cross-laminated timber. As a result, an increasing competitiveness of timber construction is expected for the future.

1.2 State of the art

Vibroacoustics in timber based constructions

Several research projects have been performed during the last years dealing with the acoustic and vibro-acoustic behaviour of timber based constructions.

During the completed project “Silent Timber Build”, new prediction tools based on the Finite Element Method (FEM) and the Statistical Energy Analysis (SEA) have been developed, with a focus on a use for calculations of the direct sound insulation for airborne and impact sound transmission. The calculation tools were validated using suitable measurements with a focus on impact sound insulation. Furthermore, a “European Timber Sound Insulation Atlas” has been developed that includes several specific measurement results of relevant timber based constructions [2].

Amongst others, essential parts of the project “Silent Timber Build” are based on investigations by Negreira [3]. In his PhD thesis, the author focuses especially on the low frequency range by the use of calculation approaches based on the FEM and suitable measurement investigations. The author discusses and emphasizes the importance of human perception, especially, for floor vibrations.

A project called “Vibroakustik im Planungsprozess für Holzbauten” was performed by the Technical University of Munich in cooperation with the University for Applied Science of Rosenheim, where hybrid methods based on FEM and SEA were developed to predict the flanking sound transmission in junctions of CLT [4].

A comprehensive and precise collection of several important topics concerning sound insulation is provided by Hopkins [5]. Here, flanking sound transmission is discussed in detail, especially, by the use of advanced SEA calculation models. Additional to the commonly used reduction of the investigations to explicit bending wave transmission, the author takes into account the transmission of different types of waves and effects like a wave conversion in the junctions that can become important especially at mid frequencies. Several topics of Hopkins book are based on his comprehensive PhD thesis [6].

An extensive compilation and analysis of measurements of the vibration reduction index of cross-laminated timber has been performed by Timpte [7] by collecting data of different, international institutions. Amongst others, Timpte discusses the partly high deviation of results of measurement investigations on comparable constructions.

Further general investigations on flanking sound transmission in general can be found, e.g., at [8, 9, 10].

Application of the finite element method

The FEM is a numerical method that can be used for calculations in building acoustics. However, calculations of the acoustic performance of cross-laminated timber results in a big challenge, caused by the complex mechanical structure and properties of timber. In a macroscopic point of view, timber is an orthotropic material depending on fiber direction showing pronounced damping mechanism. In a microscopic point of view, the material timber allows the absorption and desorption of moisture. Furthermore, the physical properties vary markedly between or within trees.

Persson [11] describes a micromechanical modelling of wood and fibre properties in his thesis. Based on experimental and numerical investigations (FEM), he discusses the influence of moisture to mechanical properties with a focus on the microstructure and the resulting

elasticity. His comprehensive investigations also show methods to include the effect of swelling and shrinking in numerical calculations of wooden structures.

Although the finite element method allows taking into account micromechanical effects like moisture content, this procedure is not suitable for calculations in building acoustics because it would result in a number of degrees of freedom that would exceed the computing resources of common IT solutions. Caused by these numerous factors, a need for simplification of the numerical models to the main sensitivity parameters is necessary.

Floden [12] describes such simplifications of the numerical models based on FEM for the prediction of sound transmission in multi-storey wooden buildings. He discusses the efficiency of different methods to reduce the substructures of the buildings and underlines the importance of including only the most relevant information. Furthermore, he describes a reduction of the details in the model to a sufficient level.

Vardaxis [13] discusses possible solutions for FE modelling of two vertical rooms based on cross-laminated timber. Caused by the numerous uncertainties of a highly detailed model, the author concludes that a reduction of complexity is necessary to obtain parameters of substructures. Additionally, Vardaxis remarks problems that can occur during comparisons of measurement and calculation results in narrow bands. These problems can be partly solved, e.g., by using one-third-octave band averaged results.

As shown subsequently in section 2.3, timber shows orthotropic material behaviour, depending on its fibre direction. Kohrmann et al. [14] states that distinguishing between all of the anatomic directions is not appropriate because in practice, wooden boards with different types of cuts are used and it is not possible to predict the application of the corresponding type of cut. To allow a determination of the material parameters using validated numerical models, several techniques can be used.

Further investigations on the use of FEM for calculation of structure-borne sound transmission can be found, e.g., at [15, 16, 17, 18, 19, 20, 21].

Model validation and parameter fitting using EMA

Model validation using experimental modal analysis is a common practice in the fields of mechanical engineering and automotive acoustics. In the last years, the application to building acoustics is increasing, especially, in timber engineering. Combining EMA, linear prediction methods and specialized fitting algorithms represents a state-of-the-art approach for determining suitable material models and parameters for CLT, which is enhanced continuously.

Free vibrating plates can be used to reduce the influence of the boundary conditions during an EMA. This was shown by Gsell et al. [22], where they combined an EMA, a orthotropic linear elastic calculation model based on Reddy's theory and nonlinear optimization algorithm to determine material parameters. The authors were able to fit accurately the investigated bending modes depending on the elastic parameters.

Based on these investigations by Gsell et al., Galzow [23] enhanced the methodology for an application to cross-laminated timber. Several panels with different layer compositions were investigated where the aim was a use, especially, for quality control in fabrication. Galzow showed the difference in results of dynamic or static measurements for determination of elastic parameters. Using dynamic measurements the results for elastic moduli can be significantly higher than those results obtained by using static investigations. The difference is significant, especially, for the shear modulus.

Similar to Galzow, Van Damme et al. [24] compared the dynamic characteristics of CLT panels to quasi-static stiffness measurements. Calculations based on the Timoshenko beam model were validated using EMA. Frequency dependent values of the orthotropic, elastic moduli have been determined up to about 1500 Hz. Van Damme et al. showed that the Young's modulus depends highly on frequency and they have observed that the bending vibration depends weakly on the Poisson's ratio. Therefore, the Poisson's ratio is of limited applicability as a control variable during a model updating process.

Also in [25], validated models are used to determine material parameters for panels of cross-laminated timber. The author developed specialized algorithms for model updating and discusses the challenges by using different types of fitting algorithms. Gradient based methods can lead to local results but not to global results and can subsequently lead to an

erroneous interpretation of the results. This is a very important fact, if fitting algorithms are used.

Filippoupolitits et al. [26] describes the development of calculation models based on the finite element method for a solid timber floor formed by dowel-connected joists. Several FE-models were validated by frequency pair tables and the so-called "Modal Assurance Criterion" (MAC) using data of EMA. Amongst others the focus lays on the support conditions. Supporting springs were chosen and their parameters have been calibrated by using this procedure of parameter fitting.

Later, Van Damme et al. [27] performed EMA on beams of CLT. These beams were cut orthogonally from a three-ply panel along the two principal directions and in difference to other publications, they compared the measured data to analytical models of Euler and Timoshenko beams. They showed that the thin-beam – respectively thin plate – models are not suitable to predict bending modes, so they used Timoshenko beams and sandwich structures.

Paolini et al. [28] used a model updating procedure based on Bayesian optimization for determination of all orthotropic material parameters. In this case, the authors investigated panels of a wall and a ceiling forming an L-shape mock-up and additionally to the material parameters, the authors include the support conditions of the panels and their connection.

In his thesis Kohrmann [29] investigated material parameter estimation using a comprehensive approach of combined FE-models and EMA measurements, especially for timber based floors at low frequencies. Kohrmann also uses the modal assurance criterion (MAC) for fitting of the mode shapes at the specific eigenfrequencies.

Further investigations on model updating using EMA can be found for example at [30].

Alternative methods are also used to validate calculation models by measurement results.

Alternative methods for parameter fitting

In [31], the elastic properties determined by Keunecke et al. [32] have been used for FE-calculations of cross-laminated-timber panels. Keunecke et al. determined the parameters

using a digital image correlating technique and compared it to several elastic material parameter sets taken from literature.

In [33], phase and time differences of experimental measured flexural wave velocity have been used to determine the elastic and stiffness characteristics of orthotropic CLT plates.

Using validated material models and suitable material parameters, FE models of full constructions can be used for predictions in building acoustics.

Kohrmann [29] investigates FE models of CLT panels within the low frequency range up to 125 Hz. Here, he complements the measurement investigations of the project "Vibwood" [14] by numerical studies. A special focus lies on determination of input data for the models and their validation by a use of measurements of Operational Modal Analysis (OMA) and EMA. Additionally, comprehensive studies on radiation efficiency and calculation of the sound radiation have been performed.

Clasen [34] shows possibilities of calculation of direct- and flanking sound transmission, especially, for typical multi-layered constructions, including porous layers. Amongst others, the author developes highly down-scaled models for validation of prediction methods based on the FEM. Partly, in-plane wave propagation is taken into account during the investigations.

Rabold [35] discusses methods for calculation of the impact sound insulation of timber based floors. The focus lays on the implementation of the tapping machine on suitable floors in a prediction method based on the FEM. The author shows some of the most important potentials of numerical calculation methods – to perform parametric and sensitivity studies. Further advantages of the methodology, like a reduction of the high time and financial effort of experimental testing, is shown by Floden [12].

Application of the statistical energy analysis

Another important numerical method for prediction of the sound insulation of building materials is the SEA. A comprehensive overview of the fundamentals of the theory is shown by Lyon and DeJong [36]. The method has already been used for the prediction of the sound transmission of different building materials for several decades. Early calculations have been performed, e.g., by Crocker and Price [37]. The applicability of SEA to coupled plates has

been shown by Wester and Mace [38]. Here, ensembles of plates and their averages are studied.

Hopkins [6] carried out very comprehensive studies using SEA and Experimental SEA (ESEA) in his thesis. The focus lays on predictions of the structure-borne sound transmission in masonry and concrete constructions. In [39], the author studies the application of the developed calculation methods especially for low modal density and modal overlap that occur at low frequencies, down to one-third octave bands of about 50 Hz. Within these frequency ranges, the methodology shows a strongly limited applicability.

Schoenwald [40] investigates the flanking sound transmission focused on lightweight framed double leaf walls using the SEA. Amongst others, the author distinguishes between resonant and non-resonant motion of the leaves. Currently, this separation is an important topic in international science and standards. The author investigates the propagation damping in the structure that is caused by high material damping. This physical effect reduces the approach of diffuse sound fields, and, as a consequence, the applicability of SEA.

Further investigations on the use of SEA for prediction of flanking sound transmission can be found, for example, at [41, 42].

Application of the boundary element method

A third numerical calculation method that can be used in building acoustics is the boundary element method (BEM). This method allows efficient calculations especially of the sound radiation of vibrating surfaces.

Early investigations on sound transmission have been made, e.g., by Wu and Dandapani [43], where they focused on the fluid-structure-fluid interaction. The efficiency of BEM calculations can be increased by using Fast Boundary Element Methods that are comprehensively discussed by Messner [44].

Katasikadelis [45] shows different ways to use the BEM for plate analysis.

Although the calculation method shows a lot of advantages like efficient calculation of sound radiation, it is rarely used in building acoustics, mostly because of the challenging coupling with other calculation methods like the FEM.

This coupling of several numerical methods plays an essential role during calculations of sound transmission in building acoustics, especially because currently no methodology exists that allows efficient calculations within the whole frequency range of building acoustics and covers all underlying physical problems at once.

Couplings of FEM and BEM are rare in building acoustics, although this procedure is often used in other disciplines, like mechanical engineering [46]. A possible application is optimizing undersea or driving vehicles, e.g., discussed by Dong et al. [47]. Further applications of a coupling of FEM and BEM in the field of technical acoustics have been shown by Müller [48].

Zhu et al [49] show a promising hybrid approach, based on a coupling of FEM and BEM in their investigations. The methodology shows high potential for calculation of direct sound transmission, considering direct sound fields and reverberant sound fields.

Coupling of FEM and SEA

A common way to allow calculations within a wide frequency range is a coupling of the FEM and the SEA. Early investigations on such couplings were performed by Steel and Craik [50] for structure borne sound transmission in a parallel arrangement of coupled plates made of concrete.

Often, this coupling of FEM and SEA is called “Virtual SEA”. Gagliardini et al. [51] describe the application for mid-frequency structure-borne sound calculations. Similar to ESEA, the necessary frequency response functions are calculated within the framework of FEM and are used afterwards in the SEA for further calculations.

Current work of the coupling of FEM and SEA has been performed by Müller and Buchschmid [52], where their investigations focus on the mid-frequency range. The authors show that especially strongly coupled structures cannot be split into separate components, which is a fundamental requirement for an application of the SEA. As a consequence, the applicability of SEA is limited and appropriate FEM approaches shall be used.

FEM and SEA can lead to inaccurate results in a special mid frequency. This is also called the “mid-frequency gap”.

Buchschmid et al. [53] presented an SEA-like approach, where they couple the SEA with FEM and include parts of the Power Injection Method (PIM) as well as the Energy Flow Analysis (EFA). The study focuses on the calculation of the structure-borne sound transmission within U-profiles of a vehicle floor pan.

Wachulec [54] discusses several approaches for calculations in the mid-frequency range using hybrid FEM and SEA approaches by detailed analysis of the power flow between subsystems for calculation of sound transmission in coupled beams and plates. Wachulec also shows the importance of taking into account in-plane motions additional to out-of-plane motion, especially during investigations in the mid-frequency range.

Langley and Shorter [55] are providing a potential solution for the problem of the mid-frequency gap. One of the advantages of their solution is that it allows a systematic analysis of a system, which cannot be analysed using classical SEA or FE methods. Further work by Langley, Shorter et al. is described, e.g., in [56, 57, 58].

In-plane wave motion

Most of the time, only bending wave transmission is taken into account for transmission calculation in building acoustics. In several cases, including in-plane wave transmission is necessary, e.g., shown by Wang and Hopkins [59] during investigations in beam frameworks.

As shown by Hopkins [5] during detailed calculations of different types of waves using the SEA, separate calculations of structural reverberation times and dampins for bending, quasi-longitudinal and transverse shear waves may be required. A consideration of in-plane components is possible, if the requirements of SEA (reverberant sound field) are fulfilled. Therefore, calculations of several types of waves are feasible, especially at mid and high frequencies using SEA.

Investigations on in-plane wave generation at plate junctions were made early on Cremer et al. [60]. Gibbs and Craven [61] showed that structure-borne sound that is converted into in-plane vibration can overcome long distances through several junctions. Only a small attenuation occurs, before the in-plane vibration is transformed to bending vibration, which again can lead to sound radiation into cavities.

Hambric and Taylor [62] used experimental methods and FEM to obtain the flexural powers in a specialized beam model. Wave decomposition theory is used to separate incident, reflected and near-field powers. The authors emphasize the importance of a consideration of compressional and torsional waves, because these types of wave contain structure-borne power additional to flexural waves.

Wachulec [54] showed that out-of-plane motions and in-plane motions are coupled at the junction of coupled plates. Dynamic properties of all types of motions have to be used to allow a comprehensive study of the dynamic behaviour, especially of the vibration of thin plates.

Kessissoglou et al. [63] investigated wave conversion in rectangular connected plates. They showed that the in-plane percentage of the total sound energy increases with an increasing frequency and number of the rectangular junctions.

Comprehensive investigations in flanking sound transmission of different types of wave have been carried out by Hopkins. In [64], the author uses calculations of the sound transmission in T-shape junctions based on SEA, where he takes into account every possible coupling of subsystems for bending, quasi-longitudinal and transverse shear wave motion separately. Therefore, the effect of wave conversion in the junction and in the plates has been considered. In [5], the author additionally showed the importance of in-plane waves on the apparent sound reduction index during investigations on two coupled rooms and a single T-shape junction. Taking into account in-plane waves, the apparent sound reduction index shows a tendency of an increasing value for direct and flanking transmission paths. At mid and high frequencies, calculations of the transmission loss through a T-shaped junction show that considering in-plane wave propagation, the transmission loss decreases for the flanking-flanking path and increases for the direct-flanking respectively flanking-direct path.

Furthermore, Hering [65] shows in very comprehensive studies that the main part of the structure-borne sound energy can be contained by in-plane waves. This energy can be converted to out-of-plane components, which finally lead to sound radiation. In his study, Hering uses the Structural Intensity (STI). The importance of in-plane waves increases for curved structures. In-plane waves can be used to influence bending waves because of their coupling with out-of-plane waves. As a consequence, a local insulation of in-plane waves can lead to a reduction of bending waves. Hering also mentioned that neglecting any type of wave at a junction may lead to a misinterpretation of the total energy flow.

Further investigations on coupling of out-of-plane and in-plane wave motions have been performed for example by [66, 67, 68].

1.3 Outline

The investigations described in this thesis focus on two overall aims: First, numerical methods are enhanced to allow calculations of the flanking sound transmission in specific junctions and fastener systems. Second, new approaches to improve the flanking sound insulation in panels of CLT are developed. The focus lays on the low and the mid frequency range. The FEM has been chosen as the main calculation method. Although the general calculation effort is significantly higher compared to other numerical methods like the SEA, the FEM also allows deeper investigations in the physical behaviour of the structure because of the possibility to model the constructions close to reality. As shown in the state of the art, for strongly coupled subsystems the FEM has to be used for calculations especially in the mid frequency range because of the limited applicability of the SEA. The modal behaviour and the physical behaviour in the junction during wave conversion is investigated. As shown in chapter 1.2, in-plane wave motion should be taken into account. Currently, investigations on panels of CLT including this effect are uncommon. Therefore, the effect of wave transformation is taken into account in the investigations described in this thesis.

Chapter 2 contains selected topics of the fundamental theory used in the consecutive chapters of this thesis. The focus lies on the fundamentals of acoustics and mechanics, as well as on standardized and numerical calculation methods.

Chapter 3 describes the development of calculation methods for junctions of CLT panels, based on the FEM. Here the focus lays on the acoustic and mechanical behaviour of the panels, their mechanical interaction and the final calculation of the flanking sound transmission in the junction by the use of special fastener systems. A frequency range within one-third-octave-bands from 200 Hz to 1250 Hz is investigated, because this frequency range is used for single-number ratings of the vibration reduction index. The survey is separated in three different steps that focus on special topics. First, single CLT panels are investigated to determine suitable calculation methods, material models and material data. Second, the single panels are connected to each other to form junctions. Special fastener systems are used and the standardized vibration reduction index is evaluated. Third, the calculation approach is

evaluated using the standardized prediction methods of the EN 12354-1 during an application to a real building situation. All steps are evaluated using measurement data from suitable, practical constructions.

Chapter 4 describes several acoustic effects that have an influence on the flanking sound transmission in panels of CLT. First, an effect called “modal (de-)coupling” is investigated that occurs in the low and very low frequency range. The effect shows a high potential for an optimization of the flanking sound insulation for impact sound. Second, an effect called “wave transformation” is investigated that occurs in the mid frequency range. This effect shows a high optimization potential for flanking sound insulation by partly compensating the effect of coincidence.

Appendix A includes further details of the measurement setups in the laboratory and in-situ.

2 THEORETIC FUNDAMENTALS

2.1 Fundamentals of mechanics

2.1.1 Vibration of a structure

The analysis of vibrating structures is very important in the fields of acoustic measurements. These structural vibrations, caused by structure-borne sound, occur in many technical areas of daily life, such as in cars or household appliances like washing machines. In normal operation, the stability of the structures should not be negative influenced by these vibrations. However, despite optimal design, undesirable effects, such as, e.g., sound radiation can occur, which can have a very annoying effect. In order to be able to detect the sound source, an investigation of the vibrating structure is necessary. In addition to the investigation of vibration problems, models can be developed based on modal analysis, which allow extensive investigations with appropriate measurement effort. First of all, the descriptive quantities (or modal parameters) are determined by measurements on the real structure. In addition to the analysis of an entire system, the modal analysis also allows investigations of individual components of the total structure. The knowledge based on these investigations allows a development of optimization measures of the system [69].

The considerations in this chapter are fundamental in the consecutive chapters of this thesis. Amongst others, they are used for measurement investigations on structures to determine the modal behaviour of the system, e.g., during an experimental modal analysis (EMA).

2.1.1.1 Vibrations and modes

The vibrations of a dynamic system are defined by their natural frequencies and the natural modes of vibration. The latter thus describes the resulting vibration shape. If the system is

excited at a frequency, which corresponds exactly to such a natural frequency (also called eigenfrequency), very high amplitudes can arise. An important criterion for an eigenfunction is the orthogonality that means that the modes are independent from each other [69]:

$$\int_S \psi_{(q)}(x,y)\psi_{(r)}(x,y)dxdy = 0 \quad \forall q \neq r \qquad (-) \quad (2.1)$$

Here, $\psi_{(r)}$ represents the eigenfunction (-).

However, the assumption of this approach requires closed bodies. This requirement is widely complied if the boundaries of the structure are showing ideal free or rigid edges. Many complex subsystems can result from connecting several systems. The modal analysis is still applicable, but with considerably higher effort. If the natural oscillations or modes of a system are known, the stationary oscillation behaviour can be described by a superposition of these modes [69]:

$$\underline{\xi}(x,y) = \sum_{r=1}^{\infty} \underline{\xi}_{(r)}\, \psi_{(r)}(x,y) \qquad (m) \quad (2.2)$$

Here, $\underline{\xi}$ represents the complex-valued displacement (m).

From the theorem (2.1) it can be stated that the oscillation behaviour of a system can be described by an arbitrary excitation from the corresponding eigenfrequencies and eigenfunctions. Equivalent to the Fourier transformation, the modal analysis thus can also be interpreted as a modal transformation [69].

2.1.1.2 Theory of systems

A linear, time-invariant system is usually assumed especially for modal analysis in acoustics. Thus the following assumptions can be stated [69]:

- **Principle of superposition:** If the system is excited simultaneously with multiple signals, the response of the total system is equal to the sum of the single responses of each individual signal.

- **Additivity:** Changing the input force by a factor causes a change in the system's response proportional to the same factor.

- **Causality:** There is no system response if no excitation signal exists. This assumption is also applied before the excitation signal is applied to the system.

- **Stability:** If the excitation signal is stopped, the vibrations will continue and decay. Thus, the system can not build up. The damping of the system determines the duration of the decay process.

- **Time invariance:** The dynamic behaviour of the system does not change with time (e.g., during experimental measurements).

Additionally, following assumption is stated during the application of the modal analysis. It has to be mentioned that this assumption is not always valid for time-invariant systems.

- **Reciprocity:** It is possible to swap the locations of excitation and response while not changing the transmission behaviour of the system. In this case, following assumption can be made

$$Y(x_1, x_2) = Y(x_2, x_1) \quad . \tag{2.3}$$

Y represents the transfer mobility, which is defined by the ratio between the Fourier-Transformed (FT) velocity observed at the point x_1 and the (FT) force exciting the system at point x_2. As a consequence, the frequency response function H_{12} between a force at an excitation point x = 1 and the response at an observed point x = 2 is equal to the frequency response function H_{21} (swapped locations), if the principle of reciprocity is fulfilled.

$$H_{12} = H_{21} \tag{2.4}$$

2.1.1.3 Vibration response of a structure

An excitation of a linear, time-invariant system in point A causes defined vibration behaviour. The resulting response of the system in point B depends on the material properties and boundary conditions of the system. Therefore, three parameters are necessary for the exact determination of the vibration behaviour: the excitation at point A (usually the value of the corresponding force), the system properties between the two points, and the response at point B (usually the acceleration, velocity or the displacement). The practical measurement of the induced force and the resulting acceleration can be carried out using force and acceleration

sensors. The measurement data allows a calculation of the transmission properties of the system. Frequency response functions define the properties of the system [69]:

$$Properties\ of\ the\ system = \frac{response}{excitation}$$

In the frequency domain, the ratio of response to excitation of the system is also referred to Frequency Response Functions (FRF). For linear systems, these functions only vary in frequency, but do not vary in the strength of the excitation. The following ratios of force and movement quantities can be used for definitions of the transfer functions [69]:

- The receptance

$$\underline{n}_{dyn}(\omega) = \frac{\underline{\xi}(\omega)}{\underline{F}(\omega)} \quad , \qquad \text{(m/N)} \quad (2.5)$$

where $\underline{\xi}(\omega)$ represents the complex-valued displacement (m) and $\underline{F}(\omega)$ the complex-valued force (N).

- The admittance or mobility

$$\underline{Y}(\omega) = \frac{\underline{v}(\omega)}{\underline{F}(\omega)} \quad , \qquad \text{(m/Ns)} \quad (2.6)$$

where $\underline{v}(\omega)$ represents the complex-valued velocity (m/s) and $\underline{F}(\omega)$ the complex force (N).

- The inertance or accelerance

$$\underline{A}(\omega) = \frac{\underline{a}(\omega)}{\underline{F}(\omega)} \quad , \qquad \text{(m/Ns²)} \quad (2.7)$$

where $\underline{a}(\omega)$ represents the complex-valued acceleration (m/s²) and $\underline{F}(\omega)$ the complex force (N).

A transfer function represents the mathematical description of the vibrating structure. However, the source of the corresponding dynamic response is not known, therefore a suitable model has to be created. A distinction is made primarily between analytical models and modal models. For complicated structures, simplifications are often required, since the generation of

a model considering all the details results in a high effort, or the generation of such a model may not be possible [69].

2.1.1.4 Analytical models

In general, a vibrating system can be considered as a specific combination of elements like masses, springs and dampers. This approach often results in very complicated distributions of such elements and their separation can be very difficult.

Such analytical models can be described mathematically by means of equations of motion, assuming suitable initial- and boundary conditions. This description is based on several differential equations characterising the systems behaviour and allows calculations of the corresponding transfer functions of the dynamic system [69].

2.1.1.5 Single oscillator (SDOF- system)

The well known homogeneous differential equation ($\underline{F} = 0$) of a SDOF-system can be used to determine the eigenvalues of the system

$$m\underline{s}^2 + c\underline{s} + k = 0 \qquad s \in \mathbb{C} \quad . \tag{2.8}$$

The non-trivial solutions for $\underline{s}$ correspond to the eigenvalues of the eigenvector, depending on the native parameters. We distinguish three different cases, which depend on the damping constant c [69]:

- Critical damping – the two eigenvalues are equal

From

$$c = c_k = 2\sqrt{mk} \tag{2.9}$$

results

$$Re(\underline{s}) = -\frac{c}{2m} \quad , \quad Im(\underline{s}) = 0 \tag{2.10}$$

- Overdamped - Exponential decay of the displacement– real eigenvalues

From

$$c \geq 2\sqrt{mk} \qquad results: \underline{s} \in \mathbb{R} \tag{2.11}$$

results

$$\underline{s} \in \mathbb{R} \tag{2.12}$$

- Underdamped system – conjugate complex eigenvalues

From

$$c < 2\sqrt{mk} \tag{2.13}$$

results

$$\underline{s} = -\frac{c}{2m} + j\sqrt{\frac{k}{m} - \left(\frac{c}{2m}\right)^2} = -\delta - j\omega_d \qquad , \tag{2.14}$$

where δ represents the modal damping (-) and ω represents the eigenfrequency (Hz).

Equation (2.14) shows that the modal damping is defined by the real part of $\underline{s}$:

$$\delta = -Re\{\underline{s}\} = \frac{c}{2m} \tag{2.15}$$

The eigenfrequency ω is defined by the imaginary part. Based on

$$\omega = Im\{\underline{s}\} = \sqrt{\frac{k}{m} - \left(\frac{c}{2m}\right)^2} = \sqrt{\omega_0^2 - \delta^2} \tag{2.16}$$

the eigenfrequency ω_0 is calculated by

$$\omega_0 = \sqrt{\frac{k}{m}} \tag{2.17}$$

For systems that show a low damping ($c \ll c_k$), the approximation of $\omega_d \approx \omega_0$ is assumed.

The damped vibration of a single oscillator is defined by $\underline{\xi} = \psi e^{-\delta t}$ in the time domain. The function $e^{-\delta t}$describes the envelope of the decaying vibration. As a consequence, the solution of the homogenous differential equation is suitable for determination of fundamental properties of the system.

Assuming a harmonic force

$$\underline{F}(\omega, t) = \underline{\hat{F}}(\omega) e^{j\omega t} \quad , \tag{2.18}$$

the stationary solution is determined.

The response of the system

$$\underline{\xi}(\omega, t) = \underline{\hat{\xi}}(\omega) e^{j\omega t} \quad , \tag{2.19}$$

shows the same frequency as the excitation.

The stationary solution is defined by

$$(-\omega^2 m + j\omega c + k)\, \underline{\hat{\xi}}(\omega) = \underline{\hat{F}}(\omega) \quad . \tag{2.20}$$

As a result, the transfer function

$$\underline{H}(\omega) = \underline{n}_{dyn}(\omega) = \frac{\underline{\xi}(\omega)}{\underline{F}(\omega)} = \frac{1}{-\omega^2 m + j\omega c + k} \tag{2.21}$$

is calculated, based on the ratio between excitation and reaction of a linear system (compare chapter 2.1.1.3). Two cases can be defined concerning the eigenfrequency ω_d.

$$\underline{H}(\omega) \approx \begin{cases} \dfrac{1}{k} & if\ \omega \ll \omega_d \\ \dfrac{1}{(-\omega^2 m)} & if\ \omega \gg \omega_d \end{cases} \tag{2.22}$$

On the one hand the stiffness, and on the other hand the mass dominates the frequency response of the system. A multiplication of the spectrum of the excitation and the tranfer function of the system in the frequency domain allows a calculation of the resulting complex-valued displacement

$$\underline{\hat{\xi}}(\omega) = \underline{H}(\omega)\underline{\hat{F}}(\omega) \quad . \tag{2.23}$$

The frequency response of a SDOF-system is defined by

$$\underline{H}(\omega) = \underline{n}_{dyn}(\omega) = \frac{\underline{\xi}(\omega)}{\underline{F}(\omega)} = \frac{1}{-\omega^2 m + j\omega c + k} \quad . \tag{2.24}$$

The damping ratio is defined by

$$D = \frac{\delta}{\omega_0} \quad . \tag{2.25}$$

The normalized excitation frequency is defined by

$$\eta = \frac{\omega}{\omega_0} \quad . \tag{2.26}$$

Based on these assumptions, the transfer function can be rewritten by

$$\underline{H}(\omega) = \underline{n}_{dyn}(\omega) = \frac{\underline{\xi}(\omega)}{\underline{F}(\omega)} = \frac{1}{k(-\eta^2 + 2j\eta D + 1)} \tag{2.27}$$

The magnitude of the resonance is increasing with decreasing damping ratio. Near the eigenfrequency of the system, the phase shows a step of –π.

2.1.2 Types of waves in solid structures

Vibrations can occur, e.g., between rigid bodies, if they are connected to each other elastically, e.g., via springs. Those vibrations of the mechanical system can be described by systems of differential equations. The natural frequencies of the system can be calculated by determining the eigenvalues of the differential equations. In general, kinetic and potential energy are stored and alternately converted to each other [70, 71].

Wave phenomena can occur in every continuum. A wave arises, e.g., if the infinitesimal elements of a solid are elastically connected in a way that the descriptive field quantities are coupled together. Then the second spatial derivative of the displacement field and the second time derivative are proportional to each other. Assuming a loss-free case, the simple wave equation can be obtained. Differential equations of higher order can occur, e.g., for bending waves [71].

In principle, only two types of waves can occur in homogeneous, solid medium - longitudinal waves (in-plane waves) and transverse waves (out-of-plane waves). Longitudinal waves are characterized by a displacement of the particles in the direction of wave propagation. Transverse waves are characterized by a displacement normal to the propagation direction. Pure shear stresses lead to shear deformations and as a consequence, the shape is changed but no volume change arises. The propagation of pure longitudinal or transverse waves is only possible in infinite large solid structures. If this condition is not fulfilled, other wave types occur that can be explained by the superposition of these two main wave types [70, 71].

Bending waves are essential in building acoustics, since they can arise in thin plates. Due to the transversal deflection of the surface of the plate this type of wave can cause a significant radiation of sound into the surrounding air. For this reason, bending waves will be discussed in more detail, especially with regard to the properties of wave propagation in plates [71].

2.1.2.1 Propagation of bending waves in plates

Bending waves are defined by a combination of longitudinal and transverse waves. They can be defined by their out-of-plane and in-plane components, therefore, bending waves are essential especially for the discussions of wave transformation in chapter 4.2. A dispersive (frequency dependent) propagation speed of the wave is an important characteristic of this type of wave. This property occurs only for bending waves and they primarily propagate in

thin plates. To describe the motion of such thin plates, Kirchhoff's plate equation can be used. Here, the definition of "thin" describes the ratio of the plate thickness to the remaining dimensions. The well known homogeneous differential equation of the Kirchhoff plate is defined by

$$\Delta\Delta\zeta + \frac{m''}{B} \cdot \frac{\partial^2 \zeta}{\partial t^2} = 0 \ , \tag{2.28}$$

where Δ represents the Laplace-operator, ζ the displacement perpendicular to the surface (m), m'' the mass per unit area (kg/m²) and t represents the time (s). Here, the so-called bending stiffness is defined by

$$B = \frac{Eh^3}{12(1-\nu^2)} \ , \quad \text{(Nm)} \tag{2.29}$$

where E represents the Young's modulus (N/m²), h the thickness of the plate (m) and ν the Poisson's ratio (-). A detailed derivation of the equations can be found, e.g., at [70].

Using an initial function of harmonic plane waves that propagates in the plate, equation (2.28) can be solved to the wave number

$$k_B^4 = \frac{\omega^2 m''}{B} \ , \quad (1/\text{m}^4) \tag{2.30}$$

where ω represents the angular frequency (Hz).

Here, two cases can be distinguished: the positive sign results in a real-valued far-field solution, which allows a propagation of the wave

$$(k_B)_{1,2} = \pm\sqrt{\omega} \cdot \sqrt[4]{\frac{m'}{B}} \ . \quad \text{(1/m)} \tag{2.31}$$

The negative sign results in an imaginary-valued near-field solution:

$$(k_B)_{3,4} = \pm j\sqrt{\omega} \cdot \sqrt[4]{\frac{m'}{B}} \ . \quad \text{(1/m)} \tag{2.32}$$

As mentioned before, the propagation speed is dispersive for bending waves. This characteristic is evident by calculation of the speed of sound c_B for bending wave:

$$from: \quad c_B = \frac{\omega}{k_B} \qquad results: \quad c_B = \sqrt{\omega} \cdot \sqrt[4]{\frac{B}{m'}} \quad , \qquad \text{(m/s)} \qquad (2.33)$$

and the bending wave-length

$$\lambda_B = \frac{2\pi}{\sqrt{\omega}} \cdot \sqrt[4]{\frac{B}{m'}} \quad . \qquad \text{(m)} \qquad (2.34)$$

It should be noted that the presented relationships apply only for frequencies where the bending wavelength is large compared to the plate thickness. For higher frequencies or smaller wavelengths, the Kirchhoff plate equation is not valid.

2.1.3 Wave propagation in fluids

Additional to solids, wave phenomena can also occur in viscous fluids. The non-linear Navier-Stokes equations represent the corresponding equations of motion in their most general form. On the one hand, these equations are the fundamentals of fluid mechanics. On the other hand, they also form the base of acoustics, since they can be simplified and linearized. The convective part of the acceleration and the viscous friction can be neglected and the gas law can be linearized, which results in the classical field equations of the frictionless, acoustic fluids [71].

The wave equation for the sound pressure p (Pa) is also called the “Helmholtz - equation” and in the frequency domain, the equation is defined by

$$\Delta p + k^2 p = 0 \quad . \qquad (2.35)$$

In this statement, the wave number k (1/m) is defined by

$$k = \frac{\omega}{c} \qquad \text{(1/m)} \qquad (2.36)$$

and the Laplace-operator Δ is defined by

$$\Delta = \left(\frac{\partial^2}{\partial x^2} + \frac{\partial^2}{\partial y^2} + \frac{\partial^2}{\partial z^2}\right) \tag{2.37}$$

Based on this equation, different solutions for plane waves or for the spherical waves can be derived, e.g., as described by Kuttruff [72].

2.1.4 Damping

A suitable damping model is essential for calculation of timber structures, as shown by Labonnote [73]. In general, damping can be described by the dissipation of mechanical energy that means an irreversible conversion into, e.g., thermal energy. Linear damping models can be assumed for small vibrations and small damping, although most of the damping mechanisms show non-linear behaviour.

Kuhl [74] specified a comparison of different damping mechanisms, shown in Table 2.1. The damping constant η (-) of the joints and the surface shows the highest influence on the total losses, followed by material damping and transmission to coupled structures. Radiation losses show a very small range of values compared to the other mechanisms, therefore they can be neglected in several real situations in building acoustics.

	Damping mechanism	**Range / η**
Energy dissipating mechanism	Material damping	10^{-4}
	Joint damping	10^{-2}-10^{-3}
	Surface damping	10^{-2}
Energy transmitting mechanism	Radiation losses (e.g., radiation to air)	10^{-5}-10^{-8}
	Flanking transmission (transmission to coupled structures)	10^{-4}

Table 2.1: Range of different damping mechanisms [74]

Kohrmann et al. [14] show a resulting total loss factor determined from investigations on CLT, shown in Table 2.2.

Construction	**Variable**	**Value (-)**
Single CLT with connection board	η	0,007 +/- 0,01

Table 2.2: Total loss factor of CLT determined by experimental investigations [14]

Van Damme et al. [27] showed in their investigations on beams of CLT that the damping ration for bending modes is lower than 2 %. So they considered the observed CLT plates as a low loss material.

During their numerical calculations of flanking walls and spring-damper joints, Clasen and Langer [75] were able to enhance the approaches and results of former investigations described in [76], but on their own appraisal they got not sufficient results. The authors traced their observation to the damping of the structure and they emphasize the importance of also taking into account other damping mechanisms.

2.1.4.1 Rayleigh damping (Proportional damping)

Proportional damping or Rayleigh damping is defined by the damping matrix

$$\boldsymbol{D}=\alpha\boldsymbol{M}+\beta\boldsymbol{K} \tag{2.38}$$

by a linear combination of the mass matrix $\boldsymbol{M}$ and stiffness matrix $\boldsymbol{K}$, where α and β are real scalars. For a SDOF system, proportional damping results in

$$\xi=\frac{\alpha\omega}{2}+\frac{\beta}{2\omega} \ , \tag{2.39}$$

where α represents the mass damping and β represents the stiffness damping. The proportional damping is a special case of viscoelastic damping [73].

2.1.4.2 Hysteretic damping

Hysteretic damping is defined by a damping force in opposite to the relative motion. This damping force is proportional to the displacement amplitude and it is in-phase with the velocity. Hysteretic damping is defined by

$$f_{\boldsymbol{D}} = k\pi\beta_h sgn(x)|x| \ , \tag{2.40}$$

where β_h represents an empirically determined constant and x represents the displacement [73].

The energy dissipated per cycle of oscillation in a hysteretic form is defined by [73]

$$\Delta E = \int_0^{\frac{2\pi}{\omega}} (f_D \times \dot{x})\, dt = \frac{d}{\omega} \int_0^{\frac{2\pi}{\omega}} \dot{x}^2 dt = \pi d X_0^2 \tag{2.41}$$

2.2 Theory of Elasticity

Assuming a rod with a length much higher than its width, one end of the rod can be loaded by tension, the other end of the rod can be clamped. A one-dimensional state of tension results in a sufficient distance from the force application point and the clamping. Within this area, the well known "Hooke's Law" [77]

$$\sigma = E\, \varepsilon \quad . \tag{2.42}$$

can be defined, where σ represents the stress, E represents the Young's modulus and ε represents the strain.

Furthermore, the tension rod shows a contraction transverse to the tension direction. Assuming a circular cross-section with a diameter d, the transversal contraction is defined by [77]

$$\varepsilon_q = \frac{\Delta d}{d} \quad . \tag{2.43}$$

Subsequently, the ratio between transversal contraction ε_q and longitudinal contraction ε_x results in the so-called "Poisson's ratio" [77]

$$\nu = -\frac{\varepsilon_q}{\varepsilon_x} \quad . \tag{2.44}$$

Typical value ranges are between $0 \leq \nu < 0{,}5$ for homogenous materials. Steel is often referred to a reference, assuming a value of about $\nu = 0{,}3$ [77].

Furthermore, the shear modulus G (N/m²) is the pendant to the Young's modulus and defines the relation between shear stress τ and shear strain γ as defined by [77]

$$G = \frac{\tau}{\gamma} \quad . \tag{2.45}$$

The relationship between Young's modulus and shear modulus can be shown by [77]

$$G = \frac{E}{2\,(1+\nu)} \quad . \tag{2.46}$$

These approaches are valid, if subsequent conditions are fulfilled [77]:

- **Linearity:** If the stresses are increased, the strains have to increase by the same amount.
- **Superposition:** As a consequence of linearity, strains and stresses in the same coordinate direction can be superimposed.
- **Isotropy:** The behaviour of the material is the same in all directions.

The Young's modulus and the shear modulus of a 3-dimensional material result in 6 equations that can be summarized in a matrix [77] [78]

$$\begin{bmatrix} \varepsilon_x \\ \varepsilon_y \\ \varepsilon_z \\ \gamma_{xy} \\ \gamma_{yz} \\ \gamma_{zx} \end{bmatrix} = \frac{1}{E} \begin{pmatrix} 1 & -\nu & -\nu & 0 & 0 & 0 \\ -\nu & 1 & -\nu & 0 & 0 & 0 \\ -\nu & -\nu & 1 & 0 & 0 & 0 \\ 0 & 0 & 0 & 2(1+\nu) & 0 & 0 \\ 0 & 0 & 0 & 0 & 2(1+\nu) & 0 \\ 0 & 0 & 0 & 0 & 0 & 2(1+\nu) \end{pmatrix} \begin{pmatrix} \sigma_{xx} \\ \sigma_{yy} \\ \sigma_{zz} \\ \tau_{xy} \\ \tau_{yz} \\ \tau_{zx} \end{pmatrix} \tag{2.47}$$

Where $\sigma_{ij,i=j}$ are longitudinal stresses and $\sigma_{ij,i\neq j}$ shear stresses.

Wood in general fulfils the assumptions of an orthotropic material model in a better way, as discussed subsequently in chapter 2.3. In this case, three planes of symmetry exist and the elastic strain-stress relations may be expressed as [78]

$$\begin{bmatrix} \varepsilon_{x'} \\ \varepsilon_{y'} \\ \varepsilon_{z'} \\ \gamma_{x'y'} \\ \gamma_{y'z'} \\ \gamma_{z'x'} \end{bmatrix} = \frac{E_{x'}}{E_{x'}} \begin{pmatrix} \frac{1}{E_{x'}} & -\frac{v_{x'y'}}{E_{y'}} & -\frac{v_{x'z'}}{E_{z'}} & 0 & 0 & 0 \\ -\frac{v_{y'x'}}{E_{x'}} & \frac{1}{E_{y'}} & -\frac{v_{y'z'}}{E_{x'}} & 0 & 0 & 0 \\ -\frac{v_{z'x'}}{E_{x'}} & -\frac{v_{z'y'}}{E_{y'}} & \frac{1}{E_{z'}} & 0 & 0 & 0 \\ 0 & 0 & 0 & \frac{1}{G_{x'y'}} & 0 & 0 \\ 0 & 0 & 0 & 0 & \frac{1}{G_{y'z'}} & 0 \\ 0 & 0 & 0 & 0 & 0 & \frac{1}{G_{z'x'}} \end{pmatrix} \begin{pmatrix} \sigma_x \\ \sigma_y \\ \sigma_z \\ \tau_{x'y'} \\ \tau_{y'z'} \\ \tau_{z'x'} \end{pmatrix} \quad (2.48)$$

Further details on the FEM and material theories can be found, e.g., at [77] or [78].

2.3 The material model of wood

Wood is a naturally grown material. In general, the physical properties of wood are orthotropic. Depending on the type of wood, the different growth conditions, bulk density or many other factors, the properties of wood, such as stiffness and strength, differ significantly from each other.

A precise modelling of the mechanical behaviour results in a big challenge, if most of the determining factors are included. E.g., a micromechanical modelling of wood needs numerous parameters and suitable values have to be determined as input parameters for the calculations, as shown by Persson [11].

Alternative approaches exist for mechanical calculation of wood, e.g., as described by Jäger [79] or Hofstetter [80]. For an application on cross-laminated timber, Stürzenbecher and Hofstetter [81] developed a mechanical calculation approach for static analysis. For vibroacoustic analysis, the chosen mechanical model plays an important role. Furthermore, the material properties can differ a lot, depending if determined by static or dynamic analysis. The properties may become frequency dependent, as shown by Santoni et al [33].

For general mechanical calculations of wood and especially for CLT, an homogenous, linear elastic, orthotropic material model has been proven within several former studies, e.g., by Kohrmann [29] or Mecking [82]. Subsequently, such a calculation approach is presented for the use in the FEM that constitutes the base of the investigations described in this thesis.

Generally, wood is an anisotropic (orthotropic) and inhomogeneous building material. The layers of early wood and late wood can show different structures within an annual ring. Wood can be assumed as homogenous, if an adequate number of annual rings exist within the considered wooden board. In acoustics, wood can be considered as homogenous, if the wavelength is much higher than the width of the annual rings [23].

The properties of wood are strongly dependent on the anatomical directions of the tree trunk. Three general directions can be defined, as shown in following Figure 2.1. The x-axis shows the longitudinal direction towards (or parallel to) fiber. The y-axis shows the tangential direction, which is transverse to the fiber and parallel to the annual rings. The z-axis shows the radial direction, which is transverse to the fiber as well as to the annual rings.

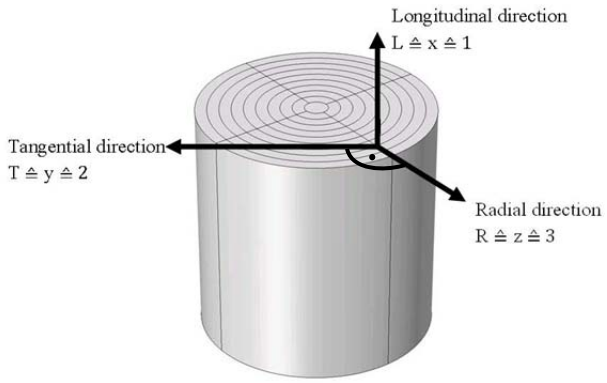

Figure 2.1: Orthogonal coordinate system of wood

A separate consideration of the directions T and R is not feasible in the field of timber engineering. For example, a CLT panel randomly consists of different types of cuts. A prediction, which type of cut has been used in a single component is nearly unfeasible. Thus, the directions T and R are summarized to the term transverse or perpendicular to the fiber. The three anatomical directions are reduced to two, depending on fiber direction (parallel or perpendicular). Based on these assumptions, the material model of timber used in panels of CLT is simplified. Table 2.3 shows a composition of typical material properties for spruce from literature. Here, static and dynamic methods have been used to determine the parameters.

Table 2.4 contains exemplarily some determined material data of CLT panels.

	Moisture content (%)	E_T/ E_L/E_R (GPa)	G_{LR}/ G_{RT}/G_{LT} (GPa)	ν_{LR} / ν_{TR} / ν_{TL} (-)	ν_{RL} / ν_{RT} / ν_{LT} (-)	Static / dynamic determination
Spruce [32]	12	0,397 / 12,8 / 0,625	0,628 / 0,053 / 0,587	0,018 / 0,48 / 0,45	0,36 / 0,21 / 0,014	Dynamic ($G_{ii'}$); others static
Spruce [83]	10	0,4 / 16,2 / 0,699	0,628 / 0,037 / 0,775	0,019 / 0,42 / 0,54	0,44 / 0,24 / 0,013	Static
Spruce [84]	12	0,43 / 11,4 / 1,11	0,742 / 0,036 / 0,686	-	-	Static
Spruce [85]	12	0,42 / 12,0 / 0,818	0,623 / 0,042 / 0,743	0,056 / 0,60 / 0,55	0,41 / 0,31 / 0,035	Static
Spruce [86]	14	0,429 / 11,3 / 0,980	-	0,049 / 0,59 / 0,56	0,45 / 0,26 / 0,028	Static

Table 2.3: Compilation of material properties of spruce [32]

	Moisture content (%)	E_T/ E_L/E_R (GPa)	G_{LR}/ G_{RT}/G_{LT} (GPa)	ν_{LR} / ν_{TR} / ν_{TL} (-)	ν_{RL} / ν_{RT} / ν_{LT} (-)	Composition
[14]	-	**0,137** / **10,981** / 0,137	**0,459** / **0,074** / 0,459	**0,05** / 0,3 / 0,05	-	
[82]	10 +/- 2	2,948 / **8,17** / **0,137**	0,168 / **0,459** / **0,103**	0,048 / **0,037** / 0,035	0,01 / 0,02 / 0,018	Floor 1
[82]	10 +/- 2	0,408 / **10,529** / **0,137** 0,137/10,981/0,137	0,168 / 0,103 / 0,459	**0,0455** / 0,037 / 0,035	0,01 / 0,02 / 0,018	Wall 2

Table 2.4: Composition of material properties for CLT

As shown in chapter 2.1.4, several damping models exist, e.g., hysteretic, Rayleigh or viscous damping. All models show different properties, as well as advantages and disadvantages, depending on their application. Energy losses from radiation or flanking transmission to adjacent components may increase the measurement values of structural loss. Therefore, a determination of the model parameters using measurement investigations is a challenging task. In most of the cases, the values are frequency dependent. Hysteretic damping is commonly used, although the damping model is not depending on frequency. E.g., Foster [87] measured spruce and determined values from about 0.015 to 0.018 within 0.4 to 70 Hz, but a

high variation occurred for different specimens. During the investigations described in this thesis, hysteretic damping has been implemented using a constant value of 0.01 for spruce [88] to allow a comprehensive investigation that is comparable with common used value ranges.

2.4 Standardized prediction methods of EN 12354 and EN ISO 10848

The standard series EN 12354 [89] represents the most common used framework to calculate the airborne and impact sound transmission between rooms. Within the framework of this prediction method, the acoustic sound transmission from one room to another is separated in several transmission paths through adjacent walls as shown in Figure 2.2

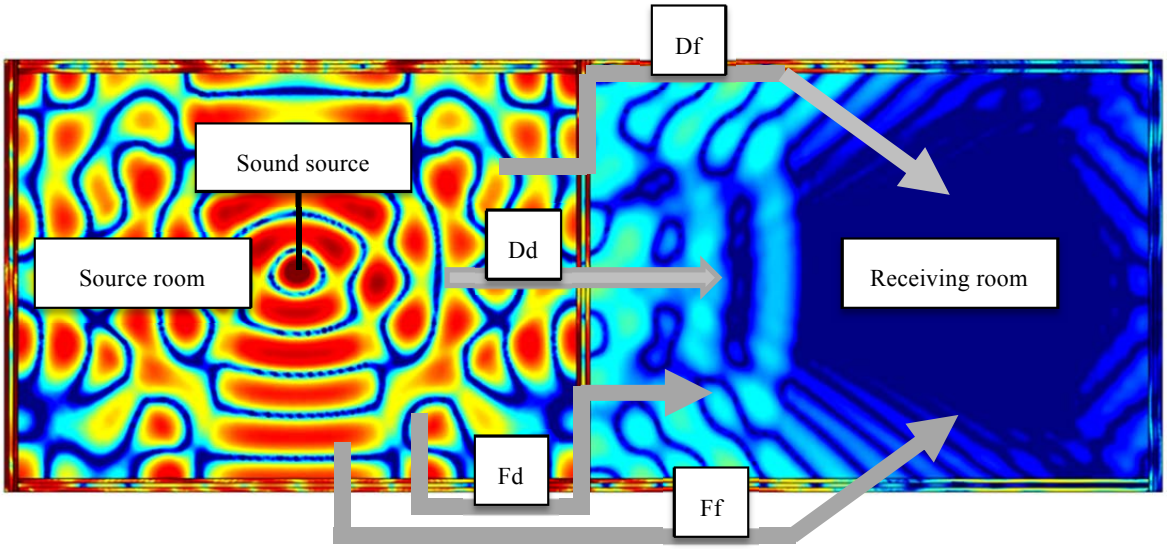

Figure 2.2: Principal numerical calculation of the sound transmission between two rooms – source room (left) and receiving room (right) – separation of the total sound transmission into single transmission paths based on the standard series EN 12354 [89]

Additional to the direct transmission (Dd), the transmission through flanking paths plays a major role (Ff, Df, Fd).

The weighted apparent sound reduction index

$$R'_w = -10\,lg\left[10^{-R_{Dd,w}/10} + \sum_{F=f=1}^{n} 10^{-R_{Ff,w}/10} + \sum_{f=1}^{n} 10^{-R_{Df,w}/10} + \sum_{F=1}^{n} 10^{-R_{Fd,w}/10}\right] \quad \text{(dB)} \quad (2.49)$$

describes the difference between the total sound energy of two adjacent rooms. $R_{Dd,W}$ represents the weighted sound reduction index for a direct transmission path and the other terms describe the weighted sound reduction index for the flanking transmission paths. Exemplarily the weighted sound reduction index for the flanking-flanking path is defined by

$$R_{Ff,w}=\frac{R_{F,w}+R_{f,w}}{2}+\Delta R_{Ff,w}+K_{Ff}+10\,lg\frac{S_S}{l_0 l_f}\ . \qquad \text{(dB)} \quad (2.50)$$

The term of the calculation that describes the acoustic behaviour of the junction, respectively the damping in the junction or the insertion loss, is the so-called “vibration reduction index”

$$K_{ij}=\frac{1}{2}\left(D_{v,ij}+D_{v,ji}\right)+10\,lg\frac{l_{ij}}{\sqrt{a_i a_j}}\ , \qquad \text{(dB)} \quad (2.51)$$

where $D_{v,ij}$ and $D_{v,ji}$ are the velocity level differences between element i and element j and vice-versa. These parameters are the determining factors for the calculation of the vibration reduction index K_{ij} and, usually, they have to be identified by experimental measurements based on the standard series EN ISO 10848 [90]. The parameters a_i and a_j represent the so-called absorption length (m) of panel *i* respectively panel *j* and are defined by the ratio of the power absorbed by the plate boundaries to the intensity incident upon them [5]

$$a_i=\frac{2.2\,\pi^2 S_i}{c_0 T_{s,i}}\sqrt{\frac{f_{ref}}{f}}=\frac{\pi^2 S_i \eta_{tot,i}}{c_0}\sqrt{f_{ref} f} \qquad \text{(dB)} \quad (2.52)$$

where f_{ref} represents a reference frequency of 1000 Hz. For every involved building component, these paths have to be separated into sub-paths. For massive constructions like concrete, the calculation can be simplified by assuming homogenous isotropic walls and rigid or supported connections of the walls. A study of literature (cf. chapter 1.2) showed that following aspects can have an influence on the vibration response of timber constructions:

- different types of vibration fields,
- coupling factor and inner damping of the different walls,
- type of acoustic waves,
- wave conversion from bending to quasi-longitudinal in the junction,
- the type, porosity and moisture of wood,
- mechanical impedance, static loads, etc.

However, many of these properties of wood reduce the precision of sound transmission calculations, as the underlying models show a limited applicability. On the one hand, this limited applicability can often lead to over-dimensioning of the buildings, which increases the building costs. On the other hand, for wooden structures, the dimensioning for critical applications, such as the requirement for increased sound insulation, especially at low frequencies is difficult. In these frequency ranges, not only the calculation methods but also the measurement methods can include a high degree of uncertainty. Recent revisions of the underlying standards have taken into account these characteristics in a more practical way. General investigations in uncertainty of the standardized prediction methods can be found, e.g., at [91, 92, 93].

The SEA [36, 37] forms the base of the EN 12354 and EN ISO 10848 prediction models. Its fundamentals have to be fulfilled in order to ensure the planning reliability of these prediction models. For massive structures, such as concrete, these criteria are satisfying fulfilled in most cases. Then calculations can be simplified by assuming homogeneous, isotropic materials and rigid connections. The dimensioning of the junction insulation can be simplified by reducing the parameters to the type of joint (branches) and the masses respectively, the associated mechanical impedances of the involved components. This assumption usually leads to a sufficient planning security.

For timber structures, several of the former mentioned aspects can have an influence on the vibration response of timber constructions and, therefore, the applicability of the standardized prediction procedures. In the following, some topics are discussed during the investigations described in this thesis.

3 PREDICTION OF THE FLANKING SOUND TRANSMISSION

In this chapter, advanced methods are developed for the calculation of flanking sound transmission of CLT panels. The focus lays on calculations of the vibration reduction index and its integration into standardized calculation methods to allow predictions of the total sound transmission between rooms. Step by step, the complexity of the investigations has been increased, starting in section 3.1 with numerical and experimental investigations on single CLT panels with clearly defined boundary conditions. Then, in section 3.2, several panels are connected to different junctions on idealized boundary conditions and special coupling methods are discussed. Finally in section 3.3, the calculation approach of the vibration reduction index is evaluated using standardized prediction methods of the total airborne sound transmission between two rooms based on the framework of the ISO 12354 [89] standard series. Each of these steps is validated using appropriate test setups in the laboratory or in-situ.

3.1 Calculation of single panels of CLT

In this chapter of the thesis, free vibrating CLT panels are investigated to decrease a potential influence of the support to the bending stiffness. In difference to the investigations discussed in the introduction of this thesis, the borads of the panels are not side glued, which can have a significant influence on its vibration behaviour. As shown by Van Damme et al. [24] the Young's modulus depends on frequency, especially, during calculations up to 1500 Hz. Here, the Young's modulus is assumed independently from frequency, but caused by the missing side gluing, a frequency dependent damping is used up to one-third octave bands of 1250 Hz

by assuming a hysteretic damping model with values that differ from the calculated one-third-octave band frequencies.

In the following, the FEM is used for numerical calculations of the vibration behaviour of several CLT panels. The geometries of the panels have been modelled using several layers of wooden boards based on a linear elastic orthotropic material model. The layers of the panels are oriented perpendicular to each other, depending on the fiber orientation. As a starting point of the investigations, material data from literature has been used for preliminary investigations. Table 4.3 contains the chosen material properties from literature, the indices 0° represent the parameters in-fiber-direction and the indices 90° represent the parameters perpendicular-to-fiber direction, as described by Kohrmann [29]. Hysteretic damping has been implemented using a constant value of 0.01 for spruce [88].

	Parameter		
	ρ	**$E_{0°}/E_{90°}$**	**$\nu_{0°/90°} - \nu_{90°/90°}$**
	(kg/m³)	**(GPa)**	**(-)**
CLT *[29]*	470	10,98 / 0,137	0,052 / 0,3

Table 3.1: Material properties of the structure

Three different CLT panels are studied, which were also used for calculations of the junctions later on in chapter 3.2. Figure 3.1 shows the geometry of the models of the panels that are named “3s wall”, “5s wall” and “5s floor” in the following chapters of his thesis, depending on their layer composition and their practical use. The corresponding sizes are shown in Table 3.2. The panels are assumed to vibrate free in all directions.

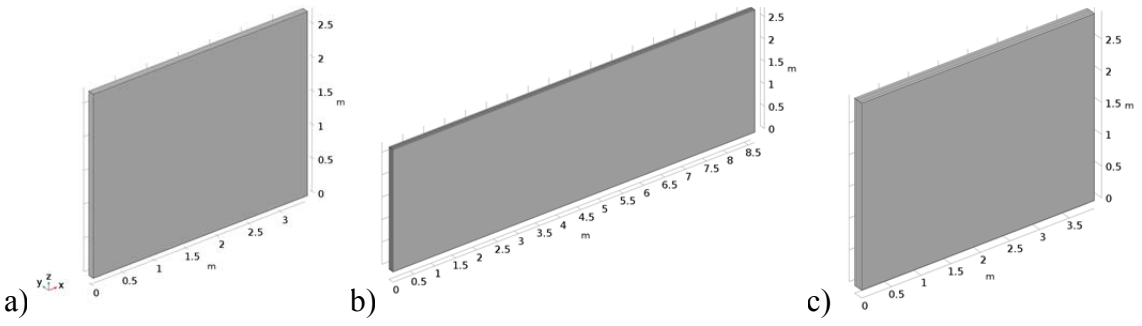

Figure 3.1: Numerical models of the single panels of cross-laminated timber –
a) 3s wall; b) 5s wall; c) 5s floor

Parameter / CLT panel	3s wall	5s wall	5s floor
Width (mm)	3400	8660	4720
Height (mm)	2730	2730	2850
Thickness (mm)	94	128	162
Layers (mm)	30/33/30	30/19/30/19/30	34/30/34/30/34
Layer – orientation (-)	transverse	transverse	longitudinal
Width of single wooden boards (mm)	160	160	160
Material	spruce	spruce	spruce

Table 3.2: Composition of the panels

3.1.1 Convergence studies and meshing strategy

A suitable meshing strategy is an essential step to allow comprehensive investigations using FEM based calculations. For this purpose, preliminary investigations have been performed to ensure a precise calculation of the vibration behaviour and furthermore, an optimized usage of the available calculation resources.

A sufficient number of elements is required for a correct sampling of the wavelength. This condition leads to an increasing number of degrees of freedom (DOF) with increasing frequency. As a consequence, a high calculation and time effort is necessary that also reduces the efficiency of the applicability of the models for scientific parametric studies. Therefore, model reductions are required, based on convergence studies. E.g., Kohrmann [29] performed studies on discretization of the geometry, respectively on the edge length of the used elements for eigenfrequencies in a low frequency range up to approximately 130 Hz. He has shown that the mean deviation of the eigenfrequencies, depending on the minimal and maximal edge length results in a value of about 1,2 %. For most of his models he has chosen a maximum length of the edges of about 0,1 m, except in the thickness direction of the single layers. In this direction a thickness of about 2 – 3 cm usually appears and the use of one element per layer is sufficient for a CLT panel.

Here, an alternative approach has been chosen to increase the efficiency of the calculations in a frequency range up to one-third-octave bands of 1250 Hz. The model of the panel “5s floor” has been chosen for convergence studies. The geometry has been discretised using tetrahedron elements and quadratic shape functions. A precise analytical solution of the eigenfrequencies of the panel was not available generally. As an alternative, the model has been calculated for

the highest number of DOF that was possible to solve using the available calculation resources. This model acts as a reference model and the aim is to reduce the DOF to a number that fulfills both requirements: a sufficiently precise calculation and a suitable calculation effort.

Figure 3.2 shows the reference model for the maximum number of 2 888 385 DOF for an eigenfrequency of 226,97 Hz exemplarily. An eigenfrequency of 227,51 Hz results, if a coarser mesh is used to obtain the same mode shape. The coloured surface shows the displacement of the model, normalized to the root-mean-squared (RMS) values of the eigenvector.

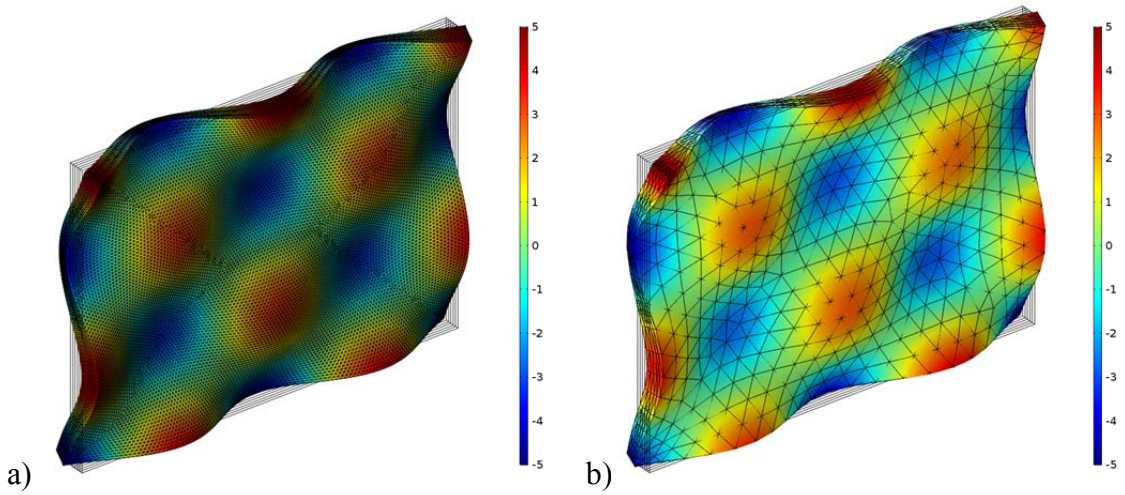

Figure 3.2: Comparison of mode shape using different mesh sizes in the one-third-octave band of 200 Hz
coloured surface: normalized displacement (-)
a) maximum element size of 0.032 m; b) maximum element size of 0.2 m

Based on this approach, the eigenfrequencies of the model have been calculated using different maximum element sizes. Table 3.3 contains the corresponding values as well as the resulting DOF. Subsequent calculations are primarily based on studies in one-third-octave bands.

To allow an efficient calculation up to 1250 Hz, the model shall be meshed for every one-third-octave band to the particular maximum element size to allow reliable calculations of the highest frequency in the single one-third-octave bands. These frequencies are the upper cut-off frequencies as described in the standard IEC 61260-1 [94]. The aim is to reduce the necessary element size especially at lower frequencies to reduce calculation effort and to

increase the applicability of the models. For this purpose, typical mode shapes near the upper cut-off frequencies of every one-third-octave band have been investigated and the mesh is adapted to the values in Table 3.3.

Maximum element size (m)	Degree of Freedom (-)
0.032	2 888 385
0.05	753 000
0.1	188 439
0.15	87 918
0.2	52 014
0.25	35 745
0.3	26 559
0.35	21 297
0.4	18 102
0.45	16 032
0.5	13 425

Table 3.3: Maximum element size of the mesh and resulting degrees of freedom

On the one hand, the convergence of the eigenfrequencies with regard to the smallest element size of 0,032 m (reference model) has been studied, as shown in Figure 3.3. The percentage of the deviations to the “overkill” solution is depicted. Using too large element sizes, a reinforcement of the elements appear that result in a higher eigenfrequency. Furthermore, certain modes can not be presented in the calculations and therefore are not taken into account. The chosen mode at the one-third octave band of 1250 Hz can only be calculated using the “overkill” solution. Coarser meshes result in an effect that may be interpreted as a reduction of the eigenfrequency of the mode, but here, the problematic possibility of an allocation of the wrong modes for coarser meshes shall be depicted.

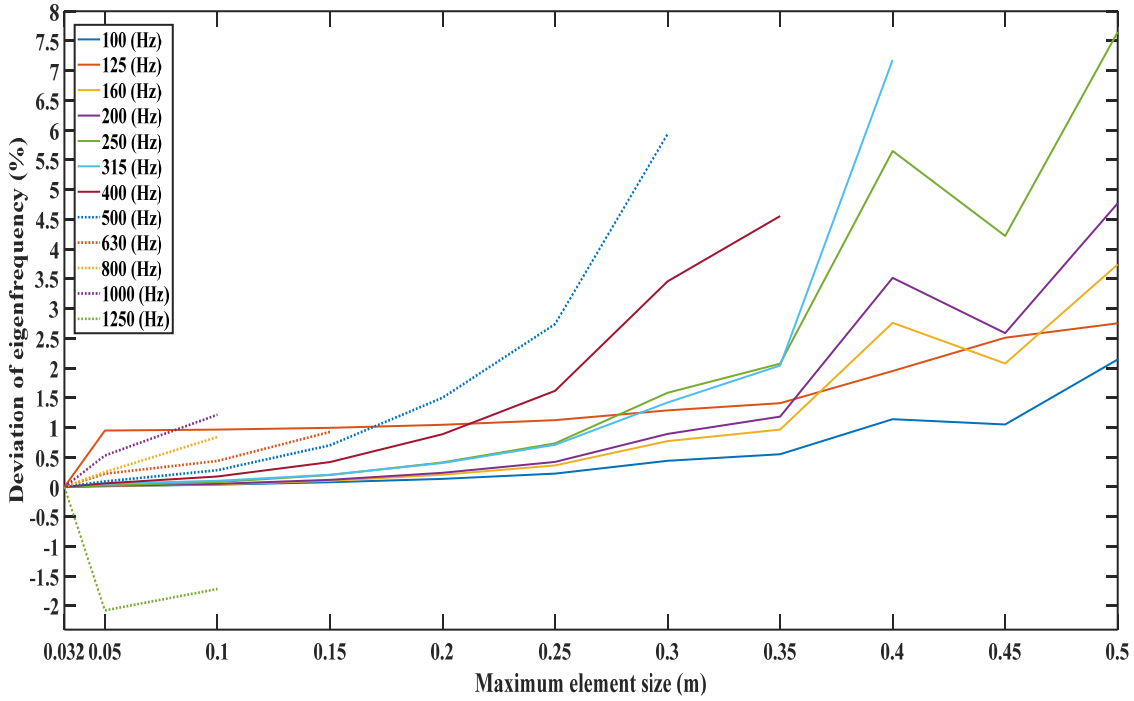

Figure 3.3: Convergence study on characteristic modes – deviation of the eigenfrequency of the observed model compared to an "overkill" model (model with a maximum element size of 0,032 m)

On the other hand, the convergence of the resulting deformation has been studied, shown in Figure 3.4. Here, the eigenvector has been normalized to its RMS values. The average of the normalized out-of-plane displacement on the front surface of the panel

$$\overline{u_{oop}^2} = \overline{\left[\frac{u_{oop}^2}{u_{oop,RMS}}\right]} \quad \text{(m)} \quad (3.1)$$

has been calculated. This quantity includes the deviation of the RMS values of the deformation as well as the spatial differences between nodes and anti-nodes for characterizing the calculated vibration using different mesh qualities. A quality criterion has been chosen that requires a relative deviation of the eigenfrequency of the observed model to the one of the precise model

$$\Delta\overline{u_{oop}^2} = \left[\frac{\overline{u_{oop,i}^2}}{u_{oop,ok}^2}\right] . \quad \text{(\%)} \quad (3.2)$$

Here, $\overline{u_{oop,ok}^2}$ represents the spatial averaged normalized out-of-plane displacement of the overkill model. Figure 3.4 shows the results of calculations of $\Delta\overline{u_{oop}^2}$ for different frequencies.

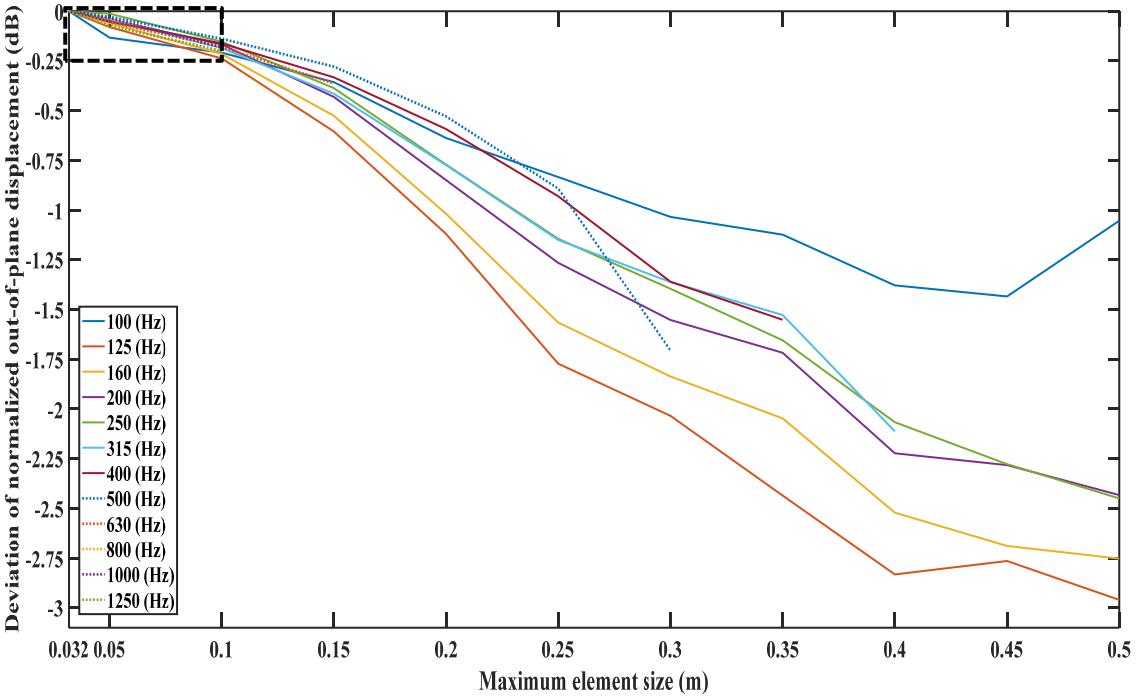

Figure 3.4: Convergence study on characteristic modes – deviation of the normalized oop-displacement compared to a model with a maximum element size of 0,032 (m)

The aim of these investigations is to reduce $\Delta\overline{u_{oop}^2}$ to a value less than 5 % or rather 0,25 dB, as shown in the dotted rectangle in Figure 3.4. Simultaneously, the relative deviation of the eigenfrequency of the observed model to the one of the "overkill" model shall be less than 2 %.

Figure 3.5 shows the resulting values for every single one-third-octave band. The chosen quality criterion holds for every eigenfrequency of the different modes. But an element length higher than 10 cm results in a significant increasing of the deviations for the normalized out-of-plane displacement (cf. Figure 3.4.). This effect may be based on the assumption that the ratio of the element edges influence the errors of the calculations additionally to the maximum element length.

One-third octave band: 1250 Hz Element size: 0,1 m Δf = -1,72 % $\Delta\overline{u^2_{oop}}$ = -4,49 % / -0,2 dB	One-third octave band: 1000 Hz Element size: 0,1 m Δf= 1,21 % $\Delta\overline{u^2_{oop}}$ = - 4,08 % /-0,18 dB	One-third octave band: 800 Hz Element size: 0,1 m Δf= 0,84 % $\Delta\overline{u^2_{oop}}$ = -4,60 % / -0,20 dB
One-third octave band: 630 Hz Element size: 0,1 m Δf= 0,44 % $\Delta\overline{u^2_{oop}}$ = -4,09 % / -0,18 dB	One-third octave band: 500 Hz Element size: 0,1 m Δf= 0,28 % $\Delta\overline{u^2_{oop}}$ = -3,13 % / -0,14 dB	One-third octave band: 400 Hz Element size: 0,1 m Δf= 0,18 % $\Delta\overline{u^2_{oop}}$ = -3,66 % / -0,16 dB
One-third octave band: 315 Hz Element size: 0,1 m Δf= 0,1 % $\Delta\overline{u^2_{oop}}$ = -4,19 % / -0,19 dB	One-third octave band: 250 Hz Element size: 0,1 m Δf= -0,08 % $\Delta\overline{u^2_{oop}}$ = -3,47 % / -0,15 dB	One-third octave band: 200 Hz Element size: 0,1 m Δf= 0,05 % $\Delta\overline{u^2_{oop}}$ = -3,79 % / -0,17 dB
One-third octave band: 160 Hz Element size: 0,1 m Δf= 0,04 % $\Delta\overline{u^2_{oop}}$ = -4,83 % / -0,22 dB	One-third octave band: 125 Hz Element size: 0,1 m Δf= 0,96 % $\Delta\overline{u^2_{oop}}$ = -5,33 % / -0,24 dB	One-third octave band: 100 Hz Element size: 0,1 m Δf= 0,04 % $\Delta\overline{u^2_{oop}}$ = -4,69 % / -0,21 dB

Figure 3.5: Chosen element size of the mesh for upper frequencies of the investigated one-third-octave bands

3.1.2 Parameter estimation

After a suitable material model has been determined, the necessary material parameters have to be identified. For this purpose, model updating procedures are common used practices that combine experimental measurements and FEM calculations. As shown in the chapter 1 and chapter 2, a usage of the linear elastic homogenous orthotropic material model results in reliable acoustic calculations of CLT panels. In difference, e.g., to the investigations of Kohrmann [29], panels without side-gluing have been examined and several CLT panels are studied simultaneously during numerical calculations.

3.1.2.1 Measurement investigations to determine reference data

Measurement investigations based on the EMA (cf. chapter 2.1.1.1) have been performed on the three CLT panels (see Figure 3.1) to determine reliable data for a model updating procedure. This measurement technique allows an identification of the modal behaviour of real constructions, and furthermore, the determination of elastic material parameters and material damping based on dynamic analyses. Additionally, it allows an analysis of specific resonance effects, which can increase the sound insulation (acoustic decoupling by using a resilient layer between several masses) or decrease of sound insulation (plate resonances or resonances of fastener systems). The frequency response functions are determined at discrete positions on several measurement paths. The measurements have been carried out for each of the mentioned panels. A composition of the spatial distribution of the transfer functions allow studies of the mode shapes, additional to an analysis of eigenfrequencies and damping ratios.

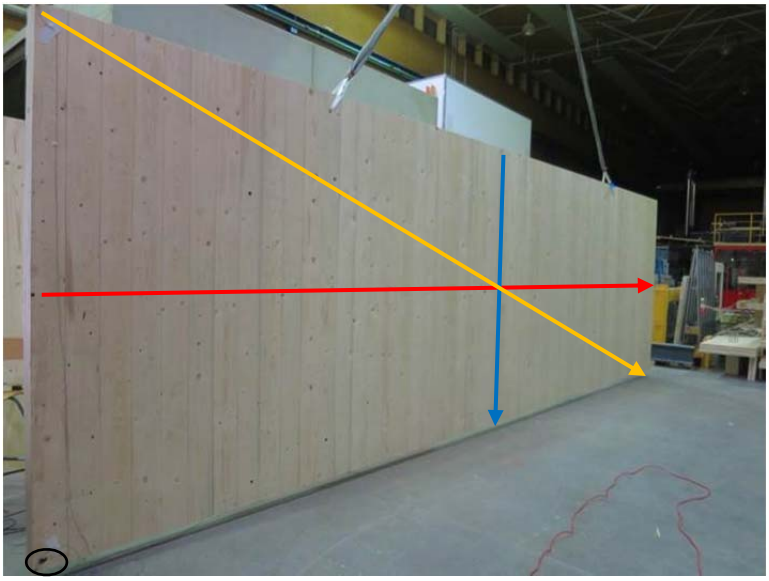

Figure 3.6: EMA on the free vibrating panel “5s wall” (width of 8.66 m) –
red: horizontal path; blue: vertical path; orange: diagonal path; black: position of the acceleration sensor

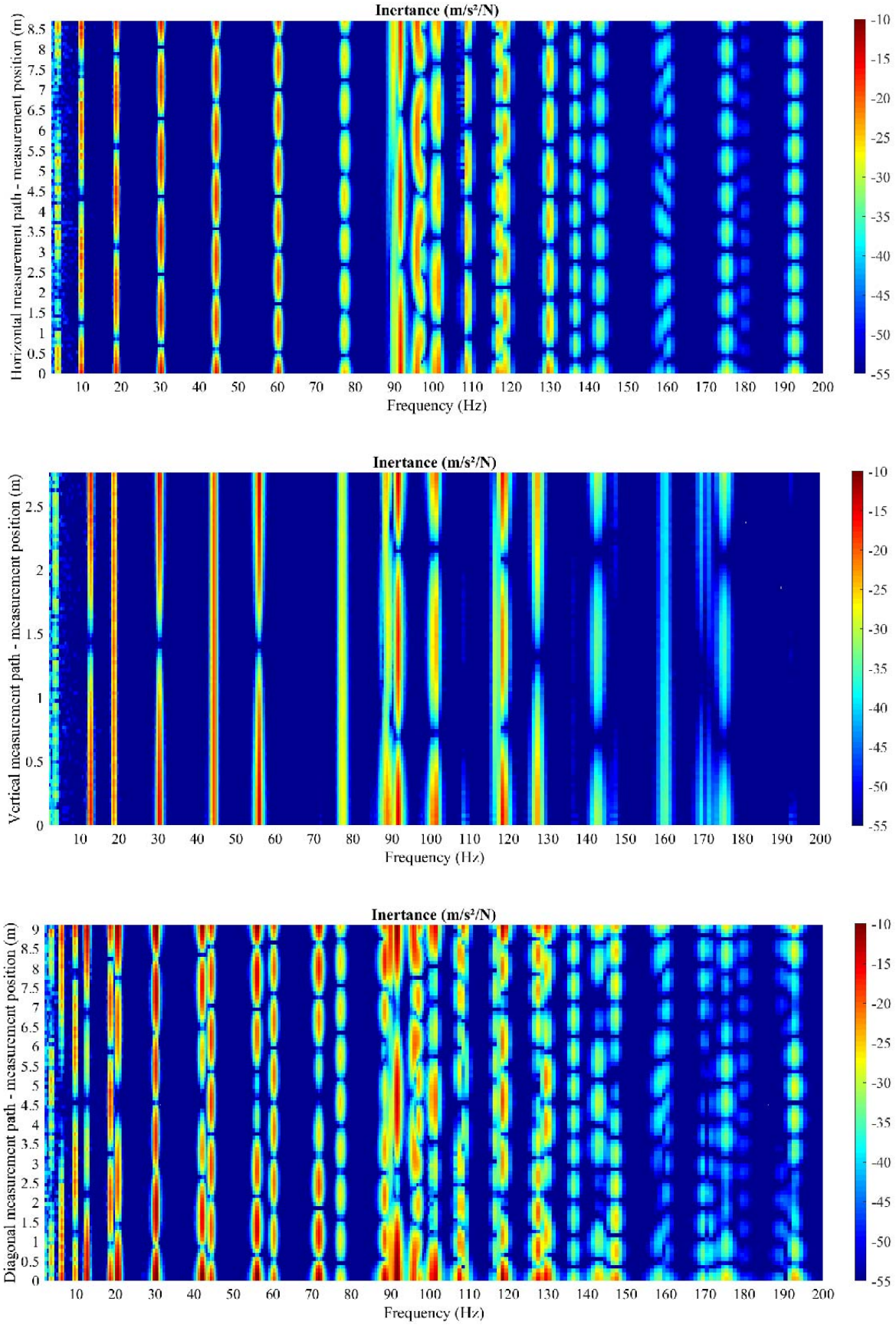

Figure 3.7: Results of the EMA - CLT panel "5s wall" – Inertance (m/s²/N) in dB re 1 m/s²/N

Figure 3.6 shows exemplarily the defined measurement paths for the specimen “5s wall”. The structure has been excited on the discrete positions using a modal hammer and the induced force has been measured. The resulting acceleration of the panel has been measured at the free vibrating edge, because here, all modes of the panel can be detected. Table 3.4 shows the chosen distances of the measurement positions for the three panels. Images and further details of the measurements on the other panels are shown in Appendix A 2 .The inertance has been calculated by using the principle of reciprocity, shown in Figure 5.7.

	3sWall			**5sWall**			**5sFloor**		
Path	horizontal	vertical	diagonal	horizontal	vertical	diagonal	horizontal	vertical	diagonal
Δx (cm)	5	5	5	8	3	10	5	5	5

Table 3.4: EMA on free vibrating panels – distance Δx of single measurement points on specified paths

3.1.2.2 Determination of suitable material parameters

The discussion of the work of, e.g., Kohrmann [29] or Paolini [28] in chapter 1.2, showed that typically, individual CLT panels have been used one by one for material parameter estimation. In difference to this procedure, simultaneous numerical calculations of several CLT panels are performed for material parameter estimations. To estimate the material parameters for the chosen material model, the mode frequencies and mode shapes have been calculated as shown in Figure 3.8 for the initial parameters of the material data shown in Table 3.5, taken from literature. The chosen material model is similar to a transversal-isotropic elastic material model (cf. [95]) with the difference that six material parameters are used instead of five material parameters.

CLT-Panel	$E_{0°}$ **(MN/m²)**	$E_{90°}$ **(MN/m²)**	$G_{0°/90°}$ **(MN/m²)**	$G_{90°/90°}$ **(MN/m²)**	$\nu_{0°/90°}$ (-)	$\nu_{90°/90°}$ (-)
Floor (5s)	10981	0,137	459	74,2	0,052	0,3

Table 3.5: Material properties based on investigations by Kohrmann [29]

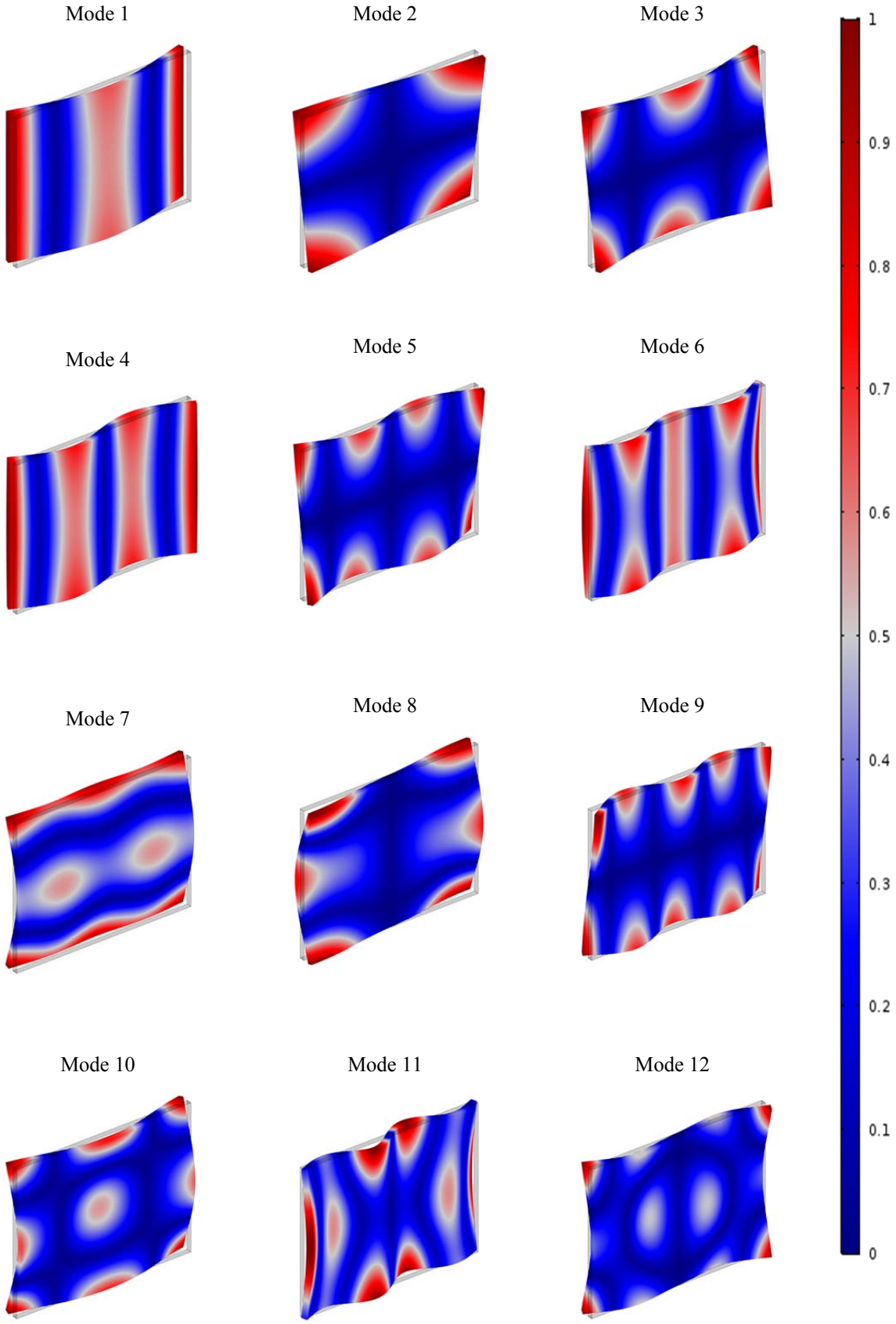

Figure 3.8: Calculation of the first ten mode shapes of the construction based on initial material parameters from (Kohrmann) - specimen: "3s wall" - coloured surface: total displacement of the panels, normalized to the maximum displacement of the single modes (-)

The eigenfrequencies of the panels are strongly dependent on elastic parameters like Young's modulus or shear modulus. A fitting of calculated and measured eigenfrequencies for the corresponding mode shapes allows a determination and validation of the consulted material parameters.

In a first step, the difference of measured and calculated eigenfrequencies

$$\Delta f = \frac{f_{m,i} - f_{s,i}}{f_{m,i}} \cdot 100 \quad (\%) \quad (3.3)$$

of comparable mode shapes is observed to allow a comparison between measured and calculated modes. Here, $f_{s,i}$ represents the calculated eigenfrequency (Hz) and $f_{m,i}$ represents the measured eigenfrequency (Hz). Similar to Greim [25] and Kohrmann [29], the RMS value of the deviation of the single eigenfrequencies

$$RMS_f = \sqrt{\frac{1}{k}\sum_{i=1}^{k}(\Delta f_i)^2} \quad (\%) \quad (3.4)$$

is obtained, where k represents the total number of the differences of measured and calculated eigenfrequencies.

In a second step, the so-called Modal Assurance Criterion (*MAC*) is used to ensure a correct calculation of the mode shapes at the specified eigenfrequencies. The fundamentals of this theory are discussed, e.g., in [96, 97, 98]. The modal assurance criterion is defined by

$$MAC(X_i, A_j) = \frac{\left|\{X_i\}^T\{A_j\}\right|^2}{\left[(\{X_i\}^T\{X_i\})\left(\{A_j\}^T\{A_j\}\right)\right]} \quad , \quad (-) \quad (3.5)$$

where i = 1,2,3,… represents the number of the experimental mode shapes, j = 1,2,3,… represents the number of the numerical mode shape, X_i represents the matrix of the correlation points from the experimental data and A_j represents the correlation points from the numerical data. *MAC* values near to 0 indicate uncorrelated modes, while *MAC* values near 1 indicate modes showing a high correlation of measurement and calculation.The EMA of the CLT panels, as described in chapter 3.1.2.1, leads to results of the eigenfrequencies and mode shapes of the panel. The results of the measurements shown in Figure 3.6 allow an interpretation of the mode shapes. Horizontal and vertical measurement path have to be interpreted with care, because they partly do not allow a full reconstruction of some mode shapes or include all mode shapes. E.g. mode 2 shown in Figure 3.8 can be only reconstructed

by the measurement results of the diagonal path. For a free vibrating plate, the diagonal measurement path includes all modes and the essential information about the mode shape that is necessary for a successful application of the *MAC*. Thus the diagonal measurement path has been used for further calculations of the *MAC*.

In a first phase of the investigations, the mode shapes (see Figure 3.8) are calculated using the initial material parameters (see Table 3.5). Table 3.8 shows the results of the calculated eigenfrequencies ($f_{s,i}$) compared to the measured eigenfrequencies ($f_{m,i}$). Most of the calculated *MAC* values gets higher than 0.7, therefore a high correlation and a correct fitting of the modes is ensured. The use of initial parameters from literature leads to high deviations for the investigated panels. The high difference in frequency of modes of higher order result in an erroneous match of the measured and calculated modes, shown in Table 3.6 by the difference in eigenfrequency. This observation is caused by the elastic material parameters of wood that show generally a high deviation. Furthermore, the fabrication of the CLT panels plays an important role, because an additional side gluing has a high influence on the resulting acoustic effective elastic parameters. As a consequence, material parameters have to be determined that correspond to the present CLT panels.

	3s wall				**5s wall**				**5s floor**			
Mode i	**$f_{m,i}$ (Hz)**	**$f_{s,i}$ (Hz)**	**MAC (-)**	**Δf_i (%)**	**$f_{m,i}$ (Hz)**	**$f_{s,i}$ (Hz)**	**MAC (-)**	**Δf_i (%)**	**$f_{m,i}$ (Hz)**	**$f_{s,i}$ (Hz)**	**MAC (-)**	**Δf_i (%)**
1	9.50	8.75	0.90	**7.9**	3.5	3.13	0.59	**10.7**	16.69	13.20	0.98	**20.0**
2	10.50	9.14	0.73	**12.9**	6.0	6.67	0.81	**-11.2**	47.56	43.45	1.00	**8.5**
3	23.00	16.70	0.99	**27.4**	9.5	8.50	0.71	**10.5**	48.69	48.49	0.87	**0.03**
4	27.00	17.94	0.97	**33.5**	12.5	10.31	0.98	**17.5**	57.06	48.95	0.88	**14.1**
5	41.50	33.15	0.90	**20.1**	18.5	16.32	0.94	**11.8**	57.06	NaN	NaN	NaN
6	52.00	NaN	NaN	**NaN**	20.5	16.97	0.98	**17.2**	89.19	NaN	NaN	**NaN**
7	66.00	NaN	NaN	**NaN**	30.0	25.04	0.94	**16.5**	116.50	NaN	NaN	**NaN**
8	71.00	NaN	NaN	**NaN**	30.0	NaN	NaN	**NaN**	119.20	NaN	NaN	**NaN**
9	79.50	NaN	NaN	**NaN**	42.0	NaN	NaN	**NaN**	121.80	NaN	NaN	**NaN**
10	86.00	NaN	NaN	**NaN**	44.0	NaN	NaN	**NaN**	125.90	NaN	NaN	**NaN**
11	93.50	NaN	NaN	**NaN**	56.0	NaN	NaN	**NaN**	147.10	NaN	NaN	**NaN**
12	99.50	NaN	NaN	**NaN**	60.0	NaN	NaN	**NaN**	150.50	NaN	NaN	**NaN**
RMS_f				**22.39**				**14.0**				**13.0**

Table 3.6: Comparison of the calculated and measured eigenfrequencies of three CLT panels - separated fitting of the of the eigenfrequencies of the single panels using initial material parameters as shown in Table 3.5

In a second phase of the investigations within this chapter, material parameters have been estimated to show its limited applicability for the present situation, using a state-of-the-art approach, e.g. shown by Kohrmann [29]. The calculated modes of each individual CLT panel have been matched to the measured modes for each single CLT panel independent from the other panels. Table 3.7 shows the best achieved solution. For the specimen "5s wall" and "5s floor", the deviation decreased compared to the solution in phase one. The specimen "3s wall" also shows a decreased deviation, except for the modes 1, 2, 9 and 10. Furthermore, mode 1 and mode 2 are reversed in frequency, which means that mode shape 1 (cf. Figure 3.8) of the measurement shows a higher frequency than mode shape 2.

	3s wall				5s wall				5s floor			
Mode i	$f_{m,i}$ **(Hz)**	$f_{s,i}$ **(Hz)**	**MAC (-)**	Δf_i **(%)**	$f_{m,i}$ **(Hz)**	$f_{s,i}$ **(Hz)**	**MAC (-)**	Δf_i **(%)**	$f_{m,i}$ **(Hz)**	$f_{s,i}$ **(Hz)**	**MAC (-)**	Δf_i **(%)**
1	9.50	10.56	0.90	**-11.2**	3.5	3.51	0.59	**-0.4**	16.5	16.65	1.00	**-0.9**
2	10.50	9.68	0.99	**7.8**	6.0	5.94	0.88	**1.0**	47.5	46.35	1.00	**2.4**
3	23.00	22.40	1.00	**2.6**	9.5	9.59	0.77	**-1.0**	48.5	48.63	1.00	**-0.3**
4	27.00	29.00	0.97	**-7.4**	12.5	12.56	0.99	**-0.5**	57.0	57.58	1.00	**-1.0**
5	41.50	41.39	1.00	**0.3**	18.5	18.55	0.98	**-0.3**	89.0	89.41	1.00	**-0.5**
6	52.00	55.84	0.54	**-7.4**	20.5	20.48	1.00	**0.1**	116.5	114.4	0.89	**1.3**
7	66.00	61.53	0.97	**6.8**	30.0	30.10	0.7	**-0.3**	119.5	119.3	0.87	**0.2**
8	71.00	68.49	1.00	**3.5**	30.0	30.15	0.96	**-0.5**	122.0	122.0	1.00	**0.0**
9	79.50	68.49	1.00	**13.8**	42.0	41.83	1.00	**0.4**	126.5	126.3	1.00	**0.2**
10	86.00	73.51	0.50	**14.5**	44.0	43.96	0.98	**0.1**	147.5	148.2	1.00	**-0.5**
11	93.50	94.26	0.97	**-0.8**	56.0	55.57	1.00	**0.8**	151.5	150.1	0.99	**0.9**
12	99.50	104.0	0.99	**-4.5**	60.0	59.82	0.98	**0.3**	197.5	197.5	0.99	**0.0**
RMS_f				**8.1**				**0.6**				**1.0**

Table 3.7: Comparison of the calculated and measured eigenfrequencies of three CLT panels - separated fitting of the of the eigenfrequencies of the single panels using material parameters as shown in Table 3.8

CLT-Panel	$E_{0°}$ **(MN/m²)**	$E_{90°}$ **(MN/m²)**	$G_{0°/90°}$ **(MN/m²)**	$G_{90°/90°}$ **(MN/m²)**	$\nu_{0°/90°}$ **(-)**	$\nu_{90°/90°}$ **(-)**
3s wall	10 037.72	280.00	398.40	581.40	0.06	0.09
5s floor	12 793.10	246.99	637.42	116.77	0.06	0.42
5s wall	11 483.00	376.00	581.00	84.70	0.05	0.14
AVG	**11 437.94**	**301.00**	**538.94**	**260.96**	**0.05**	**0.22**

Table 3.8: Determined elastic material properties based on fittings of eigenfrequencies of single CLT panels - separated fitting of the of the eigenfrequencies

Table 3.8 shows the resulting material parameters for the separated fitting of measured and calculated modes. The specimens “5s wall” and “5s floor” show comparable values that differ in an expected range for a timber based structure. The specimen „3s wall“ shows lower values of the elastic parameters, especially for the Young’s modulus. This effect is caused by the missing side-gluing of the wooden boards of the layers that result in a reduced stiffness especially at the topping layers. The specimen “3s wall” shows a reduction of Young’s modulus in fiber direction of about 22 % compared to the specimen “5s floor” and about 13 % compared to the specimen “5s wall”. Figure 3.9 shows the cross-section (upper view) of the specimen “3s wall”. Small gaps are evident caused by the shrinkage of the wooden boards. The single boards do not get full contact in horizontal direction. The bending stiffness decreases especially for low frequencies, and the influence of the gaps increases for higher frequencies.

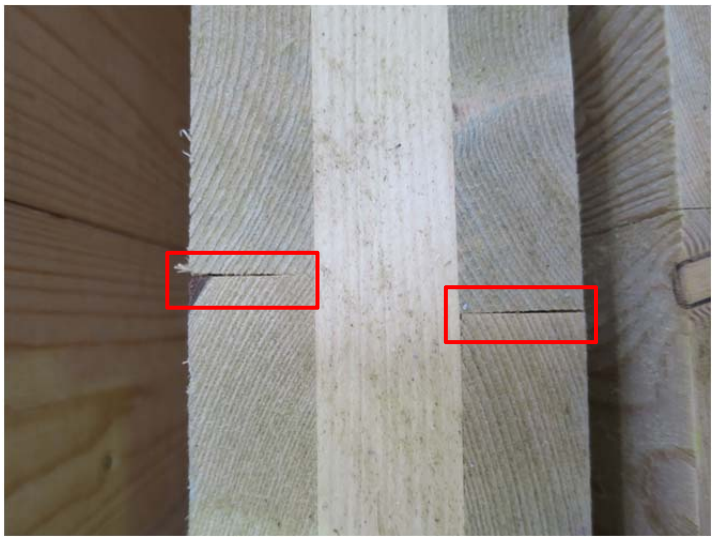

Figure 3.9: Single CLT 3s wall – gaps caused by shrinkage of the topping layers

In a third phase, the estimated material parameters of the individual CLT panels during phase two have been averaged. Calculations of the mode shapes have been compared to the measured values. The aim of these investigations is to show the influence of this effect of reduced bending stiffness caused by gaps to the usage of averaged material parameters. Table 3.9 shows the results of these investigations. In general, the deviation of the fitting increases for every panel. Therefore, the usage of averaged values does not lead to satisfying results. As mentioned by Kohrmann [14], the determined parameters should hold for every CLT. For this purpose, the fitting of the eigenfrequencies has been performed for all three different CLT panels simultaneously to get overall valid parameters.

	3s wall				5s wall				5s floor			
Mode i	**$f_{m,i}$ (Hz)**	**$f_{s,i}$ (Hz)**	**MAC (-)**	**Δf_i (%)**	**$f_{m,i}$ (Hz)**	**$f_{s,i}$ (Hz)**	**MAC (-)**	**Δf_i (%)**	**$f_{m,i}$ (Hz)**	**$f_{s,i}$ (Hz)**	**MAC (-)**	**Δf_i (%)**
1	9.50	11.09	0.90	**-16.7**	3.5	3.45	0.59	**1.3**	16.5	15.58	1.00	**5.5**
2	10.50	11.15	0.99	**-6.2**	6.0	5.81	0.88	**3.2**	47.5	43.89	1.00	**7.6**
3	23.00	25.24	1.00	**-9.8**	9.5	9.49	0.76	**0.1**	48.5	47.06	1.00	**3.0**
4	27.00	30.47	0.97	**-12.9**	12.5	12.33	0.99	**1.3**	57.0	55.71	0.97	**2.3**
5	41.50	45.48	1.00	**-9.6**	18.5	18.49	0.98	**0.0**	89.0	86.93	1.00	**2.3**
6	52.00	58.84	0.50	**-13.2**	20.5	20.23	1.00	**1.3**	116.5	114.34	0.54	**1.9**
7	66.00	73.95	0.97	**-12.0**	30.0	30.04	0.96	**-0.1**	119.5	121.26	0.97	**-1.5**
8	71.00	67.32	1.00	**5.2**	30.0	30.34	0.70	**-1.1**	122.0	121.51	1.00	**0.4**
9	79.50	78.79	1.00	**0.9**	42.0	42.12	1.00	**-0.3**	126.5	128.12	1.00	**-1.3**
10	86.00	99.59	0.43	**-15.8**	44.0	44.90	0.97	**-2.0**	147.5	148.25	1.00	**-0.5**
11	93.50	95.98	0.57	**-2.7**	56.0	56.64	0.99	**-1.1**	151.5	152.11	0.99	**-0.4**
12	99.50	111.2	0.99	**-11.8**	60.0	61.98	0.97	**-3.3**	197.5	202.07	0.99	**-2.3**
RMS_f				**10.8**				**1.7**				**3.2**

Table 3.9: Comparison of the calculated and measured eigenfrequencies of three CLT panels - separated calculation of the of the eigenfrequencies of the single panels using the same averaged material parameters as shown in Table 3.8

In phase four of the investigations, the material parameters have been determined by a simultaneous fitting of the calculated and measured modes of all three CLT panels. The results are shown in Table 3.9, Table 3.10 shows the final values of the estimated elastic parameters for the non-side glued CLT panels. For all single modes, the deviation has been reduced to values lower than 10 % and for all panels, the RMS values have been reduced to values lower than 6 %. These results indicate a good fitting and a high reliability of the estimated vales.

$E_{0°}$ (MN/m²)	$E_{90°}$ (MN/m²)	$G_{0°/90°}$ (MN/m²)	$G_{90°/90°}$ (MN/m²)	$\nu_{0°/90°}$ (-)	$\nu_{90°/90°}$ (-)
12192.49	138.78	543.55	123.13	0,05	0,16

Table 3.10: Determined elastic material properties based on fittings of eigenfrequencies of single CLT panels - simultaneous calculation of the of the eigenfrequencies

	3s wall				**5s wall**				**5s floor**			
Mode i	$f_{m,i}$ (Hz)	$f_{s,i}$ (Hz)	MAC (-)	**Δf_i (%)**	$f_{m,i}$ (Hz)	$f_{s,i}$ (Hz)	MAC (-)	Δf_i (%)	$f_{m,i}$ (Hz)	$f_{s,i}$ (Hz)	MAC (-)	Δf_i (%)
1	9.50	10.27	0.90	**-8.1**	3.5	3.42	0.59	**2.4**	16.50	15.47	1.00	**6.2**
2	10.50	11.11	0.99	**-5.8**	6.0	5.78	0.88	**3.6**	47.50	46.18	1.00	**2.8**
3	23.00	24.76	1.00	**-7.6**	9.5	9.35	0.77	**1.6**	48.50	47.61	1.00	**1.8**
4	27.00	28.23	0.97	**-4.5**	12.5	12.25	0.99	**2.0**	57.00	55.60	1.00	**2.5**
5	41.50	43.76	1.00	**-5.4**	18.5	18.14	0.98	**2.0**	89.00	86.32	1.00	**3.0**
6	52.00	54.85	0.86	**-5.5**	20.5	20.02	1.00	**2.3**	116.50	114.75	0.90	**1.5**
7	66.00	69.15	0.68	**-4.8**	30.0	29.56	0.70	**1.5**	119.50	117.31	0.87	**1.8**
8	71.00	71.49	1.00	**-0.7**	30.0	29.58	0.96	**1.4**	122.00	120.84	1.00	**1.0**
9	79.50	81.89	1.00	**-3.0**	42.0	41.21	1.00	**1.9**	126.50	123.74	1.00	**2.2**
10	86.00	90.70	0.88	**-5.5**	44.0	43.39	0.97	**1.4**	147.50	145.11	1.00	**1.6**
11	93.50	99.15	0.99	**-6.0**	56.0	54.99	1.00	**1.8**	151.50	146.07	0.99	**3.6**
12	99.50	104.57	0.99	**-5.1**	60.0	59.38	0.98	**1.0**	197.50	192.86	0.99	**2.4**
RMS_f				**5.5**				**2.1**				**2.8**

Table 3.11: Comparison of the calculated and measured eigenfrequencies of three CLT panels - simultaneous calculation of the eigenfrequencies of the panels using material parameters as shown in Table 3.10

It has to be mentioned that different studies of the convergence behaviour of the fitting of calculated and measured modes showed a tendency that for the first modes of the panels, the Young's moduli are the determining factors to match the eigenfrequencies. For higher modes, the investigations showed a tendency that the shear modulus is the determining factor for fitting of the eigenfrequencies. The Poisson's ratio shows a low influence to the eigenfrequency, compared to the other elastic parameters. Therefore, it can be set to a fixed comprehensible value. This is an important finding, because a parameter fitting of calculated and measured eigenfrequencies the number of the variation parameters has to be set to a minimum with respect to the most influencing parameters. Otherwise, a correct fitting is not possible or the duration of calculation procedure may increase significantly. These aspects should be considered in future investigations, e.g. to increase the efficiency of the fitting algorithms where the specific variation values are specially addressed to the corresponding effects respectively to modes of low or high frequency. In this case, also the simultaneous calculation of a high number of panels could be possible.

3.1.2.3 Determination of a suitable damping model

Numerical calculations of the acoustic behaviour of structures require a correct consideration of the underlying damping mechanism [75]. E.g. Kohrmann [29] used Rayleigh damping for his investigations in CLT panels. The panels show side gluing that leads to mechanical fully connected layers and the panels can be approximated by continuous plates.

In this thesis, CLT panels that are not glued on the side of the single boards are investigated. As shown in Table 3.8, this missing side-gluing has an influence on the material properties especially of the panel "3s wall", because gaps reduce the bending stiffness of the 3-plyed panel significantly. The gaps add a damping effect that is included in the measured total loss factor. Furthermore, an effect of damping on propagating waves is expected at higher frequencies, where the wavelength is lower than the size of the gap. In this case, the gap acts as a discontinuity and effects like reflection or diffraction can increase the total damping.

Caused by these reasons, Rayleigh damping seems not to be a suitable damping model for non-side glued CLT panels, but rather a frequency dependent isotropic total loss factor [69]

$$\eta_{ges} = \frac{2{,}2}{f T_s} \quad (-) \qquad (3.6)$$

has been used that is calculated depending on the frequency f (Hz) and the (measured) structure-borne reverberation time T_S (s).

This total loss factor includes all damping mechanisms as shown in Table 2.1. The measurement has been performed on single panels that are suspended supported. Therefore, flanking transmission to coupled structures is suppressed as well as joint damping. The dominating damping mechanisms are material damping with a range of about 10^{-4} (-) and radiation losses with a range of about 10^{-5} to 10^{-8} (-), which are included in the total loss factor, as well as further damping losses, e.g., caused by the gaps between and within the wooden boards.

Figure 3.10 shows the resulting total loss factor for the two panels 3s wall and 5s floor, as well as their averaged value. The corresponding structure-borne reverberation times can be found in appendix A in Figure 5.9.

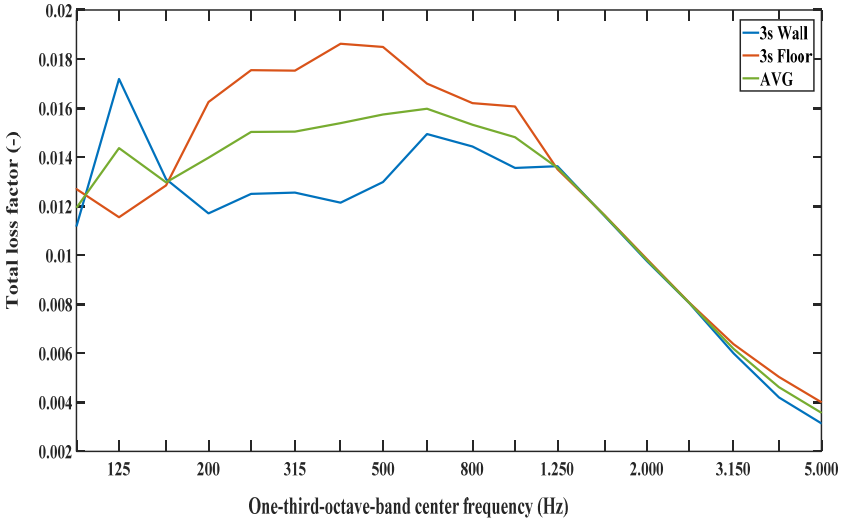

Figure 3.10: Total loss factor of different panels and their averaged values

The total loss factor is used for further calculations of connected panels of CLT by an approximation during the use of hysteretic, isotropic damping. Within each single one-third octave band, different values are used for the hysteretic, isotropic damping model according to the measured values of the total loss factor.

3.2 Coupling of several CLT panels

Versatile composition possibilities of CLT panels (e.g. quality of timber, thickness and number of layers, direction of the topping layer, difference in geometric dimensions, ...) combined with the numerous types of fastener systems result in a nearly innumerable number of possible designs of junction in timber engineering. The use of numerical calculations can reduce the high measurement efforts for the development of innovative constructions. Nevertheless, highly detailed calculation models lead to impracticable calculation times by using the FEM. Therefore, simplifications of the models have to be introduced to allow a use of the final calculation approaches, e.g., for sensitivity studies during an optimization process, where a lot of different variations of an initial situation have to be calculated.

The investigations described in this chapter focus on numerical studies of two test setups that are typical for a practical use. First, a T-shaped junction based on two flanking walls and a separation wall is investigated, the latter is formed by two independent CLT panels. For this situation, the CLT panels are connected using typical timber screws. A second situation is based on the same T-shaped junction, though using angle brackets and one single screw (this

acts more as a mounting aid) to connect the panels. Both situations are integrated in prediction calculations of the total sound insulation on a real building example, as described subsequently in chapter 3.3.

3.2.1 Measurement investigations to determine reference data

Measurement investigations based on the standardized methods of EN ISO 10848 (details see chapter 2.4) have been performed on the test setup of a T-shaped junction of CLT panels to determine reliable data for a model updating procedure. Figure 3.11 shows the test setup without panel 4. Figure 3.12 shows the details of the final junction. The separation wall is formed by CLT panels 3 and 4. The cavity with a depth of 6 cm is filled with mineral wool with a thickness of 5 cm to avoid contact between the CLT panels. Table 3.12 contains the sizes and the layer compositions of the used CLT-panels.

Figure 3.11: Test setup for measurements on a T-shaped mock-up without wall 4

Parameter (unit)	Wall 1	Wall 2	Wall 3	Wall 4
Width (mm)	4600	3700	4200	4200
Height (mm)	2720	2720	2720	2720
Layers (mm)	30/19/30/19/30	30/19/30/19/30	30/33/30	30/33/30
Layer – direction (-)	vertical	vertical	vertical	vertical

Table 3.12: Size of the mock-up for measurements on T-shaped junctions of CLT panels

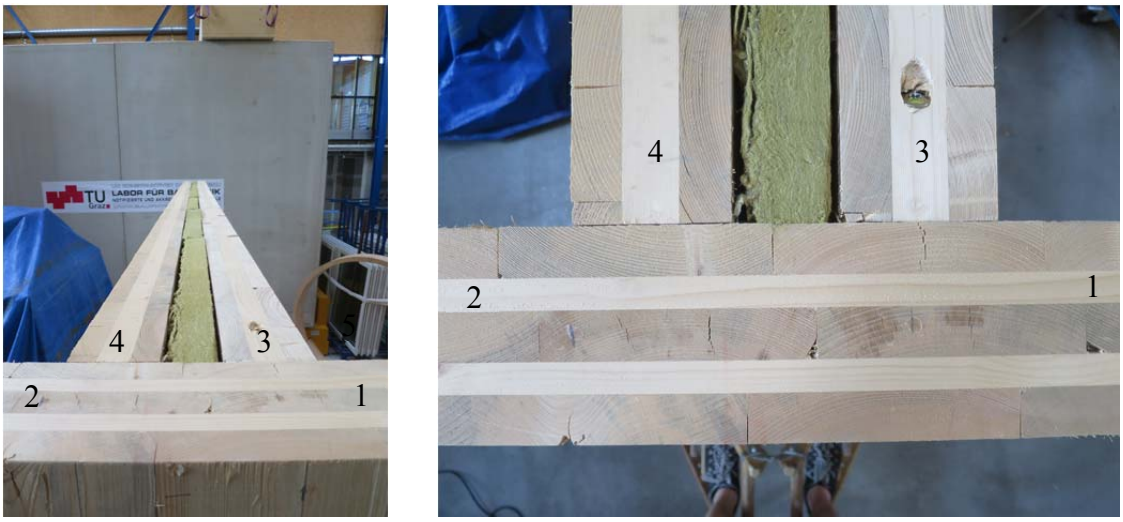

Figure 3.12: Junction of the test setup including wall 4 and mineral wool – designation of the different panels

The panels have been connected using different fastener systems. For the first situation, screws for typical use in timber engineering have been used with a distance of 34 cm between the single screws. For the second situation, two angle brackets have been used. The specifications of the fastener systems are listed in Table 3.13.

a) b)

Figure 3.13: Different fastener systems of the used junctions –
a) connection using 6 screws; b) connection using 2 angel brackets

Fastener System	Screws	Angle brackets	Screws (for angle brackets)
Producer	Würth Handelsges.m.b.H.	Würth Handelsges.m.b.H.	Würth Handelsges.m.b.H.
Type	Article number: 0176808220 080x220/100 wheel head Dm 20 mm, TX 40 yellow, galvanised partial thread	Article number: 5390201105961 105X105X90X3,0 Type A, including bridge steel, galvanised	Article number: 018421080 10X80/50 hexagon screw AW 40 steel, A2K partial thread
Width (mm)	-	90	-
Length (mm)	220	105	80
Thickness (mm)	8	3	10

Table 3.13: Specifications of the used fastener systems

Measurements of the vibration velocities have been performed on the interior surfaces of the panels, normal to the surfaces. More than 30 measurement positions and three excitation points have been defined for each panel to minimize uncertainties, because of the standard deviation of the measurement procedure. A list of the used measurement equipment can be found in the Appendix in Table 5.1. Further details of the test setup and measurements are shown in Appendix A 3 . Figure 3.14 shows the graphs of the determined vibration reduction indices (cf. chapter 2.4).

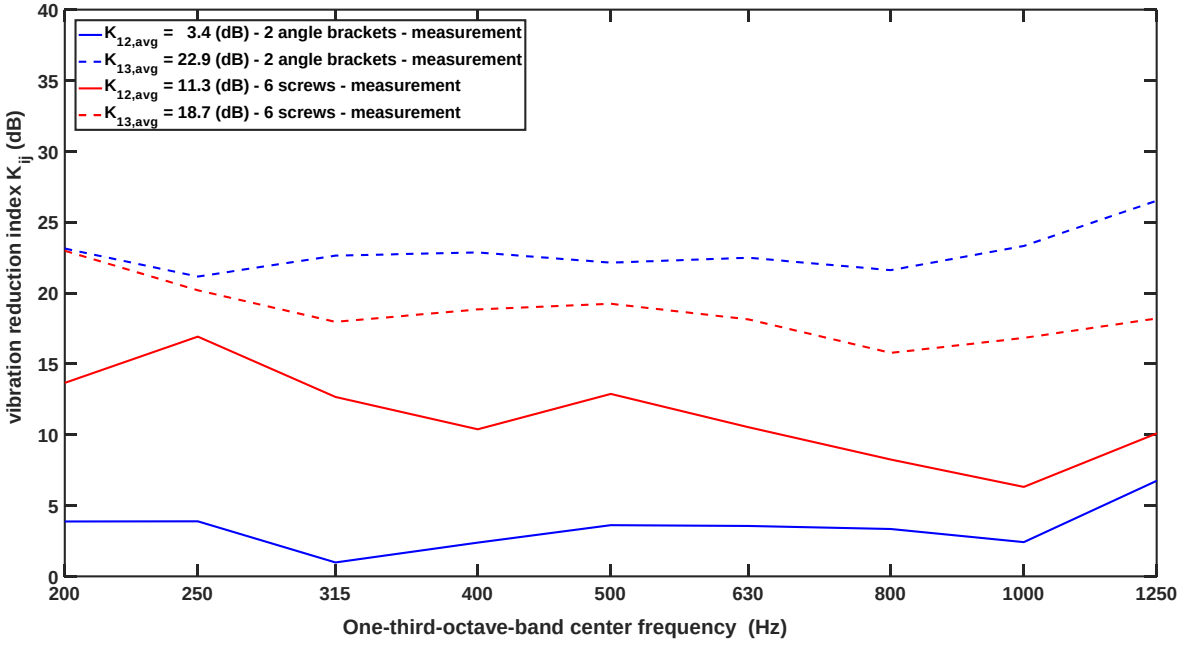

Figure 3.14: Results of the measurement investigations - vibration reduction index for the different situations

As expected, the vibration reduction index of the flanking-flanking path ($K_{12,avg}$) shows very low values caused by the continuous flanking panel, especially, for the situation using the two angle brackets.

3.2.2 Numerical calculations and validation of coupling several CLT panels

The high number of variations of junctions can be reduced and approximated by the definition of acoustic coupling stiffness and a coupling damping. Current approaches for coupling of CLT panels have been discussed during the introduction in chapter 1.2. E.g. in [99] the authors used an isotropic connection stiffness for the coupling of an L-shaped junction of CLT. Using a parameter fitting, they got an Elastic modulus of 5,94 (N/mm²) for the connection, depending on an EMA of the construction.

In difference to their work, here a frequency dependent coupling stiffness has been assumed for coupling of the blunt joint of the panels. Furthermore, the used fastener systems have been implemented in a practical way. During the investigations it is assumed that the total sound transmission in a junction of coupled CLT panels can be separated into two main transmission paths:

- On the one hand, a sound transmission occurs, based on the coupling stiffness and the contact pressure at the contact area (blunt joint) of the two panels.

- On the other hand, a sound transmission occurs, based on the rigid connection caused by the fastener systems (see chapter 3.2.3 and chapter 3.2.4).

Based on these assumptions, a numerical model of the mock-up in the laboratory, as described in chapter 3.2.1, has been developed. Following Figure 3.15 shows the resulting model. The CLT panels have been implemented using the material models and parameters, determined on investigations on single CLT panels shown in chapter 3.1.2. The panels have been excited using a harmonic force of 100 N perpendicular to the surface. The standard requires a minimum of three excitation points on each panel with a distance of 1 m to each other. As a consequence, the numerical models have been solved 9 times for each single frequency that would lead to a high calculation effort. To reduce this calculation effort, the model could be solved one time using a rain-on-the-roof excitation for a set of three simultaneous excitation points per wall.

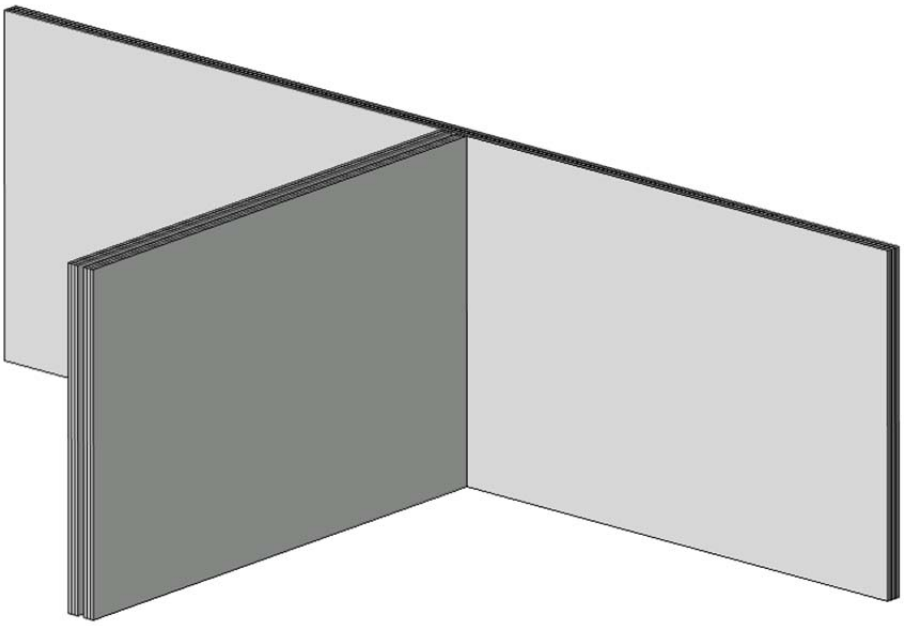

Figure 3.15: Numerical model based on the FEM for a T-shaped junction

Using this approach, errors are expected for the evaluation of spatial averaged values for the vibration response on the excited walls caused by the small remaining area on the surface of the walls. Therefore, in difference to the specifications of the standard, the excitations points have been chosen in the free vibrating corners of the panels on the opposite side of the panels, as shown in Figure 3.16. This procedure additionally significantly reduces the overall calculation resources.

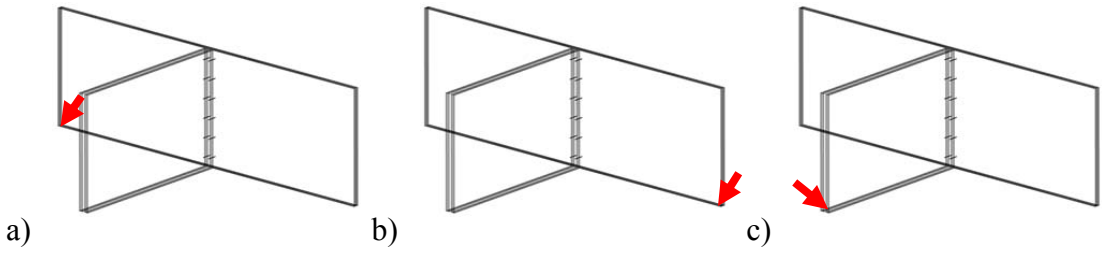

Figure 3.16: Excitation of the CLT panels perpendicular to their surfaces – a) wall 1; b) wall 2; c) wall 3

The velocity on the surface of the panels has been evaluated in the distance of 0.5 m from the boundaries and in the distance of a minimum of 1 m from the excitation points, as defined in the standard EN ISO 10848 and shown in Figure 3.17.

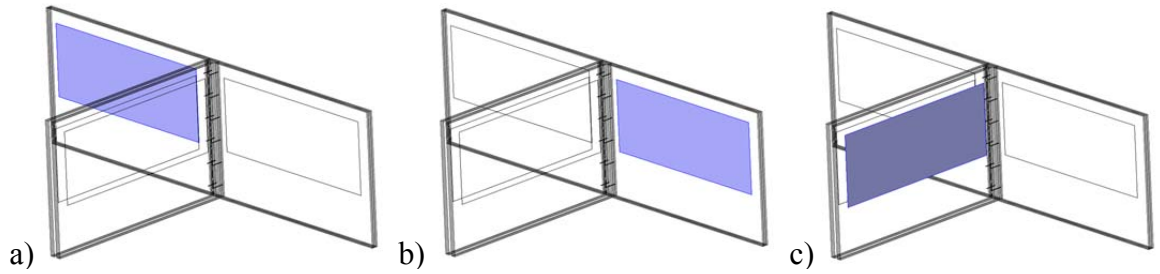

Figure 3.17: Area for averaging of velocity components – a) wall 1; b) wall 2; c) wall 3

The first main transmission path, based on the blunt joint of the CLT panels, is controlled by a frequency dependent coupling stiffness in the contact area, as shown in Figure 3.18 (blue area). This coupling stiffness is described by isotropic springs in every node point of the coupling area. The springs are defined by a frequency dependent spring constant per unit area k_A (N/m/m²).

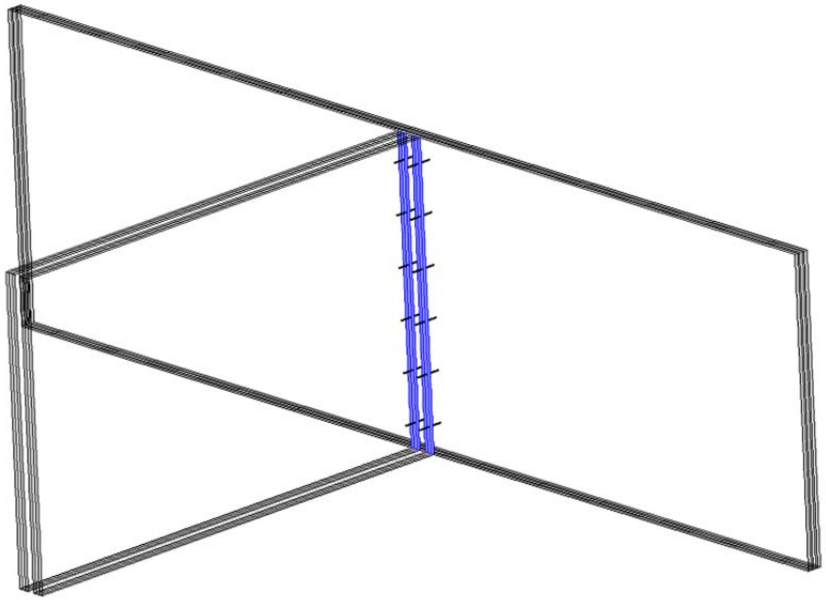

Figure 3.18: Coupling area of the CLT panels (blue) – isotropic coupling stiffness defined by springs in every node point of the area

The second transmission path is defined by the used fastener system. In the following, screws and angle brackets made of steel are investigated. This path is not controlled by a parameter, because of the rigid connection between steel and timber. A linear elastic, isotropic material model including hysteretic damping has been chosen for the steel parts, using parameters as shown in Table 3.14. Further details for the implementation are described in chapter 3.2.3 and chapter 3.2.4.

Parameter			
ρ	**E◦**	**ν◦**	**η**
(kg/m³)	**(GPa)**	**(-)**	**(-)**
7850 [100]	200 [100]	0.3 [100]	10^{-4} [88].

Table 3.14: Material properties of the structure

The model has been solved for every frequency and every excitation point. 10 frequencies were solved for every one-third-octave bands within a range of 200 Hz to 1250 Hz. The estimation procedure of the vibration reduction indices using numerical calculations is discussed in the following.

3.2.2.1 Calculation procedure of the vibration reduction index

As shown in chapter 2.4, the vibration reduction index is calculated by

$$K_{ij} = \frac{1}{2}\left(D_{v,ij} + D_{v,ji}\right) + 10\,lg\,\frac{l_{ij}}{\sqrt{a_i a_j}}\ , \tag{3.7}$$

where $D_{v,ij}$ and $D_{v,ji}$ are the velocity level differences between element i and element j and vice-versa (dB), l_{ij} is the length of the junction (m) and a_i and a_j are the equivalent absorption lengths of the junction.

The equivalent absorption length

$$a_i = \frac{2.2\,\pi^2 S_i}{c_0 T_{s,i}}\sqrt{\frac{f_{ref}}{f}} = \frac{\pi^2 S_i \eta_{tot,i}}{c_0}\sqrt{f_{ref} f}\ , \tag{3.8}$$

is defined by the ratio of the power absorbed by the panel boundaries, to the intensity incident upon them [5], where S_i represents the area of the panel (m²), $\eta_{tot,i}$ represents the total loss factor (-), c_0 represents the speed of sound in air (m/s), f represents the current frequency (Hz) and f_{ref} represents a reference frequency of 1000 (Hz).

Here, the total loss factor $\eta_{tot,i}$ includes the losses of all effects of Table 2.1 that are considered in the FEM model. As discussed within chapter 2.1.4, several dissipation mechanisms can occur. In chapter 3.1, the measured total loss factor for a single, free vibrating panel has been discussed that includes material damping and radiation losses but excludes a structure-borne sound transmission to adjacent CLT panels because of the missing

coupling. By coupling several CLT panels, e.g., to T-shaped mockups, transmission losses have to be considered in the calculation procedures. For the current model of a T-shaped junction, the total loss factor

$$\eta_{tot,i} = \eta_{int} + \eta_{trans} \tag{3.9}$$

results from internal losses η_{int} and losses caused by flanking transmission η_{trans}. Radiation losses do not appear because no coupling of the structure to a surrounding fluid like air is implemented.

As shown by Hopkins [5], the power absorbed by the plate boundaries is defined by

$$W_{abs} = \omega\eta_{tot,i}E = \omega\frac{2{,}2}{fT_{s,i}}E \quad , \tag{3.10}$$

where $\eta_{tot,i}$ is the total loss factor (-), E is the plate energy (J), $T_{s,i}$ represents the structure-borne reverberation time of panel i (s) and ω represents the angular frequency (Hz).

Richter et.al [101] investigated several measurement methods for structural damping using different approaches. Measurements of the structure-borne reverberation time are a suitable way to experimentally determine the damping. But for numerical calculations this seems not to be applicable, because then expensive time dependent calculations have to be performed. As an alternative, a modification of the so-called power injection method (PIM) has been used to estimate the loss factors. In [102] a similar method for a use for calculations of CLT panels by applying a hybrid FEM/SEA approach is shown.

In general, the coupling loss factor is defined by

$$\eta_{ij} = \frac{E_j}{E_i}\eta_{int,j} \quad , \tag{3.11}$$

where E respresents the energies of panel i and the connected panel j (J) and $\eta_{int,j}$ represents the internal loss factor of the connected panel j.

Assuming the power absorbed by the boundary is equivalent to the total dissipation energy of the receiving structure, the total loss factor is calculated by combining and transforming equation (3.9) and (3.10) to

$$\eta_{tot,i} = \eta_{int,i} + \eta_{trans,i} = \frac{W_{abs,i}}{\omega E_i} = \frac{W_{diss,i}}{\omega(E_{kin,i} + E_{pot,i})} + \frac{W_{diss,j} + \sum W_{diss,k}}{\omega(E_{kin,i} + E_{pot,i})} \quad , \tag{3.12}$$

where $W_{diss,i}$ represents the dissipated energy in the excited panel i, $W_{diss,j}$ respresents the dissipated energy in the junction j, $\sum W_{diss,k}$ represents the sum of the dissipated energies in all connected panels for k = 1,2,…, $E_{kin,i}$ represents the kinetik energy of the excited panel i and $E_{pot,i}$ represents the potential energy of the excited panel i. Here, the ratio of the dissipated energies to the total energy of the excited panel is used for calculation of the total transmission loss factor.

The total dissipated energies of the connected walls k

$$W_{diss,k} = \iiint w_{diss,k}\, dxdydz \tag{3.13}$$

are determined by integrating the dissipation energy density $w_{diss,k}$ for wall k = 1,2,… . The energy in the source panel is calculated by a volume integration of the sum of the kinetic energy density $e_{kin,i}$ and the potential energy density $e_{pot,i}$, as show in equation (3.14)

$$E_{kin,i} + E_{pot,i} = \iiint e_{kin,i} + e_{pot,i}\, dxdydz \quad . \tag{3.14}$$

The dissipation energy density is integrated within the total structure, therefore also in-plane waves are considered. This approach has been chosen, because in the junction a wave transformation can happen that can have a significant influence on the structure-borne sound transmission (cf. chapter 1.2).

3.2.2.2 Comparison of measured and calculated values – aspired precision of the numerical calculations

Timpte [7] showed that the measured vibration reduction index can lead to high deviations especially for frequency dependent values. Table 3.15 shows Timpte's studies on comparable specimen of T-shaped junctions using a continuous flanking wall, a similar situation as described in this thesis. The flanking paths *Fd* and *Ff* are depicted, depending on an analysis of n = 23, respectively n = 16 measurements on different specimen/test setups. Within the investigated frequency range of this thesis (200 Hz to 1250 Hz), the standard deviation (SD) of the measured vibration reduction indices values (K_{ij}) result in high deviations from 2,1 dB

(at 200 Hz) to 8,5 dB (at 1250 Hz). This study shows that the measurement procedure itself can cause high uncertainties. These errors have to be kept in mind during the validation of numeric calculations. The standard deviation of the single number ratings of the vibration reduction indices ($K_{ij,200\text{-}1250}$) result in values of 2.8 dB, respectively 2.6 dB. These investigations show that the measurement procedure and as a consequence, the determined resulting reference data are governed by uncertainties. One sources of uncertainty can be the spatial sampling of the vibration field. In general, uncorrelated measurements at different positions have to be carried out, e.g., by choosing positions with a distance of $d \geq \lambda_B/2$ from each. The bending wave length λ_B is depending on the material properties and frequency. Ideally the distance of the measurement grid should be calculated for each specimen seperatly for the lowest measured frequency. To avoid the resulting high effort during the application of standardized measurements of EN ISO 10848 series, a minimum distance of 0,5 m between single measurement positions is a pragmatic base for the definition of the measurement grid. But a resulting uncertainty especially for measurement values at low frequencies can occur. This can be shown in Table 3.15 and Table 3.16, where the standard deviations are higher at frequencies of 100 Hz and 125 Hz, compared to frequencies of 400 Hz or 500 Hz.

Inclunding all these aspects, an aspired aim of the numerical calculations discussed in the following is a reduction of deviations between measured and calculated values of 2 dB for frequency dependent values. For the single number ratings of the vibration reduction index, a maximum deviation of 1 dB is aspired.

Vibration reduction index K_{ij} in dB																						
	$K_{ij,200\text{-}1250}$	50 Hz	63 Hz	80 Hz	100 Hz	125 Hz	160 Hz	200 Hz	250 Hz	315 Hz	400 Hz	500 Hz	630 Hz	800 Hz	1000 Hz	1250 Hz	1600 Hz	2000 Hz	2500 Hz	3150 Hz	4000 Hz	5000 Hz	n
Min	6.3	4.3	2.8	1.4	-1.1	0.6	0.7	2.0	3.2	4.4	6.1	4.5	6.1	4.4	5.9	5.1	6.4	7.2	8.9	10.2	8.9	14.1	
AVG	11.3	10.1	9.5	9.7	8.3	7.8	7.5	9.1	9.4	9.6	10.0	11.1	11.1	12.2	13.8	15.4	16.9	18.0	20.8	21.7	23.1	24.9	23
Max	15.1	14.0	16.8	15.2	14.3	13.7	13.3	14.3	15.2	15.4	16.2	14.9	15.2	20.1	22.5	28.6	33.9	36.5	33.6	35.6	38.1	44.4	
SD	2.8	3.0	3.4	3.8	4.0	4.2	3.5	3.4	3.4	3.1	2.9	3.2	2.4	4.5	5.5	7.5	7.9	8.8	8.3	8.1	7.9	7.8	

Table 3.15: Vibration reduction index for T-junction wall-wall without resilient layer, *Fd*-path [7]

Vibration reduction index K_{ij} in dB																						
	$K_{ij,200\text{-}1250}$	50 Hz	63 Hz	80 Hz	100 Hz	125 Hz	160 Hz	200 Hz	250 Hz	315 Hz	400 Hz	500 Hz	630 Hz	800 Hz	1000 Hz	1250 Hz	1600 Hz	2000 Hz	2500 Hz	3150 Hz	4000 Hz	5000 Hz	n
Min	3.7	-1.1	-1.2	2.2	0.7	0.4	-0.2	2.0	0.9	0.2	3.8	3.3	2.3	0.0	0.7	-2.0	-2.4	-3.1	-2.1	-1.7	-0.7	0.4	
AVG	7.6	3.2	3.4	5.5	5.3	5.7	4.1	5.1	6.1	5.8	6.4	7.5	7.6	8.7	10.1	11.5	12.3	12.8	12.5	14.0	15.6	17.4	16
Max	13.0	10.6	8.4	11.9	12.8	11.0	14.0	10.1	11.5	10.4	11.7	11.3	12.3	17.2	19.0	25.9	29.0	27.7	26.5	28.3	32.3	39.3	
SD	2.6	2.5	2.2	2.8	3.5	3.7	3.4	2.1	2.6	2.7	2.2	2.3	2.8	5.3	5.8	8.5	9.5	10.2	9.9	10.2	10.3	11.2	

Table 3.16: Vibration reduction index for T-junction wall-wall without resilient layer, *Ff*-path [7]

3.2.3 Coupling of CLT panels using screws

Screws are typical used fastener systems in timber engineering. In this section, a numerical model of a T-shaped junction of CLT panels, connected by several screws is discussed. The general model of the T-shaped junction has been defined by the description discussed in chapter 3.2.1. The screws have been approximated by metal rods with comparable specifications like the real screws, as shown in Table 3.13. The metal rods have been fully coupled to the surrounding structure.

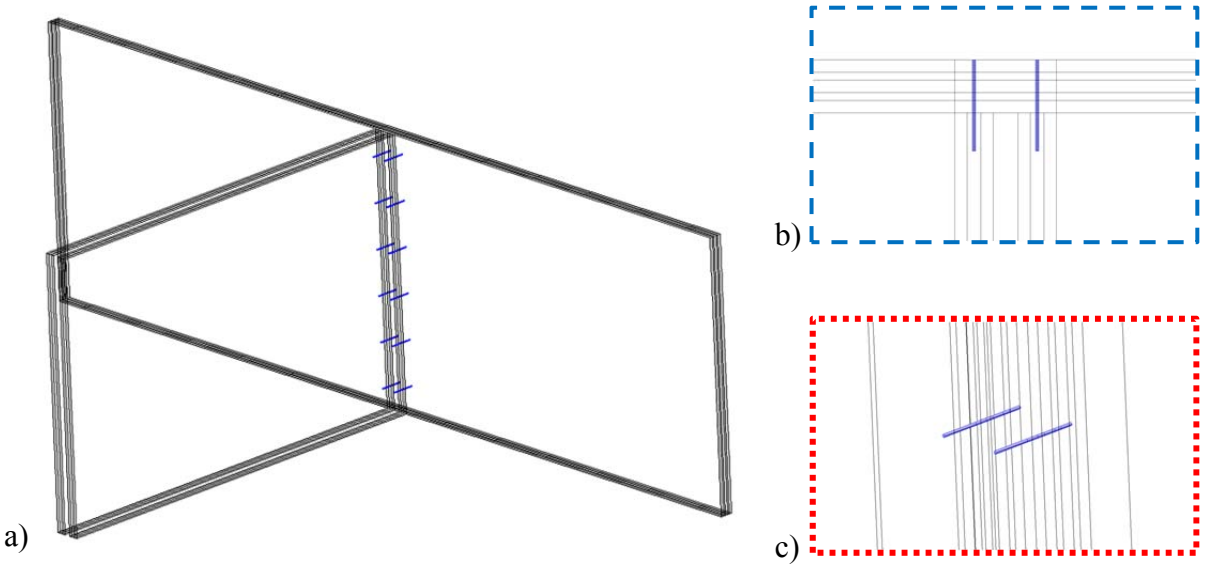

Figure 3.19 shows the resulting model and a detailed view of two investigated screws.

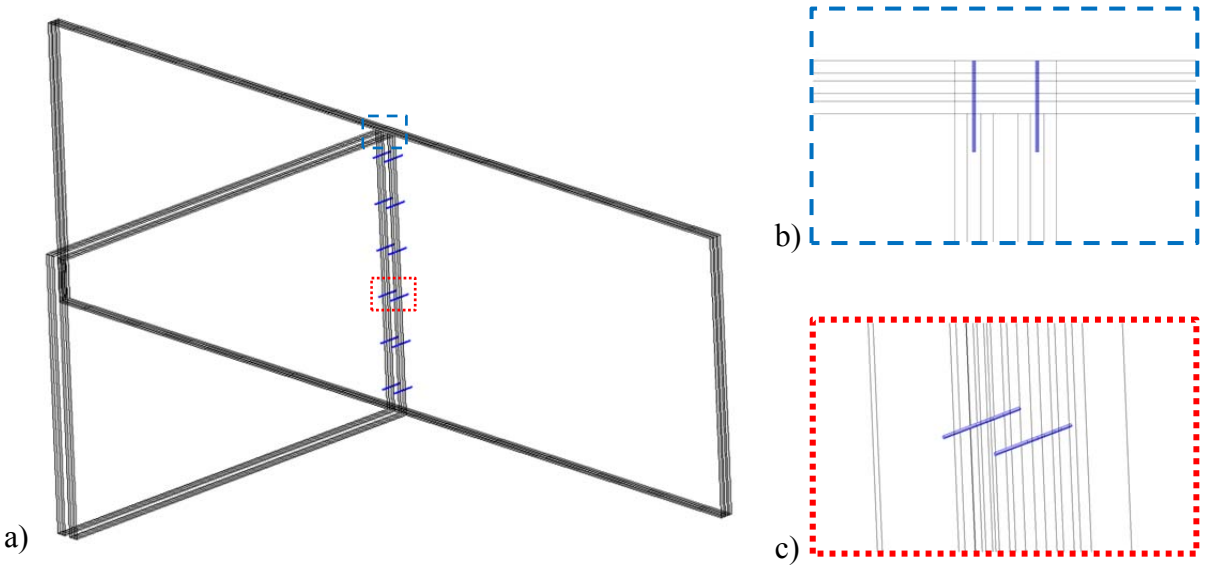

Figure 3.19: Calculation model of discrete screws (steel) – a) overall view; b) horizontal cross section / upper view of the junction; c) detailed view of two metal screws

Based on these approaches, several parametric studies have been performed to determine conditions for the coupling of the CLT panels that allow a practical calculation of the vibration reduction index. As mentioned previously, the transmission caused by the coupling stiffness of the coupling area is varied by the parameter k_A (spring constant per unit area). The difference of the frequency dependent values for the vibrations reduction indices, as well as the difference of the single-number quantity ratings have been analysed to allow a comparison of the measured and calculated values.

Figure 3.20 shows a graph of the calculated values listed in Table 3.17 and a comparison to the measured reference values of the vibration reduction indices. Calculation and measurement show a high correlation, especially for mid frequencies between 400 Hz and 800 Hz. The single number rated values result in a minor underestimation of 0.2 dB for the flanking-flanking path (K_{12}) and a minor overestimation of 0.3 dB for the flanking-direct path (K_{13}). At one-third-octave bands of 250 Hz and 315 Hz, the studies show a tendency for overestimating values for the calculation that can be caused by modal effects in the measurement configuration. At high frequencies of 1000 Hz and 1250 Hz, the calculation underestimates the vibration reduction indices. In this frequency range, it is obvious that additionally to a coupling effect, damping effects have to be taken into account in the investigations. Furthermore, apart from bending modes, thickness modes can occure in the panel.

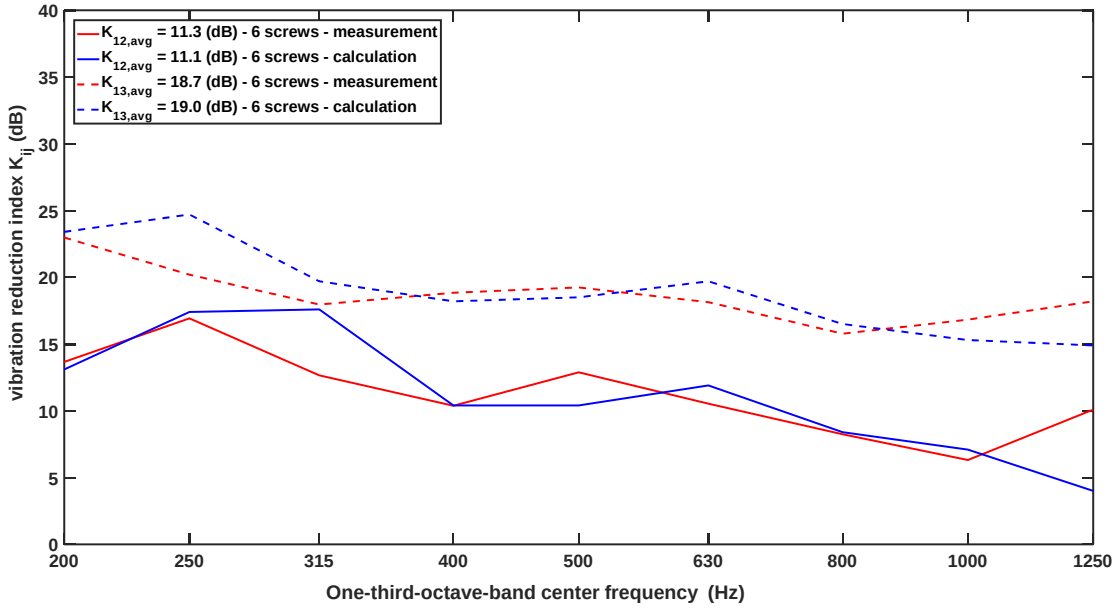

Figure 3.20: Numerical calculation of a T-junction using screws– comparison of measured and calculated vibration reduction indices

As mentioned by Hopkins (cf. section 1.2), different wave types have to be calculated using different damping approaches. It is assuemd that these thickness modes may require higher values for material damping than bending modes, which is not considered in the current model. The existance of further damping mechanism or a separation of thickness and bending modes have not been analysed in this thesis but may be investigated in future studies.

	K_{12} (Ff)			K_{13} (Ff)		
Frequency (Hz)	**Measured (dB)**	**Calculated (dB)**	**Difference (dB)**	**Measured (dB)**	**Calculated (dB)**	**Difference (dB)**
200	13.7	13.1	-0.6	23.0	23.4	0.4
250	16.9	17.4	0.4	20.2	24.7	4.5
315	12.7	17.6	5.0	18.0	19.7	1.7
400	10.4	10.4	0.0	18.8	18.2	-0.6
500	12.9	10.4	-2.5	19.2	18.5	-0.7
630	10.5	11.9	1.4	18.1	19.7	1.5
800	8.3	8.4	0.2	15.8	16.5	0.8
1000	6.3	7.1	0.7	16.8	15.3	-1.5
1250	10.1	4.0	-6.1	18.2	14.9	-3.3
$K_{ij,200\text{-}1250}$	**11.3**	**11.1**	**-0.2**	**18.7**	**19.0**	**0.3**

Table 3.17: Comparison of calculated and measured values of a T-shaped junction – screwed situation

Figure 3.21 shows the spring constant per unit area of the coupling area (left ordinate) and the total loss factor for the springs of the coupling area (right ordinate respectively, dotted graph) that results in these values for the vibration reduction indices. A separate model has been implemented for every one-third-octave band, using these different frequency dependent values. Especially at low frequencies, an increasing spring constant per unit area is obtained to allow a correct percentage between the different flanking paths. At high frequencies the spring constant results in lower values.

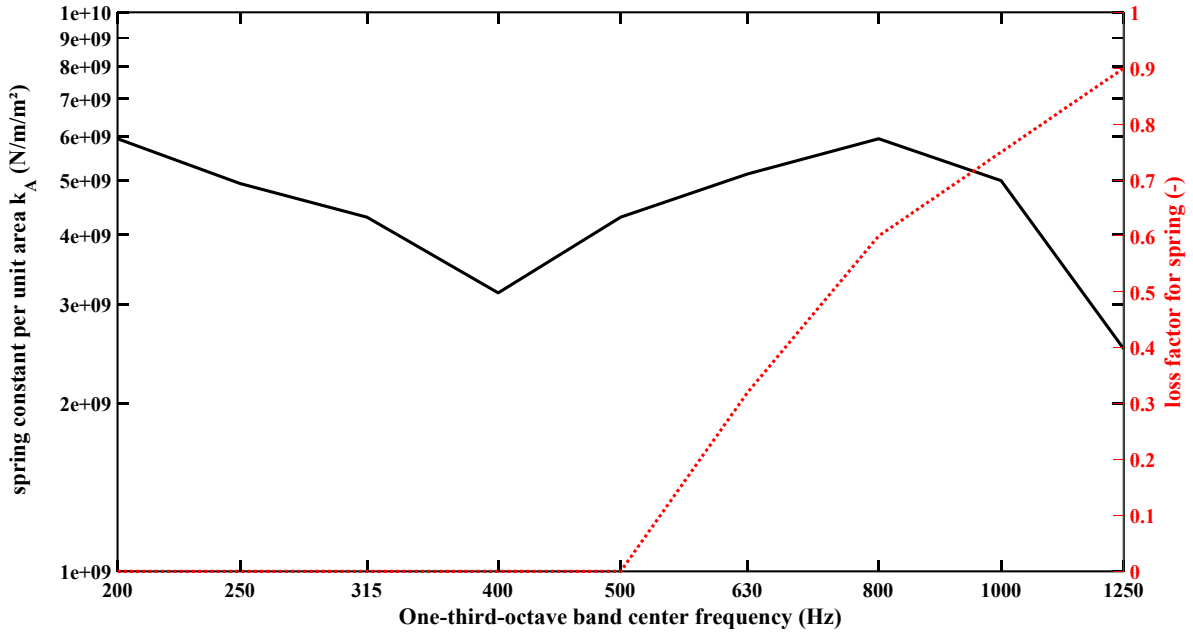

Figure 3.21: Coupling of the CLT panels – spring constant per unit area k_A and loss factor for springs - situation using screws

3.2.4 Coupling of CLT panels using angle brackets

In addition to screws, angle brackets are typical used fastener systems in timber engineering. Similar to the former described investigations for screws, a T-shaped calculation model has been defined, as shown in Figure 3.22.

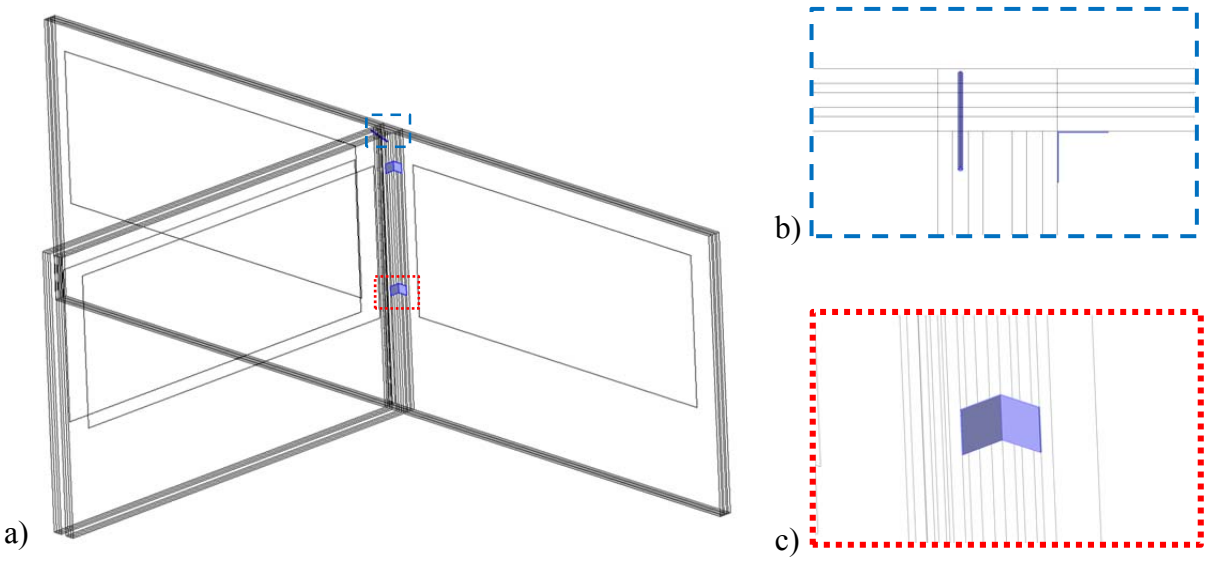

Figure 3.22: Implementation of discrete screws and angle brackets (steel) – a) overall view; b) horizontal cross section / upper view of the junction; c) detailed view of an angle bracket

The general model of the T-shaped junction has been defined by the description in chapter 3.2.1. The angle brackets have been implemented using a similar geometry and the specifications as shown in Table 3.13. A linear elastic, homogenous material model of steel has been chosen. The second CLT panel of the separation wall has been mounted using one screw as a mounting aid, which has been implemented as described in former chapter 3.2.3.

In difference to the investigations described in former chapter 3.2.3, separated coupling areas of the corresponding CLT panels have been defined for connection of the single leafs of the separation wall and the flanking wall because of the different types of mounting. The determined values for the damping model in the contact layers have been used for all coupling areas of the CLT panels as shown in Figure 3.21. Additionally, the contact areas of the angle brackets and the CLT panels have been defined by a separated, independent coupling stiffness. As a consequence, three independent parameters for coupling stiffness's are defined for parametric studies of the resulting vibration reduction index. Similar to chapter 3.2.3, the difference of the frequency dependent values for the vibrations reduction indices, as well as the difference of the single-number quantities have been analysed to allow a comparison of the measured and calculated values.

Figure 3.23 shows a graph of the resulting values of Table 3.18 for the calculated values, compared to the measured reference values for the vibration reduction indices.

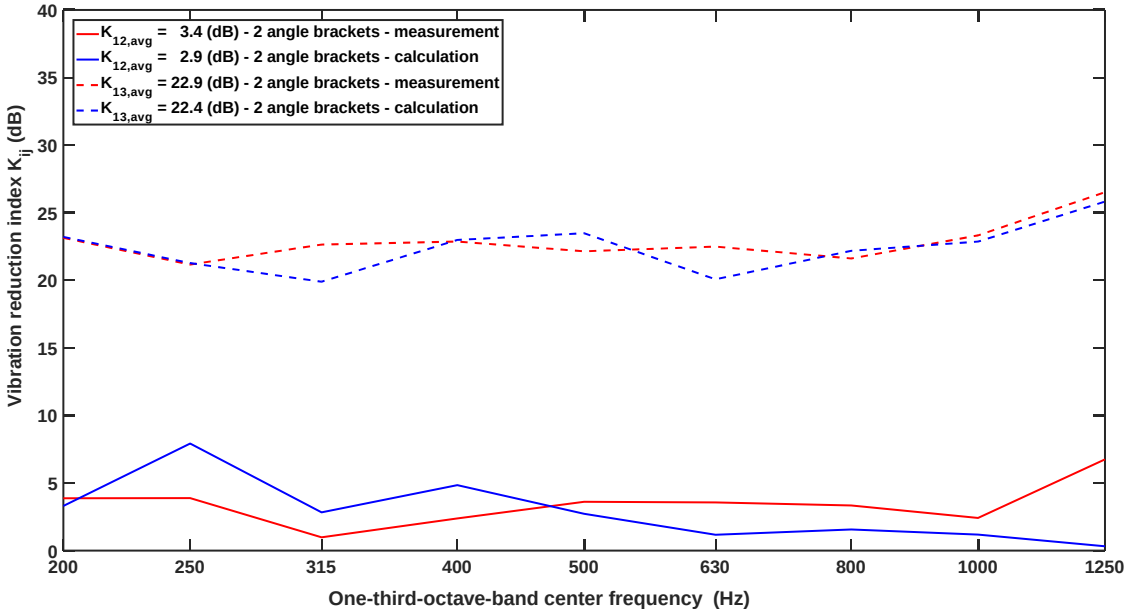

Figure 3.23: Numerical calculation of a T-junction using angle brackets and one screw – comparison of measured and calculated vibration reduction indices

Also for this situation, calculation and measurement show a high correlation. The single number rated values result in an underestimation of 0.5 dB for the flanking-flanking path (K_{12}) and 0.5 dB for the flanking-direct path (K_{13}). At one-third-octave bands of 250 Hz and 315 Hz, the parametric studies showed a tendency for overestimating values for the calculation that might be caused by modal effects in the measurement configuration. At high frequencies, especially at 1250 Hz, the calculation underestimates the vibration reduction indices that confirms the observations in section 3.2.3 of an additional physical effect in the measurements which causes an additional damping and is not included in the numerical model.

	K_{12} (Ff)			K_{13} (Ff)		
Frequency (Hz)	**Measured (dB)**	**Calculated (dB)**	**Difference (dB)**	**Measured (dB)**	**Calculated (dB)**	**Difference (dB)**
200	3,9	3,3	-0,6	23,1	23,2	0,1
250	3,9	7,9	4,0	21,2	21,3	0,1
315	1,0	2,8	1,9	22,6	19,9	-2,8
400	2,4	4,8	2,5	22,9	23,0	0,1
500	3,6	2,7	-0,9	22,1	23,5	1,3
630	3,6	1,2	-2,4	22,5	20,1	-2,4
800	3,3	1,6	-1,8	21,6	22,2	0,6
1000	2,4	1,2	-1,2	23,3	22,9	-0,5
1250	6,7	0,3	-6,4	26,5	25,8	-0,7
$K_{ij,200\text{-}1250}$	**3,4**	**2,9**	**-0,6**	**22,9**	**22,4**	**-0,5**

Table 3.18: Deviation of calculated and measured values of a T-shaped junction –situation using angle brackets

Figure 3.24 shows the frequency dependent values for the stiffness of the coupling that results in the discussed values for the vibration reduction indices. Caused by the different connections of the leafs of the separation wall, different coupling layers have to be defined and varied, using independent spring constants per unit area. These spring constants per unit area are represented by $k_{A,3}$ for the leaf of the separation wall connected by the screw (mounting aid), $k_{A,4}$ for the leaf of the separation wall connected by the angle brackets and $k_{A,AB}$ for the connection of the angle brackets and the CLT panels. Furthermore, a loss factor for the springs of coupling area $k_{A,3}$ and $k_{A,4}$ have been chosen, as determined in former surveys in section 3.2.3. The investigations here show that below 800 Hz, the coupling stiffness of $k_{A,4}$ and $k_{A,AB}$ differ a lot because the angle brackets are connected using a thick screw for each side of the bracket. Compared to this connection, the two CLT panels form a

blunt joint showing a reduced interaction force and, therefore, a coupling stiffness less than the one of the 6 screws, as shown in Figure 3.21. For one-third-octave bands of 800 Hz and 1000 Hz, the comparable coupling stiffness's result. For 1250 Hz, again the spring constants differ, but this might also be traced to a higher reference of the measurements. It appears an additional physical effect exists that causes damping and is not included in the numerical investigations. It is assumed that the numerical model of the hysteretic damping is no longer valid within this frequency range.

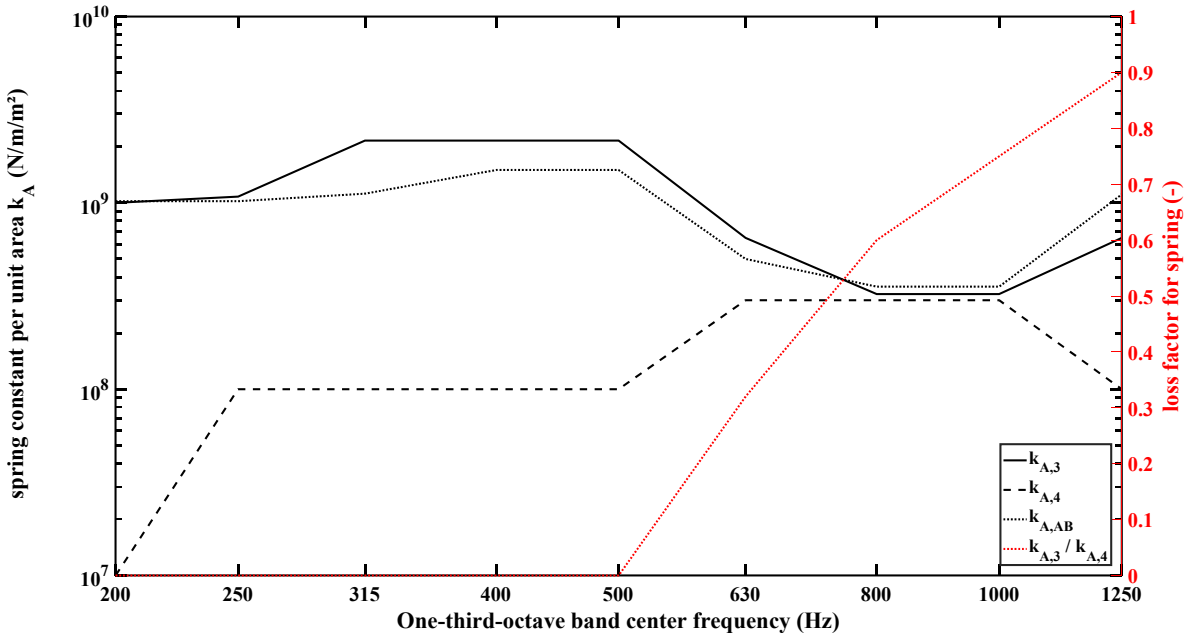

Figure 3.24: Coupling of the CLT panels - spring constant per unit area - $k_{A,3}$: leaf of the separation wall connected by the screw (mounting aid); $k_{A,4}$: leaf of the separation wall connected by the angle brackets; $k_{A,AB}$: connection between angle bracket and CLT panels

3.3 Comparison of the full calculation approach to standardized measurements

In former chapters, several variables have been calculated respectively measured that act as input parameters for the prediction of the sound insulation of adjacent rooms based on the EN ISO 12354 series. In the following, the total sound insulation is calculated for a typical building situation and is compared to standardized measurements of the resulting quantities.

First, measurement investigations have been performed to obtain reference data for the calculation procedure. Second, the actual situation has been analysed extensively to ensure a correct application of the standardized prediction method. Here, focus lays on a correct definition of the flanking paths of first order that include the (double-leaf) separation wall, as

well as on investigations of an influence of additional flanking paths of 2nd order that usually are not included in the standardized calculation approach. Finally, the numerical calculated values for the vibration reduction index, as described in chapter 3.2, are validated using the developed calculation approach.

3.3.1 Measurement investigations to determine reference data

To determine suitable reference values for further calculations of the sound insulation between rooms, measurements of the standardized level difference (field measurements of airborne sound insulation) have been performed, based on the standard ISO 16283-1 [103].

The measurements have been performed in two rooms of the building shell of a multi-storey residential building as shown in Figure 3.25. The rooms are built with raw CLT panels without additional linings. The chosen rooms are the main rooms within two different dwellings that are separated by a typical separation wall of CLT. Both rooms show the same size of 9.12 m x 2.92 m x 2.84 m (width x depth x height). The geometric details result in a volume of the source room, as well as of the receiving room of about 75,6 m³. Further details of the rooms, like the horizontal cross-sections, can be found in appendix A 3 .

Figure 3.25: Building shell of the investigated situation

The horizontal transmission between the two rooms results from the direct transmission path through the separation wall, as well as the flanking transmission paths of the flanking walls and ceilings/floors. The interior vertical junction is constructed as shown in Figure 3.26, which is the same as used for the laboratory measurements described in chapter 3.2. Here, one panel of the separation wall is fixed, using an oblique mounted screw, and the other panel is fixed using two angle brackets. For the exterior junction, the panels of the separation walls are mounted to the flanking walls using several screws as shown in chapter 3.2.

Figure 3.26: Details of the vertical (interior) junction between the two rooms

The measurements have been carried out using accredited calibrated measurement equipment (class 1) as shown in appendix A 1 in Figure 5.3 (devices g-n). For this situation, a weighted standardized level difference of 41,7 dB has been determined. Further details of the measurement results can be found in the measurement report in Figure 3.27.

Figure 3.28 show some detailed illustrations of the measurement situation. The airborne sound field has been excited using 4 different positions of a dodecahedron loudspeaker. The sound pressure in the rooms has been determined using high precision microphones that are mounted on rotating microphone booms near the center of the rooms. Window or door openings of the walls have been sealed and additional absorption material has been added to the room to increase the modal overlapping and, therefore, the reliability of the measurement procedure.

Standardized level difference according to ISO 16283-1

Field measurements of airborne sound insulation between rooms

Client: Laboratory for Building Sciences, Inffeldgasse 24, A-8010 Graz, Austria — Date of test: 21.10.2016

Description: Building shell of a multi-storey dwellings
3rd staircase
1st storey
Apartment 3/5 to 3/6

Object: Separation wall: 94 mm CLT 3-layer (30/34/30 mm, top layer orientation: vertical) - 60 mm rock wool -
94 mm CLT 3-layer (30/34/30 mm, top layer orientation: vertical)
Interior flanking wall: 128 mm CLT 5-layer (30/19/30/19/30 mm, orientation top layer: vertical)
Exterior flanking wall: 128 mm CLT 5-layer (30/19/30/19/30 mm, orientation top layer: vertical); do or cutout
Floor: 162 mm CLT 5-layer (34/30/34/30/34 mm, orientation top layer: towards separation wall

Source room: Apartment 3/5 - living room		Receiving room: Apartment 3/6 - living room	
Condition:	10,4 °C - 73,8 % - 98,5 kPa	Condition:	10,4 °C - 73,8 % - 98,5 kPa
Type:	CLT without facing shell	Type:	CLT without facing shell
Location:	Wiener Neustadt	Location:	Wiener Neustadt

Area of common partition: 25.87 m²
Source room volume: 76 m³
Receiving room volume: 76 m³

Frequency f [Hz]	1/3 octave [dB]
50	17.2
63	16.0
80	21.6
100	27.2
125	30.2
160	33.2
200	30.7
250	31.1
315	33.5
400	35.7
500	36.0
630	38.1
800	38.6
1000	41.9
1250	46.2
1600	48.9
2000	50.2
2500	52.8
3150	53.6
4000	59.5
5000	61.3

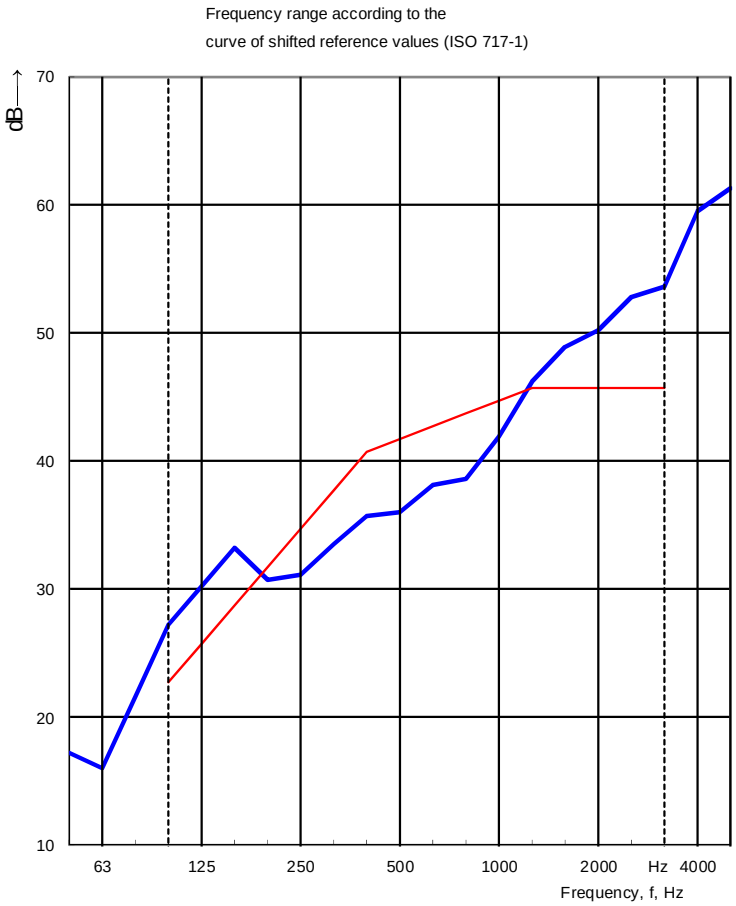

Rating according to ISO 717-1
$(C;C_{tr})$ = 41.7 (-1.1 ; -4.1) dB

Evaluation based on field measurement results obtained in one-third-octave bands by an engineering method.

$C_{50\text{-}3150}$ = -1.7 dB $C_{50\text{-}5000}$ = -0.7 dB $C_{100\text{-}5000}$ = -0.2 dB
$C_{tr,50\text{-}3150}$ = -7.9 dB $C_{tr,50\text{-}5000}$ = -7.9 dB $C_{tr,100\text{-}5000}$ = -4.1 dB

Name of test institute: Laboratory for Building Sciences, Inffeldgasse 24, A-8010 Graz, Austria
No. of test report: B14-025-080006-320_buhaso

Date: 21.10.2016 Signature:

Figure 3.27: Test report of in-situ measurements of the standardized level difference

Figure 3.28: Test setup for measurements of the airborne sound transmission

3.3.2 Preliminary investigation - flanking paths including a double-leafed separation wall

Based on the determined geometric parameters of the building situation as described in the former section, standardized calculations based on EN 12354-1 [89] have been performed using parameters determined from numerical calculations and specialized laboratory measurements.

First of all, preliminary investigations have been performed that deal with the definition of the flanking paths that include the double-leafed separation wall. For calculations using the framework of EN 12354-1, the weighted sound reduction index of the entire separation wall is used as shown, e.g., in Figure 2.2., assuming that the separation wall can be approximated as a single component of the overall system of two adjacent rooms. Table 3.19 shows the size of the walls and floor of the rooms that are used for standardized calculations and the definitions of the direct and flanking paths during the standardized procedures.

Building component	Width (m)	Heigth (m)	area (m²)	Composition
Separation wall	9,12	2,84	25,87	94 mm CLT 3-layer (30/33/30 mm, top layer orientation: vertical) 60 mm rock wool 94 mm CLT 3-layer (30/33/30 mm, top layer orientation: vertical)
Interior flanking wall (F=f=1)	2,92	2,84	8,29	128 mm CLT 5-layer (30/19/30/19/30 mm, orientation top layer: vertical)
Exterior flanking wall (F=f=2)	2,92	2,84	8,29	128 mm CLT 5-layer (30/19/30/19/30 mm, orientation top layer: vertical)
Floor (F=f=3)	9,12	2,92	26,63	168 mm CLT 5-layer (30/19/30/19/30 mm, orientation top layer: towards separation wall)
Ceiling (F=f=4)	9,12	2,92	26,63	168 mm CLT 5-layer (30/19/30/19/30 mm, orientation top layer: towards separation wall)

Table 3.19: Size of the elements of the rooms

Furthermore, measured data of the weighted sound reduction index of the panels and measured data of the vibration reduction index have been used, as shown in Table 3.20. Based on the assumption of transmission paths of 1st order as defined in the standard and the fact that the floors and the ceilings of the different sides of the rooms are totally separated by a gap of about 2 cm between the CLT elements (see Figure 3.26 left), a vibration reduction index of 30 dB is assumed for the flanking-flanking paths of the floor and of the ceiling that can be interpreted as a fully acoustic decoupling of the corresponding elements. Based on these

assumptions, the standardized level difference has been calculated for different situations, as discussed in the following.

Building component	R_w (dB)	K_{Ff} (dB)	K_{Fd} (dB)	K_{Df} (dB)
Separation wall:	60 (measured)	-	-	-
Interior flanking wall (F=f=1)	33 (measured)	**3,4 (measured)**	**22,9 (measured)**	**22,9 (measured)**
Exterior flanking wall (F=f=2)	33 (measured)	**11,3 (measured)**	**18,7 (measured)**	**18,7 (measured)**
Floor (F=f=3)	37 (measured)	30,0 (assumed)	**12,9 (measured)**	**12,9 (measured)**
Ceiling (F=f=4)	37 (measured)	30,0 (assumed)	**12,9 (measured)**	**12,9 (measured)**

Table 3.20: Prediction based on EN 12354-1 – input parameters used during preliminary investigations

Table 3.21 shows the results of the standardized calculations. This "conservative" approach leads to an overestimation of the total sound insulation of 3,3 dB compared to the measurements. The deviation is caused by the fact that the single leafs of the separation wall are supposed to be separated subsystems, as shown in Figure 3.12 for panel 3 and panel 4. Therefore, a single leaf, respectively CLT panel has to be used to allow feasible calculations.

Building component	Path	Rw_{avg} (dB)	Additional lining (dB)	K_{ij} (dB)	$10*\log(S/l_f)$ (dB)	sum (dB)
Separation wall:	R_{Dd} =	60	0			60,0
	R_{1d} =	46,5	0	22,9	9,6	79,0
	R_{2d} =	46,5	0	18,7	9,6	74,8
	R_{3d} =	48,5	0	12,9	4,5	65,9
	R_{4d} =	48,5	0	12,9	4,5	65,9
Interior flanking wall (F=f=1)	R_{D1} =	46,5	0	22,9	9,6	79,0
	R_{11} =	33,0	0	3,4	9,6	46,0
Exterior flanking wall (F=f=2)	R_{D2} =	46,5	0	18,7	9,6	74,8
	R_{22} =	33,0	0	11,3	9,6	53,9
Floor (F=f=3)	R_{D3} =	48,5	0	12,9	4,5	65,9
	R_{33} =	37,0	0	30,0	4,5	71,5
Ceiling (F=f=4)	R_{D4} =	48,5	0	12,9	4,5	65,9
	R_{44} =	37,0	0	30,0	4,5	71,5

	Calculation	Measurement	Difference
$D_{nT,w}$ =	**44,8**	41,7	**3,1**

Table 3.21: Prediction based on EN 12354-1 – separation wall that deals acts as a single subsystem

Table 3.22 shows the used data and the results of this "progressive" calculation method. For this purpose, the involved flanking paths are defined using a single CLT panel (3s, 94 mm, 30/34/30). This single CLT panel shows a measured weighted sound reduction index R_w of 31 dB. Using the modified calculation approach, the overestimation of the calculated standardized level difference is significantly reduced to a neglectible value of 0,1 dB. Furthermore the calculation shows that the flanking sound insulation of the interior walls R_{11} is the determining factor (lowest value) of the total sound insulation, caused by the low vibration reduction index. Therefore, the overall standardized level difference is sensitive concerning this flanking path.

The calculations show that using a single CLT panel instead of the total separation wall leads to values of practical use. As a consequence, these preliminary investigations lead to a calculation framework that is reliable for further calculation procedures.

Building component	Path	$R_{w,avg}$ (dB)	Additional lining (dB)	K_{ij} (dB)	$10*\log(S/l_f)$ (dB)	sum (dB)
Separation wall:	R_{Dd} =	60	0			60,0
	R_{1d} =	32,0	0	22,9	9,6	64,5
	R_{2d} =	32,0	0	18,7	9,6	60,3
	R_{3d} =	34,0	0	12,9	4,5	51,4
	R_{4d} =	34,0	0	12,9	4,5	51,4
Interior flanking wall (F=f=1)	R_{D1} =	32,0	0	22,9	9,6	64,5
	R_{11} =	33,0	0	**3,4**	9,6	**46,0**
Exterior flanking wall (F=f=2)	R_{D2} =	32,0	0	18,7	9,6	60,3
	R_{22} =	33,0	0	11,3	9,6	53,9
Floor (F=f=3)	R_{D3} =	34,0	0	12,9	4,5	51,4
	R_{33} =	37,0	0	30,0	4,5	71,5
Ceiling (F=f=4)	R_{D4} =	34,0	0	12,9	4,5	51,4
	R_{44} =	37,0	0	30,0	4,5	71,5

	Calculation	Measurement	Difference
$D_{nT,w}$ =	**41,8**	41,7	**0,1**

Table 3.22: Prediction based on EN 12354-1 – separation wall that is divided into two subsystems

3.3.3 Predictions using numerical calculated vibration reduction indizes

The values of the numerical calculations of the vibration reduction index have been validated by using the corresponding values in the discussed calculation approach. The resulting input parameters are shown in Table 3.20. The measured vibration reduction indices of the horizontal junctions are replaced by the numerical calculated values as discussed in chapter 3.2.

Building component	R_w (dB)	K_{Ff} (dB)	K_{Fd} (dB)	K_{Df} (dB)
Separation wall:	60 (measured)	-	-	-
Interior flanking wall (F=f=1)	33 (measured)	**2,9 (calculated)**	**22,4 (calculated)**	**22,4 (calculated)**
Exterior flanking wall (F=f=2)	33 (measured)	**11,1 (calculated)**	**19,0 (calculated)**	**19,0 (calculated)**
Floor (F=f=3)	37 (measured)	30,0 (assumed)	12,9 (measured)	12,9 (measured)
Ceiling (F=f=4)	37 (measured)	30,0 (assumed)	12,9 (measured)	12,9 (measured)

Table 3.23: Prediction based on EN 12354-1 – input parameters using measured and numerical calculated values

Table 3.24 shows the procedure and the results of this "progressive" calculation approach. In general, the usage of the numerical determined vibration reduction indices results in a minor underestimation of the total sound insulation, respectively the standardized level difference $D_{nT,w}$ of 0,1 dB. In this case, final standardized level difference is sensitive on the input parameters for the flanking path R_{11}, especially, its vibration reduction index and the direct sound insulation of the panel.

In general, the numerical calculations, as discussed in chapter 3.2, lead to satisfying results. The underestimation is mainly caused by the slight underestimation of the vibration reduction index for flanking path R_{11} for the connection using angle brackets. As analysed in the corresponding section 3.2.4, the underestimation at the one-third-octave-band of 1250 Hz mainly leads to the low value for the single-number quantity for the vibration reduction index. This underestimation in high frequency might be caused by a physical effect in the real situation that leads to higher values but is not included in the numerical calculations. If this physical effect will be included in future investigations, it is expected that also this

underestimation will be corrected and the already satisfying precision of the results can be additionally increased.

Building component	Path	$R_{w,avg}$ (dB)	Additional lining (dB)	K_{ij} (dB)	$10*\log(S/l_f)$ (dB)	sum (dB)
	R_{Dd} =	60	0			60,0
	R_{1d} =	32,0	0	22,4	9,6	64,0
Separation wall:	R_{2d} =	32,0	0	19,0	9,6	60,6
	R_{3d} =	34,0	0	12,9	4,5	51,4
	R_{4d} =	34,0	0	12,9	4,5	51,4
Interior flanking wall	R_{D1} =	32,0	0	22,4	9,6	64,0
(F=f=1)	R_{11} =	33,0	0	**2,9**	9,6	**45,5**
Exterior flanking wall	R_{D2} =	32,0	0	19,0	9,6	60,6
(F=f=2)	R_{22} =	33,0	0	11,1	9,6	53,7
Floor	R_{D3} =	34,0	0	12,9	4,5	51,4
(F=f=3)	R_{33} =	37,0	0	30,0	4,5	71,5
Ceiling	R_{D4} =	34,0	0	12,9	4,5	51,4
(F=f=4)	R_{44} =	37,0	0	30,0	4,5	71,5

	Calculation	Measurement	Difference
$D_{nT,w}$ =	**41,6**	41,7	**-0,1**

Table 3.24: Prediction based on EN 12354-1 using numerical calculated values of the vibration reduction index

3.4 Summary

This chapter of the thesis deals with several studies on a development of calculation methods for the sound transmission in CLT panels and junctions, based on the FEM. A frequency range within one-third-octave-bands from 200 Hz to 1250 Hz has been investigated, because this frequency range is used for single-number quantities for the vibration reduction index. The investigation has been separated in three different steps that focus on special topics and every step has been validated using experimental measurements. First, single panels of cross-laminated timber are investigated to determine suitable calculation methods, material models and material data. Compared to former studies, typical panels that show no side-gluing have been investigated. A suitable meshing strategy has been developed for further numerical

calculations of this kind of panels. The investigations showed that a linear elastic homogenous orthotropic material model can be used to calculate the vibration response of CLT. Using material parameters and data from investigations of side glued panels result in errors for non-side glued panels, because shrinking of the topping layers leads to a gap that reduces the stiffness of the panels. Furthermore, a simultaneous parameter fitting of several CLT panels lead to more precise solutions than using averaged material data determined from single analyses of the panels. The final results indicate a good fitting and a high reliability of the estimated vales. Using a parameter fitting process for calculated and measured eigenfrequencies, the number of the variation parameters has to be set to a minimum with respect to the most influencing parameters. Otherwise a high calculation effort can lead to impracticable calculation times.

Based on the investigations on single CLT panels, these panels have been connected to each other to form junctions. Fastener systems like screws and angle brackets have been used and the standardized vibration reduction index has been determined. The numerical calculated vibration reduction indices show a good agreement compared to measured results. Coupling stiffness's and loss factor for the springs have been used for the contact surfaces of CLT and fastener systems. At high frequencies of 1000 Hz and 1250 Hz, a tendency has been observed that the calculation underestimates the vibration reduction indices. Within this frequency range, an additional physical effect might be taken into account in the numerical model. On the one hand, the quality of contact of the CLT panels may have an influence on the structure borne sound transmission at higher frequencies. Figure 3.29 shows the resulting junction of two CLT panels. The interior layer gets full contact to the surface of panel 2. The exterior layers partly have no contact to the surface of panel 2.

Figure 3.29: Blunt joint of two CLT panels

On the other hand, the deviations might be caused by a specific effect called “element attenuation” (cf. [104]) that describes the decrease in level of the propagating wave under far-field conditions. The effect can cause overestimations during measurements of vibration reduction indices. It is assumed that, in principle, the effect is considered in the FE-model caused by the chosen calculation method, but a detailed validation of the approach has not been carried out. Therefore, this and the prior hypotheses have not been proven within the surveys of this thesis but they should be a topic for future studies.

Furthermore, this numerical calculation approach of the vibration reduction index is validated using the standardized prediction methods of the EN 12354-1 by a comparison to the measurement results of a real building situation. For this purpose, a too general interpretation of the standard leads to significant overestimations of the sound insulation. Using such a “conservative” approach, the standardized level difference is overestimated by about 3,3 dB compared to the measurements. A “progressive” interpretation of the standard has to be used to obtain plausible results. Here, the involved flanking paths of a double leafed separation wall (two CLT panels) have to be defined using only single leafs, respectively single CLT panels. This calculation procedure leads to reliable results. Finally, the numerical determined values result in a minor underestimation of the total sound insulation, respectively the standardized level difference $D_{nT,w}$ of 0,1 dB. Therefore the developed numerical calculations lead to satisfying results.

4 SPECIAL PHYSICAL EFFECTS

This chapter describes two acoustic effects that can have an influence on the flanking sound insulation of CLT. It can be shown that independent physical effects occur in different frequency ranges. The effects in the junction strongly depend on the properties and the interaction of the connected panels. Therefore, variations of the compositions of the panels result in a change of the impact of these physical effects and can be used, especially, for optimization of the flanking sound insulation in the specific frequency ranges.

In section 4.1, an effect called “modal (de-)coupling” is investigated that occur in the very low and low frequency range. The effect shows a high potential for optimization of the constructions, especially for increasing the flanking sound insulation for impact sound.

In section 4.2, an effect called “wave transformation” is investigated that occur in the mid frequency range. The effect shows a high optimization potential for flanking sound insulation at mid frequencies, where also the effect of coincidence arises.

4.1 Modal (de-)coupling

In several building situations, timber constructions often allow an advanced sound insulation at higher frequencies caused by, e.g., the high material damping. But at low frequencies, timber constructions often show a reduced sound insulation, because of the low density that dominates the sound insulation. Additional linings on the walls or floors increase the sound insulation especially at frequencies above 100 Hz but they have less effect on the sound insulation at lower frequencies.

Typical measurement results are shown for instance in Figure 4.1 to show the limitations of these “classical” optimization modifications and subsequently, the potential of the approach described in this section. Here, the impact sound pressure levels of various modifications of a typical CLT floor are compared, based on standardized measurements [105]. Here and subsequently in this thesis, a reference value of 20e-6 Pa for the sound pressure levels is used. The measurements have been performed by the Laboratory for Building Science, Graz University of Technology. The results show that the level increases with decreasing frequency. Caused by the low mass of the CLT panel, plate resonances like bending modes are strongly excited at low frequencies. The sound insulation can be increased significantly by the use of additional linings like a resilient layer and a floating floor or an additional suspended ceiling. Nevertheless, these typical modifications have less influence below 100 Hz.

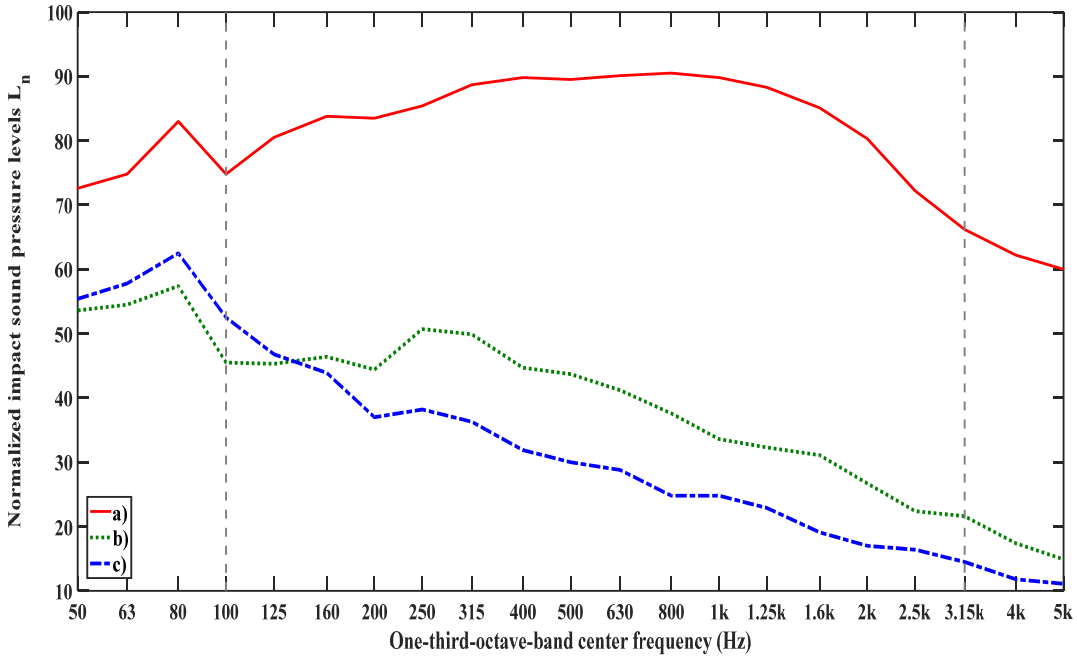

Figure 4.1: Comparison of floors – a) CLT, 5s, 140 mm b) former situation a) but adding gravel filling, resilient layer and floating floor to the construction; c) former situation b) but adding a suspended ceiling

At low frequencies, improvements can be made by additional masses, e.g., gravel fillings. But this action decreases main advantages of the construction material like low cost and fast building. Alternatively, an additional resilient layer and a floating floor can reduce the direct sound transmission and additional linings on the walls can reduce flanking sound insulation. Improvements of the sound insulation are caused by a decoupling effect of a resonating system for frequencies above the corresponding eigenfrequency of the system. For

frequencies near the eigenfrequency of the added system, the sound insulation of the overall construction can get worse. Furthermore this eigenfrequency can coincide with the bending mode frequencies of the panels. As a consequence, additional linings can have a non-satisfying effect at low and very low frequencies. Excitation by walking noise can result in a noise spectrum containing sound energy especially at low frequencies. As a result, the modes of the panel are strongly excited and a noise of high level occurs at single eigenfrequencies. This noise can have a very annoying effect on inhabitants because of its tonal character. Compared to evaluations of noise immission, such a tonal character is taken into account by adding a surcharge of several decibels [106].

Alternatively, an improvement of the sound insulation can be achieved by a use of the effect of modal (de-)coupling. Amongst others, flanking sound transmission – especially at low frequencies - is depending on the correlation of the vibration fields of the coupled panels. In general, every single panel shows eigenfrequencies and mode shapes that characterize the vibration behaviour of the component. The junction may couple these "local" modes to "global" modes, if two or more components have similar eigenfrequencies.

The distinction of local and global modes was investigated, e.g., by Hopkins [6]. He observed that approximate global modes by considering exclusively local modes of the uncoupled system leads to unsatisfying results, though appropriate junction boundary conditions for an uncoupled plate are assumed. Therefore, drawing conclusions on global modes based on local modes of uncoupled systems may lead to unsatisfying results. This aspect has been taken into account during the investigations described in this thesis during calculations of the full structure. In [107], Hopkins showed the relevance of significant global modes in investigations using measurement data and calculations based on FEM and SEA for concrete/masonry walls. Especially, the measured mobility on constructions of H-shape junctions shows the importance of considering global modes at low frequencies. Global modes are related to the whole structure, like vibrations of the entire building [5].

The former described approach of a decoupling of local modes to avoid global modes that leads to a reduced sound transmission can be compared to an advanced approach of the classical SEA called the "Statistical Modal Energy Distribution Analysis", e.g., described by Maxit and Guyader [108]. The fundamentals of this calculation method are based on a dual mode formulation [109], where the interaction of each single mode of one subsystem is coupled separately to each single mode of another subsystem. This approach was used

especially for calculations of coupled plates [110]. Applications, e.g., to cavity–panel–cavity systems are described by Aragonés et al. [111]. A similar calculation approach called „MODal ENergy analysis“ (MODENA) is described by Totaro and Guyader [112] and provides a pure tone analysis of sound power flow.

Variations of material parameters that have an influence on the eigenfrequencies, e.g., the Young’s modulus can be used to reduce the coupling of local modes. Amongst others, Gibbs and Craven [61] investigated the influence of a variation of stiffness or plate thickness on coupled panels of concrete at frequencies higher than 100 Hz. They have shown that difference on stiffness or plate thickness can have strong influence on flanking sound transmission. In building practice, materials like concrete allow only small variations in bending stiffness, because the range of changing panel thickness or Young’s Modulus is strongly limited or a change is not possible.

Cross-laminated timber shows a high potential range for variations of the bending stiffness, caused by the high number of possible compositions of the panels. Here, we investigate the effect of modal (de-)coupling by numerical studies, based on the FEM. Variations of bending stiffness of connected panels result in modal (de-) coupling at frequencies lower than 100 Hz.

Besides the coupling of structural subsystems, also the modal coupling of structures and cavities has an important influence. For direct sound insulation of timber-joist floors (impact sound), Larsson and Amiryarahmadi [113] investigated the modal coupling of the floor to the receiving room at frequencies below 100 Hz. They concluded that the impact sound pressure depends of the floor modes and they investigated how the floor modes are coupled with the room modes. High impact sound levels arise especially if unfortunate combinations of room size and floor properties are chosen. The importance of this plate/cavity coupling is an important aspect shown in this thesis in the next section.

4.1.1 Fundamental assumptions

The resonant structure borne sound transmission can be described by the transfer mobility between oscillating subsystems. To show the fundamentals of this approach for coupled panels, numerical studies have been performed based on the FEM, with a focus on flanking sound transmission.

4.1.1.1 Numerical calculations

Figure 4.2 shows the calculation model and the chosen boundary conditions. The model contains two coupled panels, a floor and a wall forming a L-shape junction, and a cavity including an air-borne sound field. The size of the room is 3m x 3m and the thicknesses of the panels are 0,1m. The wall has been coupled to the air-borne sound field. The floor panel has been excited using a rain-on-the-roof excitation of the surface (unit force and arbitrary phase over the surface).

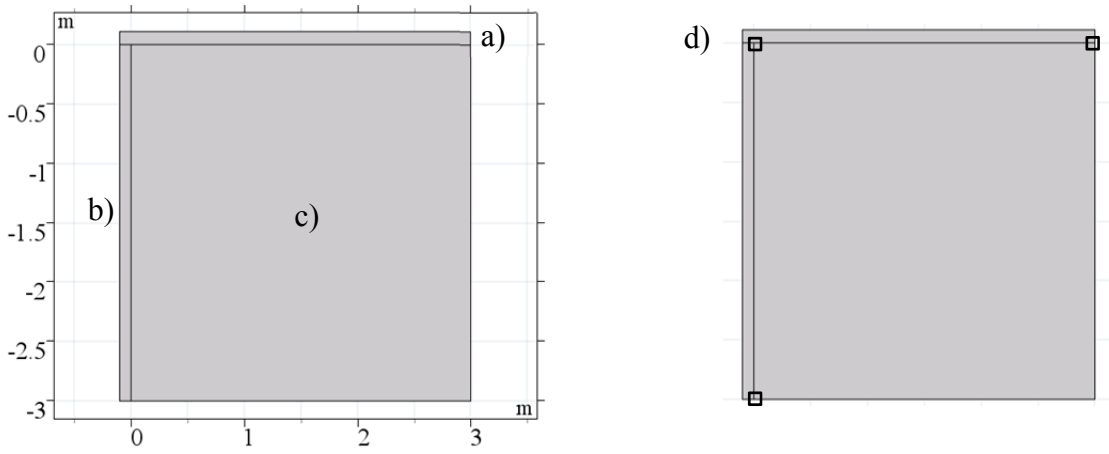

Figure 4.2: Geometry and boundary conditions: a) panel 1; b) panel 2; c) air-borne sound field; d) fixed constraint at edges and in the corner (single point)

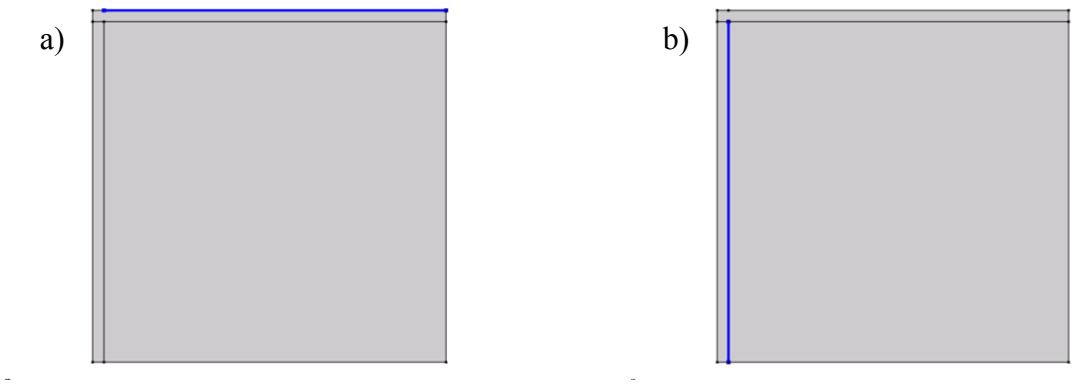

Figure 4.3: Geometry and boundary conditions: a) rain-on-the-roof excitation b) coupling of structure and air-borne sound field

A linear elastic, isotropic material model has been chosen to calculate the structure. The corresponding values are shown in Table 4.1. A hysteretic damping with a value of 0,1 (-) has been chosen. Quadratic shape functions have been used for the structure and the cavity. Figure 4.4 shows the resulting mesh based on triangle elements, the model results in

55137 DOF. The model has been studied in the frequency domain within a frequency range of 20 Hz to 100 Hz. 5000 frequencies have been calculated using a linear distribution within the chosen frequency range.

	Material data			
Parameter	**ρ (kg/m³)**	**E (GPa)**	**ν (-)**	**c (m/s)**
structure	470	10,7	0,2	-
air	1,2	-	-	343

Table 4.1: Material data of the structure and of the air

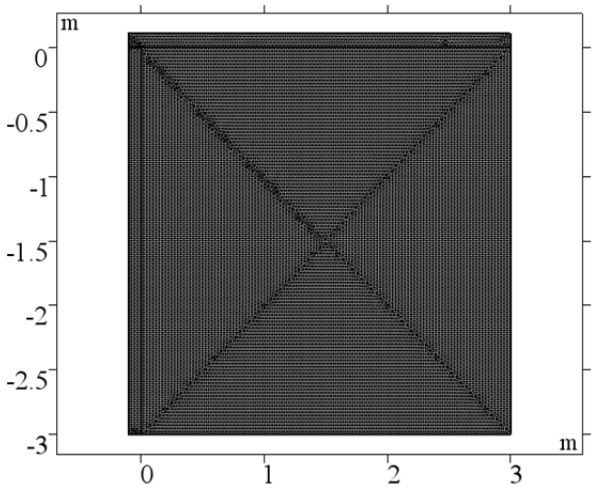

Figure 4.4: Final mesh of the numerical model for fundamental studies

For further calculations, parts of the geometry are selected to evaluate physical parameters, shown in Figure 4.5.

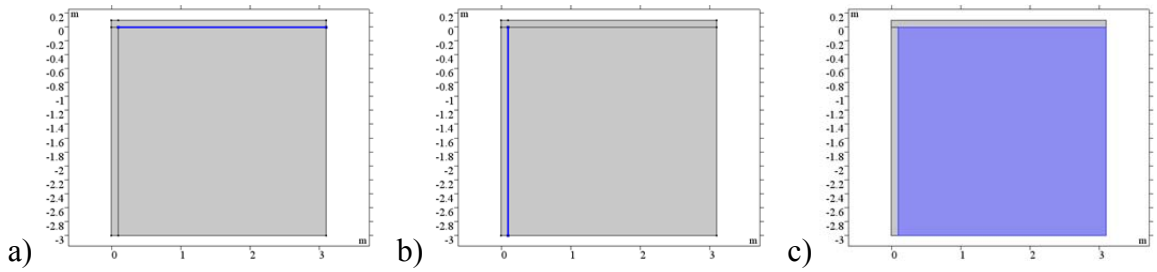

Figure 4.5: Selections for evaluation of physical parameters– a) boundary 1 (b_1) of panel 1; b) boundary 2 (b_2) of panel 2; c) domain 1 (d_1) of the cavity

4.1.1.2 Results and discussion

Each of the subsystems in Figure 4.6 shows local modes. If the eigenfrequencies of two systems coincide, a global mode occurs that result in a high flanking sound transmission.

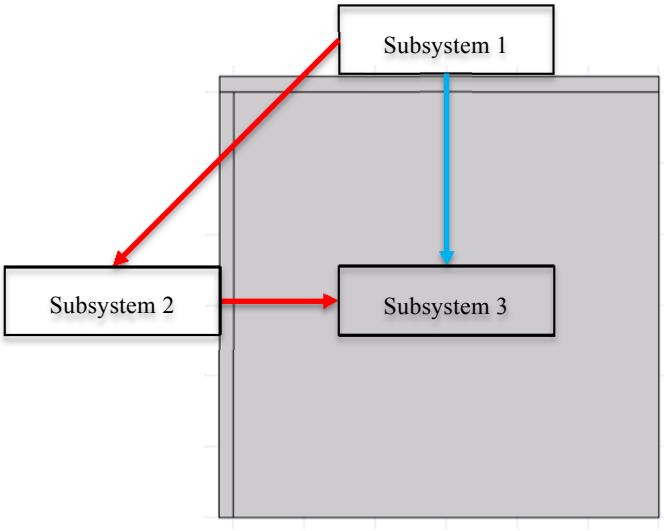

Figure 4.6: Subsystem structure for the numerical model – direct sound transmission (blue); flanking sound transmission (red)

Global modes arise if the panels show the same size, boundary conditions and material data. A decoupling of global to local modes can be achieved, if the properties are changed in a suitable way. First, the model has been solved to obtain global modes using identical material parameters for the two panels. Second, the Young's modulus of panel 2 has been changed to 60 % of the Young's modulus of panel 1 to decouple the local modes of the two panels. For both situations, the resulting sound pressure level in the air-borne sound field has been evaluated.

The spatial averaged sound pressure level of the solution of the model can be calculated by

$$L_{p,d1} = 10 \lg \left[\frac{\overline{|p^2|}_{d1}}{p_0^2} \right], \quad \text{(dB)} \quad (4.1)$$

where $\overline{|p^2|}_{d1}$ represents the spatial averaged sound pressure within domain 1 (Pa) and p_0 represents the reference sound pressure with a value of $20e^{-6}$ (Pa). This reference value is generally used subsequently in this thesis.

Figure 4.7 shows the results of the spatial averaged air-borne sound pressure level within the room, normalized to the maximum of the two situations. Caused by the global mode at 57,175 Hz (red), a strong resonant peak occurs because the first two resonances of the cavity arise at the same frequency due to the sqared room. Furthermore, the material damping of the panels is the only damping mechanism considered in this model. Using the lower Young's modulus of panel 2 (green), the normalized impact sound level is significantly reduced for a broad range of frequencies. The difference in stiffness of the two walls results in a slight "detuning" of these two modes of the cavity. As a consequence, two different resonance frequencies arise for these two modes.

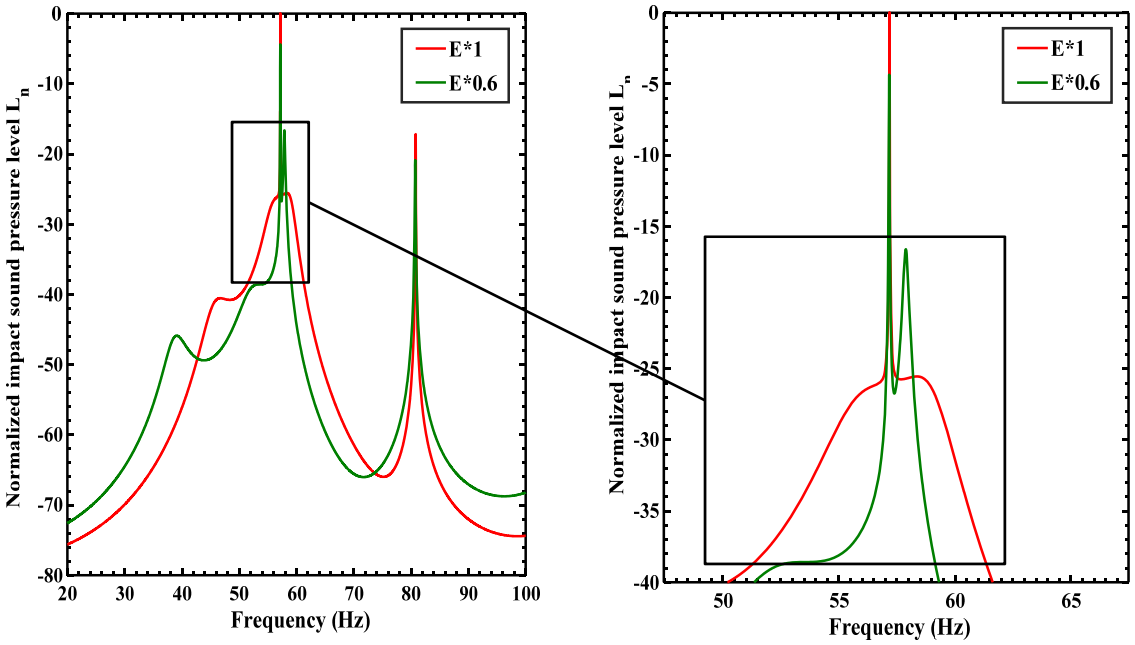

Figure 4.7: Normalized sound pressure level in the cavity by using different values for the Young's modulus of panel 2 – calculation using identic Young's moduli of the two panels (red); calculation using a reduced Young's modulus of panel 2 (green)

A second reason for the high difference between these two solutions is shown in Figure 4.8. A global mode of the structure occurs, if the panels show identical material parameters, boundary conditions and sizes (a). Additionally, the cavity reveals a mode at nearly the same eigenfrequency as both panels. A reduction of the stiffness of panel 2 leads to a shift of its (local) eigenfrequencies. As a result, a reduction of the coupling of the local modes of panel 1 and panel 2 arises. Furthermore, the influence of the coupling of panel 2 and the cavity on the sound transmission is reduced. The impact of this global mode is reduced shown by the decreased sound pressure level in the cavity.

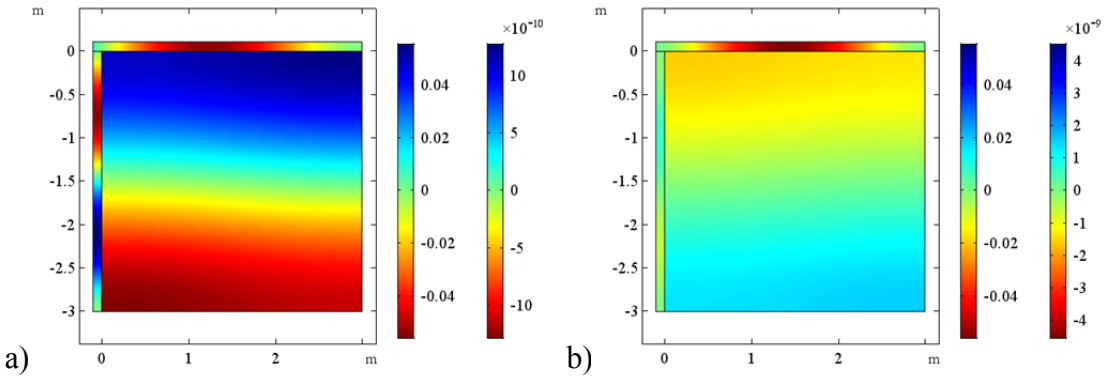

Figure 4.8: Global mode caused by identic material parameters – a) Frequency = 57,18 Hz;
b) Frequency = 57,16 Hz (left colorbars: sound pressure (Pa), right colorbars: out-of-plane displacement (m)

It has to be mentioned that a variation of the stiffness of one of the panels also slightly influences the eigenfrequency of the global mode, shown in Figure 4.7.

A local mode is a natural property of a single finite plate or a cavity. Compared to this, a global mode is a natural property of several coupled subsystems. To quantify the influence of this global mode especially on flanking sound transmission, the discrete correlation of eigenfrequencies of single components as well as their vibration response is studied in the following

The eigenfrequencies of the cavity and the structure has been analysed for different models to separate the single modes of the corresponding subsystems. Uncoupled calculations of cavity and structure have a slight influence on their eigenfrequencies and mode shapes. In contrast to the structure, this influence is assumed negligible for theoretical and also practical reasons. One the one hand the high difference in mechanical impedance of air and CLT results in a very low repercussion. On the other hand, calculations of real sized, fully coupled models e.g. in 3D (see section 4.1.2) result in very time consuming calculations, therefore the applicability of extensive parametric studies is strongly limited today.

In contrast, a separate calculation of the local modes of single, uncoupled panels instead of a calculation of the whole structure can result in a significant error in eigenfrequencies and mode shapes. As mentioned by Hopkins [6], local modes of the uncoupled system can not simulate the global mode exactly, although a correct boundary condition of the junction is considered. In a nutshell, two uncoupled models have been studied, one for the cavity by assuming sound hard boundaries and one for the solid structure.

Based on these assumptions, three parameters have been developed to analyse and evaluate the correlation of these global modes. A correlation first order indicates the correlation of the eigenfrequencies of the cavity to the structure. As a consequence, this parameter indicates, if there generally arises a problematic coupling between structure and cavity, independent, whether flanking transmission or direct transmission occurs or not. This discrete correlation of first order for a global mode is defined by

$$G^{I} = \frac{\min(f_c,f_s)}{\max(f_c,f_s)}, \qquad (-) \qquad (4.2)$$

where f_c represents the eigenfrequency of the cavity (Hz) and f_s represents the eigenfrequency of the solid structure (Hz). The minimum of the compared eigenfrequencies is normalized to the maximum of the compared eigenfrequencies to get a value range between 0 to 1. This value range allows a comprehensible comparison of further correlation subsequently. Furthermore, G^I quantifies the proportion of the lower to the higher eigenfrequency. A high value near 1 (-) indicates a high correlation of eigenfrequencies of the structure and the cavity.

A correlation of second order of a global mode includes the correlation of local modes of coupled panels, additionally to the correlation of the eigenfrequencies. Therefore, it describes the structure borne sound transmission from the first subsystem to the second subsystem. For the present case, the transmission from the floor to the flanking panel is focused. As already mentioned, drawing conclusions from calculations of the eigenfrequencies of uncoupled panels to global modes can lead to errors, thus the full structure is calculated. As a result, the coupling of the local modes, respectively the impact of a local mode to the global mode can be described by the ratio of the averaged out-of-plane displacements of the single panels. If a global mode occurs, the ratio reaches a value of nearly 1 (-). Fully decoupled local modes show values nearby 0 (-). This discrete correlation of second order of a global mode is defined by

$$G^{II}_{i,j} = G^{I} \cdot \sqrt{\frac{\min\left[\overline{|u|}_{bi},\overline{|u|}_{bj}\right]}{\max\left[\overline{|u|}_{bi},\overline{|u|}_{bj}\right]}}, \qquad (-) \qquad (4.3)$$

where *i* represents the first panel (e.g., floor) and j represents the second panel (e.g., flanking wall). Here, the minimum of the averaged out-of-plane displacements is normalized to the maximum of the out-of-plane displacements to get a value range between 0 and 1. A high value near 1 indicates a high correlation of the eigenfrequencies of structure and cavity (G^I),

and additionally a high correlation of the vibration response of the single structural components.

A correlation third order for a global mode additionally includes the spatial correlation of the out-of-plane deformation of one of the single panels and the sound pressure in the cavity at the corresponding boundary. As shown in the global mode in Figure 4.8, panel 1 and panel 2 have a high spatial coupling of the structure and the cavity. This discrete correlation third order of a global mode is defined by

$$G_{i,j}^{III} = G_{i,j}^{II} \cdot \sqrt{\max_{bj}\left[\frac{|u|_{bj}}{\max(|u|_{bj})} \cdot \frac{|p|_{bj}}{\max(|p|_{bj})}\right]} \qquad (-) \qquad (4.4)$$

where u_{bj} represents the out-of-plane deformation and p_{bj} the sound pressure at the boundary b of panel j (wall). The second term of equation (4.4) indicates the maximum (max_{bj}) of the spatial correlation of an anti-node of a mode of a panel and the anti-node of the mode of the cavity. The out-of-plane deformation at the boundary has been normalized to the maximum of the out-of-plane deformation at the boundary. This normalization has been chosen additionally for the sound pressure at the boundary to ensure that the two different physical parameters get a comparable (dimensionless) value range. This procedure is chosen because the correlation even of one anti-node of a mode of a panel and one anti-node of a mode of the cavity at one single position leads to a distinctive excitation of the cavity.

If all resulting G^{III} get values nearby 1 (-), this seems to be the worst case because then, the eigenfrequencies and the mode shapes of all components of the structure and the cavity shows a high correlation.

Table 4.2 shows an overview of the introduced quantification using correlation of global modes of different order:

Correlation	$\mathbf{G^{I}}$	$\mathbf{G^{II}}$	$\mathbf{G^{III}}$
Value range (-)	0 - 1	0 - 1	0 - 1
Correlation of eigenfrequencies - structure / cavity	YES	YES	YES
Correlation of eigenfrequencies - panel / panel	NO	YES	YES
Spatial correlation of anti-nodes - panel / cavity	NO	NO	YES

Table 4.2: Characterization of global modes using variables for correlation of different order

Based on these definitions, the discrete correlation different order has been calculated using the described calculation model. In general, every mode of the structure has been compared to every mode of the cavity. Figure 4.9 and Figure 4.10 show the results. For case 1, the values for all correlation variables get high values, especially in the range of the first cavity modes at about 57 Hz. As shown in Figure 4.8, especially the eigenfrequency of the first structural mode is highly coupled to a mode of the cavity (G^{I}). Additionally, the panels are strongly coupled (G^{II}) and the panel 2 and the cavity show a spatial correlation of anti-nodes of the corresponding mode shapes. Compared to case 1, case 2 shows different eigenfrequencies of structure and cavity (G^{I}). The coupling of the local modes of the panels is reduced (G^{II}), therefore, the high spatial correlation of one mode is less problematic. Here, a high spatial correlation means that G^{II} and G^{III} get nearly the same values. All values of G^{II} and G^{III} are less than 0,5 (-) and as a consequence, the sound pressure level in the cavity is reduced. Similar to, e.g., the optimal difference of the dimensions of a measurement room with a minimum of 10 % that result in a difference of eigenfrequencies of 10 %, also here the frequency decoupling should be more than 10 % ($G^{I} < 0.9$).

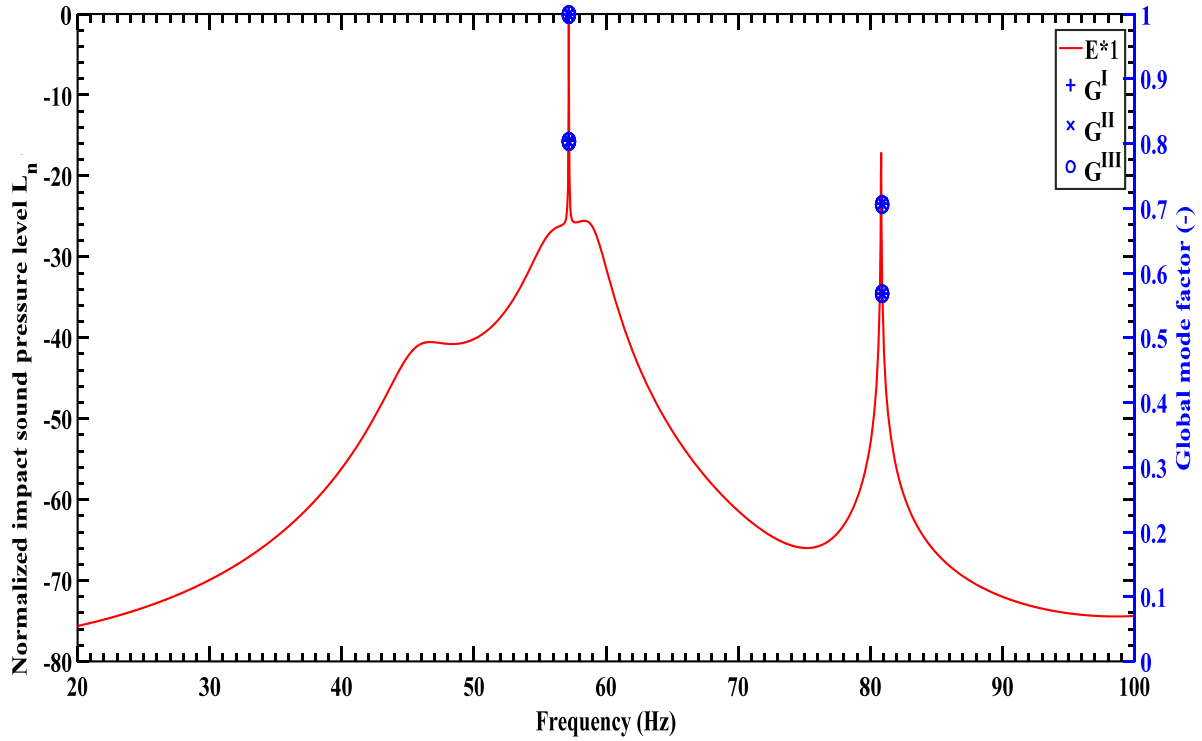

Figure 4.9:Calculation of discrete correlation – case 1

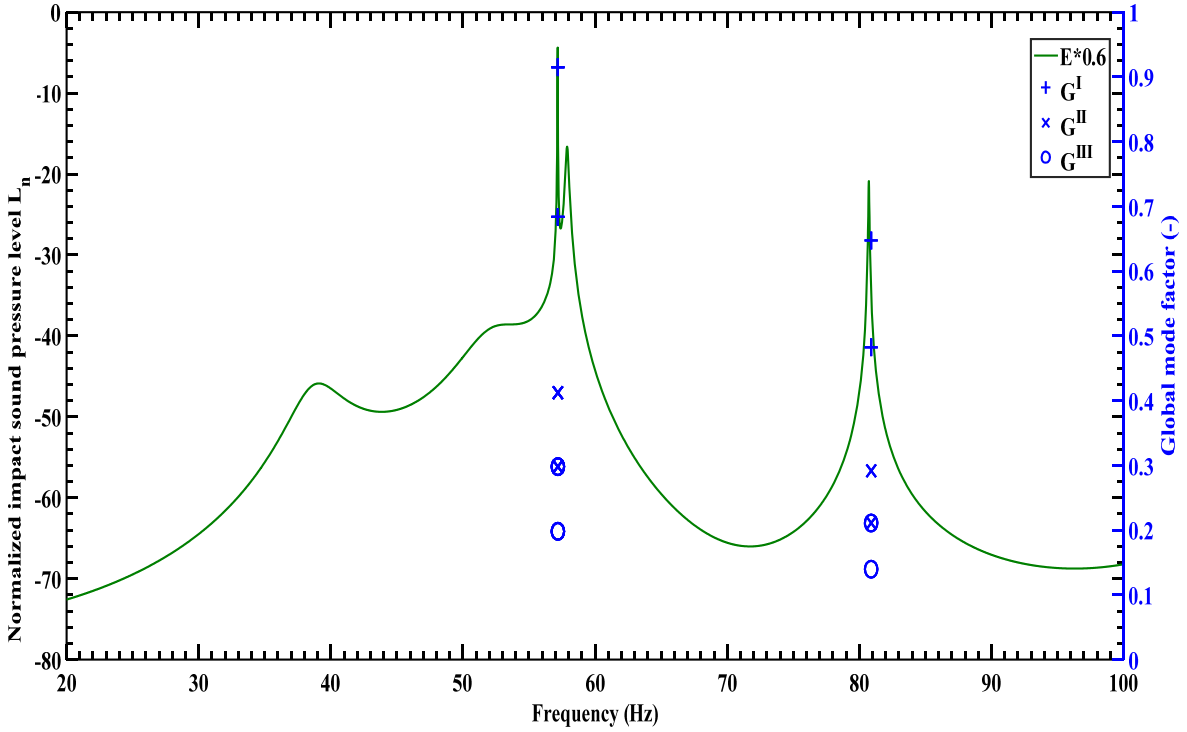

Figure 4.10: Calculation of discrete correlation – case 2

In the next section, the approach that the impact of a global mode can be reduced by a separation of its local modes will be extended for applications to CLT.

4.1.2 Application to cross-laminated-timber

4.1.2.1 Numerical Calculations

Based on the assumptions stated in the former chapter, 3D-calculation models of two adjacent rooms based on panels of CLT have been investigated. The aim is to investigate the influence of modal coupling, especially to impact sound insulation.

Figure 4.11 shows the resulting calculation model with a size of 2,9 m x 5,2 m x 2,6 m. These dimensions lead to a base area of about 15 m² of the final room, what corresponds to the base area of a typical sleeping room. To set practical boundary conditions for the junctions, the upper walls are additionally implemented to form horizontal junctions of T-shape.

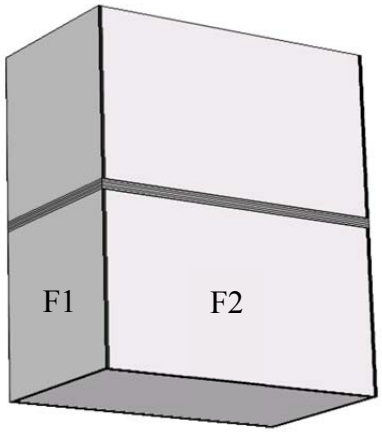

Figure 4.11: Geometry of the numerical model of two vertical rooms - F1: flanking wall 1; F2: flanking wall 2

The panels of CLT have been modelled using several layers of wooden boards based on a linear elastic, orthotropic material model. The layers of the panels are perpendicular to each other, depending on the fiber orientation. In chapter 3.1, material parameters for calculations of cross-laminated timber have been determined for panels without side-glued wooden boards. Today, side-glued panels are more popular, therefore calculations of this type of panel is preferred in this chapter. Table 4.3 contains the chosen material properties from literature, the indices 0° represent the parameters in-fiber-direction and the indices 90° represent the parameters perpendicular-to-fiber direction, as described by Kohrmann [29]. To allow a comprehensible investigation that is comparable with common used values, hysteretic damping has been implemented using a constant value of 0.01 for spruce [88]. The fiber direction of the floor has been chosen parallel to the longer flanking wall (F2).

	Material data			
Parameter	**ρ** **(kg/m³)**	**$E_{0°}/E_{90°}$** **(GPa)**	**$\nu_{0°/90°}$ - $\nu_{90°/90°}$** **(-)**	**c** **(m/s)**
CLT [29]	470 kg/m³	10,98/ 0,137	0,052/ 0,3	-
air	1,2	-	-	343

Table 4.3: Material data of the structure and of the air

Rigid boundary condition has been chosen, shown in Figure 4.12. The floor was excited using a rain-on-the-roof excitation with a unit force and an arbitrary phase. The geometry has been meshed using tetrahedron elements with a maximum element size of 0.15 m.

The cavity has been meshed with a maximum element size of 0.55 m. This is based on the calculation of the well known sampling of waves, based on wavelength/5 of highest frequency, e.g., shown by Petritsch [114]. The minimum number of degrees of freedom for 3-dimensional cavities can be defined by

$$g_{D,min} = 12^3 \frac{V_D}{\lambda_{min}^3} = 1728 \frac{V_D}{\lambda_{min}^3} = 1728 \frac{f_{max}^3 V_D}{c^3} \quad (-) \qquad (4.5)$$

where V_D represents the Volume of the Domain (m^3), λ_{min} the minimum wavelength (m), f_{max} the highest, investigated frequency (Hz) and c^3 the speed of sound (m/s). For this room, the minimum number of degrees of freedom by using quadratic shape functions is 2294 (-). The implemented room results in 12913 degrees of freedom, caused by the small element sizes near the boundaries. Exclusively the flanking walls have been coupled to the cavity to focus the investigations on flanking sound transmission.

Quadratic shape functions have been used for the structure, as well as the airborne sound field of the cavity. The calculation approach results in approximately 550 000 DOF, depending on the number of layers of the CLT panels.

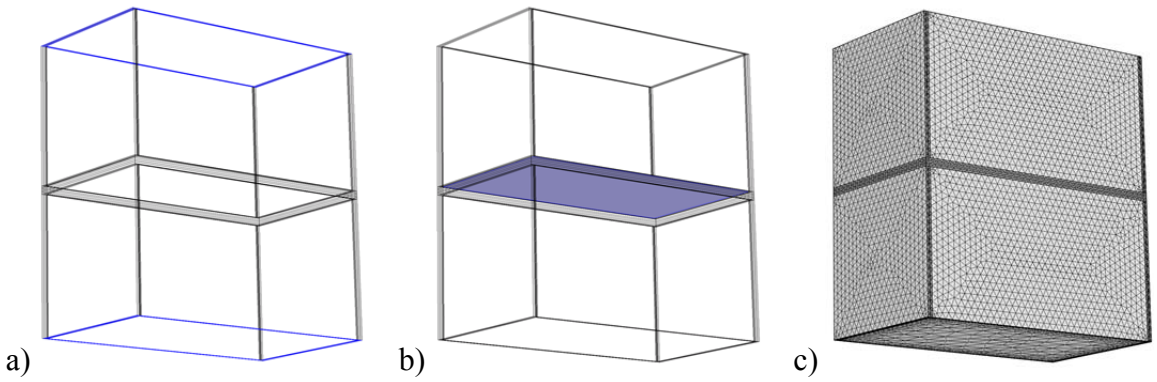

Figure 4.12: a) Fixed constraints of the model (displacement equal to zero);
b) rain-on-the-roof excitation of the floor; c) Resulting mesh of the geometry using tetrahedron elements

Based on this calculation model, the layers of the flanking panels have been varied using designs as shown in Table 4.4. The layers of the floor were kept constant. Every possible combination of the resulting flanking walls has been calculated. The investigated frequency range was defined from 17 Hz to 113 Hz. These are the rounded lower and upper cut-off frequencies of the one-third-octave bands at centre frequencies of 20 Hz and 100 Hz.

329 frequencies were solved using a logarithmic distribution within the mentioned frequency range.

	Thickness (mm)					
	Floor	Wall – Composition				
Panel Nr.		1	2	3	4	5
Layer 1	34	19	27	30	40	19
Layer 2	30	19	34	34	40	19
Layer 3	34	19	27	30	40	19
Layer 4	30					19
Layer 5	34					19

Table 4.4: Designs of the walls for parametric study

Combination	***1***	***2***	***3***	***4***	***5***	***6***	***7***	***8***	***9***	***10***	***11***	***12***	***13***
Composition -	1	2	3	4	5	1	2	3	4	5	1	2	3
Composition –	1	1	1	1	1	2	2	2	2	2	3	3	3

Combination	***14***	***15***	***16***	***17***	***18***	***19***	***20***	***21***	***22***	***23***	***24***	***25***
Composition -	4	5	1	2	3	4	5	1	2	3	4	5
Composition –	3	3	4	4	4	4	4	5	5	5	5	5

Table 4.5: Combinations of the panels of the flanking walls for parametric study

For further calculations, respective quantities have been defined as shown in Figure 4.13. Here, the bottom boundary of the floor (a), the interior boundary of flanking wall 1 (b) and flanking wall 2 (c), as well as the volume / domain of the cavity (d) have been used for further calculations.

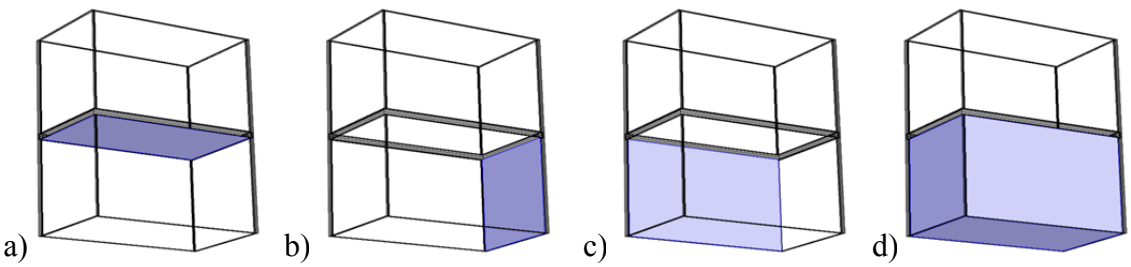

Figure 4.13: Definition of parts of the geometry- a) boundary 1 (floor); b) boundary 2 (flanking wall 1); c) boundary 3 (flanking wall 2); d) domain 1 (source room)

4.1.2.2 Results and Discussion

The results of the calculations show the influence of global modes for the panel designs as described in Table 4.4. Caused by the low mass and high bending stiffness of the CLT panels, they show a low modal density and -overlap especially in the frequency range of 20 Hz to

100 Hz. Variations in bending stiffness lead to a shift of the eigenfrequencies of the single panel. These variations can be caused, e.g., by a variation of the designs of the single panels. Using an adjusted combination of the panels, the eigenfrequencies can be separated from each other to reduce the acoustic response of adjacent panels respectively for the air-borne sound field, as shown in chapter 4.1.1.2. For this purpose, the model has been solved for all 25 possible solutions of the compositions shown in Table 4.4. First, the spatial averaged sound pressure level in the receiving room has been calculated and averaged over the whole frequency range.

Figure 4.14 shows the results for the impact sound level of the investigated combinations that differs depending on the combination of the panels. Furthermore, the discrete correlations of different order for global modes as described in section 4.1.1.2 are calculated for each possible combination of the 12 relevant modes of the cavity and of the 90 relevant modes of the structure. These correlations are calculated for each solution, respectively combination shown in Table 4.5, which results in a total of 1080 factors for G^{I}, 2160 factors for G^{II} and 2160 factors for G^{III}. The sums of the correlation factors with values higher than 0.8 G^{I} , G^{II} and G^{III} are illustrated. The aim is to determine correlations between the final sound pressure level in the cavity and global modes. Several solutions show that a high number, especially, of high ordered global modes might result in a high averaged sound pressure level in the cavity, e.g. solution 24, where also a global mode with a correlation of third order occurs.

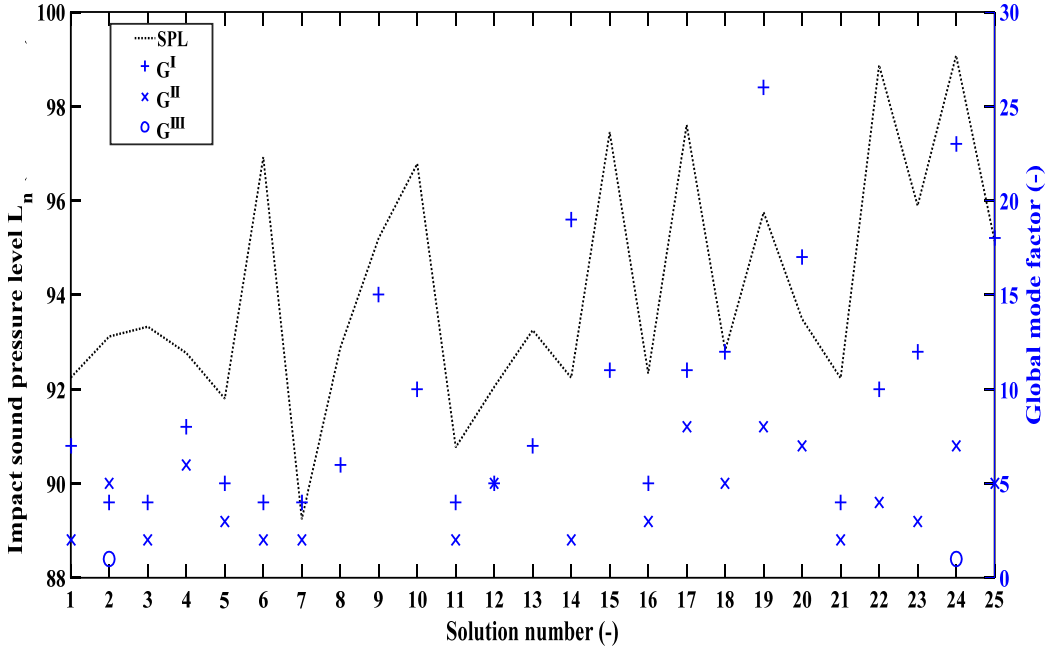

Figure 4.14: Spatially and frequency averaged sound pressure level for all possible combinations / solutions, compared to the number of discrete correlation factors of different order within the investigated frequency range

Solution 7 and solution 24 have been chosen because an uncommon effect has been noticed. A typical rule of thumb in building acoustics states that increasing mass leads to an increasing sound insulation. Here, a different observation was made. Solution 7 shows low sound pressure level and global modes, subsequently defined as case 1 and solution 24 shows a high sound pressure level and global modes, subsequently defined as case 2. But in difference, solution 7 (case 1) is based on calculations on CLT panels with less thickness and therefore, less mass than solution 24, thus this rule of thumb is inversed. Table 4.6 contains the corresponding composition of the CLT panels of these solutions.

	Thickness (mm)				
	Floor	Case 1 (solution 7)		Case 2 (solution 24)	
		F1	F2	F1	F2
Layer 1	34	27	27	40	19
Layer 2	30	34	34	40	19
Layer 3	34	27	27	40	19
Layer 4	30				19
Layer 5	34				19
Panel	162	88	88	120	95
F1+F2		176		215	

Table 4.6: Comparison of a low-level (case 1) and a high-level (case 2) solution

Figure 4.15 and Figure 4.16 show the resulting sound pressure level in the cavity, compared to the global modes and the corresponding mode shapes of the structure and the cavity. A different kind of coupling of the subsystems is observed for the two situations that lead to different sound pressure levels in the receiving room. For both situations, the same damping mechanism has been chosen in the models (hysteretic damping with a constant value of 0.01 for spruce). Modes in case 1 are defined by g_1-g_4 and modes in case 2 are defined by r_1-r_4. Caused by the same sizes of the rooms for both cases, the mode shapes and the eigenfrequencies of the room are assumed to stay constant ($a_1 - a_4$). The sound pressure level is normalized to the maximum of the two situations within the investigated frequency range.

A global mode showing a correlation of 1st order occurs for the mode of the cavity (a_1) at 33 Hz that is strongly coupled to the first mode of the floor of case 1 (g_1). But the first mode of the floor of case 2 (r_1) shows a stronger coupling caused by the less difference in eigenfrequency and this leads to an increasing sound pressure within the range from 17 Hz to about 40 Hz.

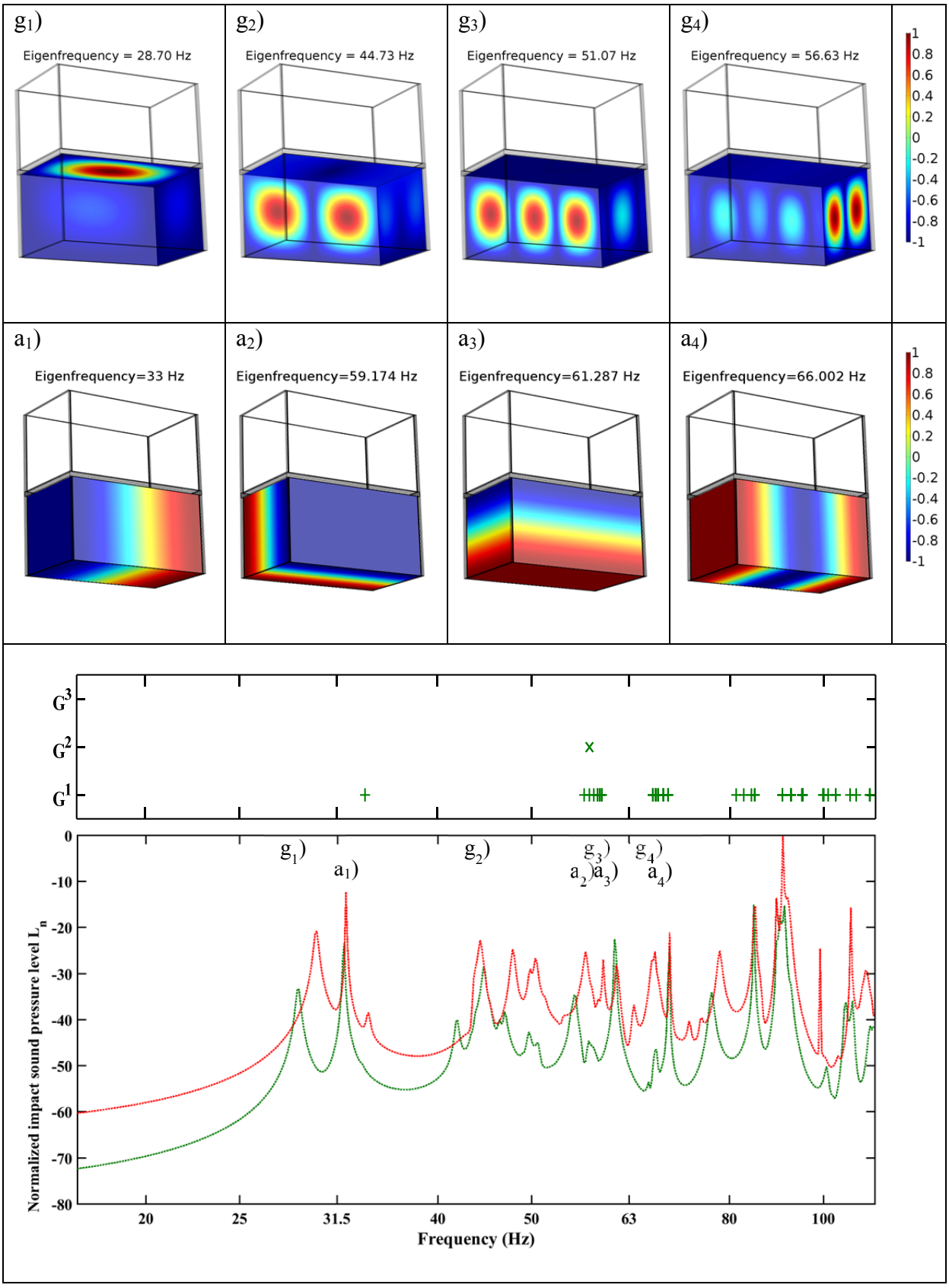

Figure 4.15: Detailed analysis of the different cases – Normalized sound pressure level of the case 1 (green) and the case 2 (red); Mode shapes of case 1 (gi) and the air-borne sound field (a_i)

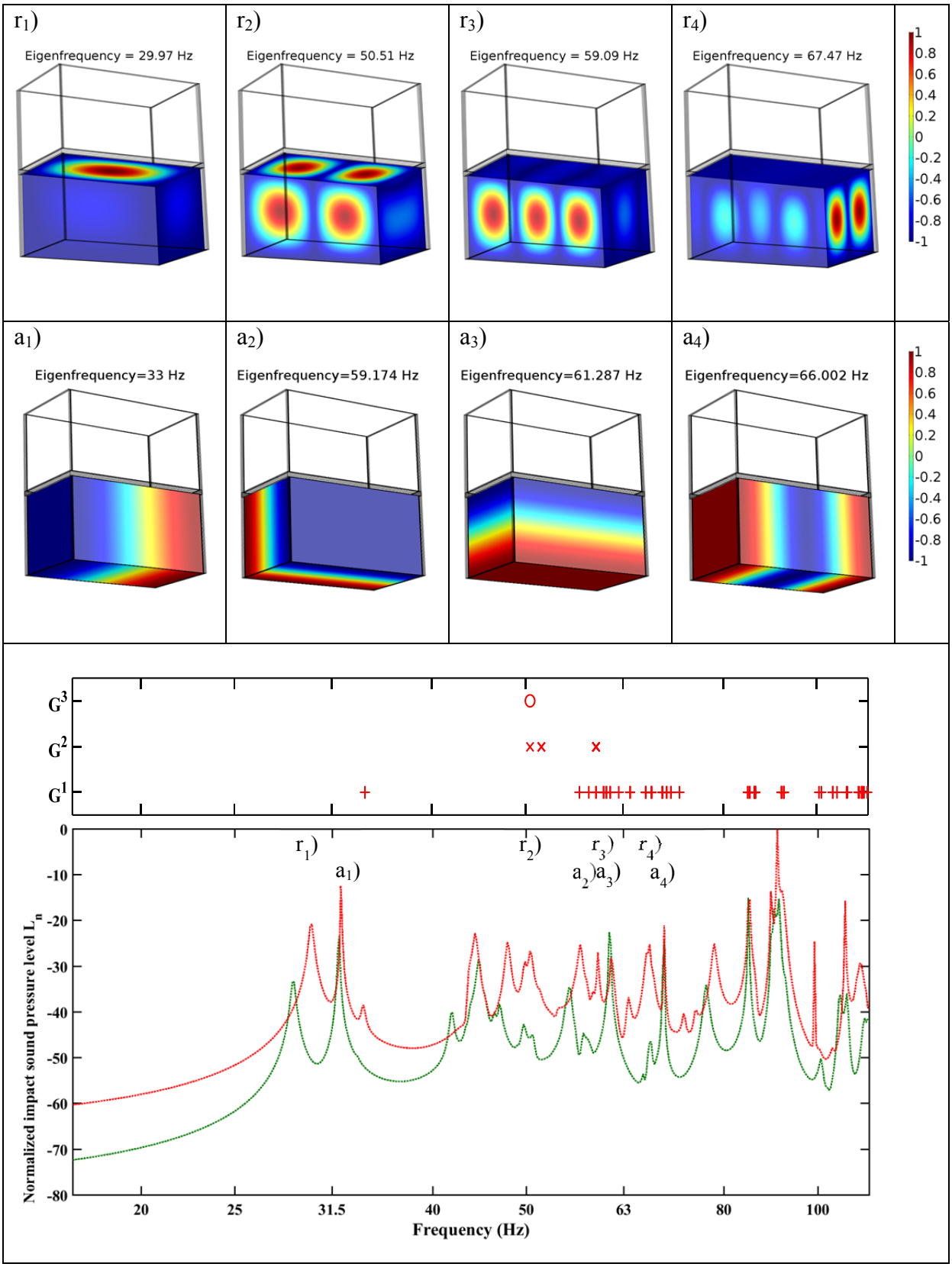

Figure 4.16: Detailed analysis of the different cases – Normalized sound pressure level of the case 1 (green) and the case 2 (red); Mode shapes of case 2 (r_i) and the air-borne sound field (a_i)

Furthermore, a global mode showing a correlation of 3rd order arises for the mode of the cavity (a_2) at 59.174 Hz. The structural mode of case 2 (r_2) shows a small difference in eigenfrequency and a high coupling of the local modes of the (excited) floor and flanking wall 2. Additionally, a comparison of the shapes of the local mode of flanking wall 2 and the cavity result in a high correlation. As a consequence, a high sound pressure occurs within the frequency range of about 47 Hz to 55 Hz. Compared to this situation, the alternative situation in case 1 does not lead to a global mode showing a correlation of any order, because on the one hand, the difference in eigenfrequency of the modes of the structure (g_2) and the cavity (a_2) is much larger. On the other hand, the local modes of the floor and the flanking wall 2 show a minor coupling. Similar to case 2, the mode shapes of the flanking wall 2 and the cavity correlate. Nevertheless, this observation does not result in a high sound pressure in the cavity.

Within the range of about 55 Hz and 83 Hz, several global modes showing a correlation of 1st order occur for both cases. Here, the increasing sound pressure level in the cavity of case 2 is caused by some modes of the structure (e.g. r_3 and r_4) that highly correlate with the eigenfrequencies several modes of the cavity (e.g. a_3 and a_4). Few of them additionally show a correlation of the mode shapes (e.g. r_4 and a_4). Compared to this situation, similar mode shapes of the structure are obvious for case 1, but the eigenfrequencies of structural modes and the modes of the cavity are more regular distributed in the frequency spectrum. Therefore, the difference in eigenfrequencies is much higher than the one of case 2. The number of discrete correlations of global modes of 1st order is significantly decreased as well as the sound pressure in the room.

A comparison of the mean values of the sound pressure within the investigated frequency range shows a level difference of 9.8 dB for the two cases, thus an improvement can be achieved by using less material for the flanking walls.

4.2 Wave Transformation

In general, the sound radiation of a panel is based on the out-of-plane movement of the structure. Nevertheless, the in-plane movement can carry a significant part of the total vibration energy. Wave transformation describes the conversion of out-of-plane components to in-plane components, e.g., in corners. This effect may become important at junctions, where incoming bending waves are transformed not only in outgoing bending waves but also in quasi-longitudinal waves. These waves may not directly contribute to the sound radiation but they can carry a significant part of the overall energy. Further, these quasi-longitudinal waves travel to other junctions (second order nodes), where they can be converted to bending waves, which again contribute to the radiated sound.

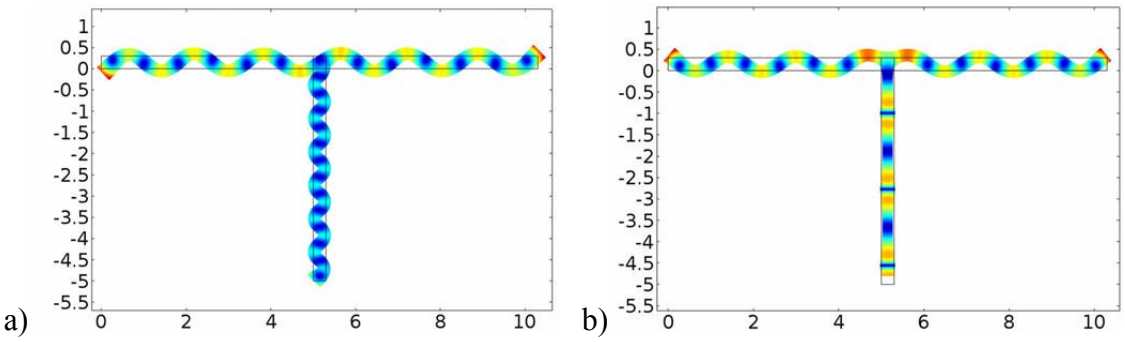

Figure 4.17: Principle of the effect of wave transformation – a) transmission of bending waves; b) conversion of bending to quasi-longitudinal waves

Here, the effect of wave transformation is studied using numerical models based on the FEM. First, the focus lies on the relevance and the impact of a path of second order on the total sound radiation into the receiving room. The frequency ranges, where the contribution of such a path seems to be significant are determined. The correct measurement of the flanking sound reduction index depends on the existing waveforms in the structure. A transformation of out-of-plane components to in-plane components can cause an error in the determination of the flanking sound reduction index, if it is determined only by the out-of-plane movement of the vibrating surface. This data is the input for calculations of the sound insulation between adjacent rooms due to EN 12354-1. If not the whole transmitted energy is determined by the measurement procedure, the error propagates in the calculation methods and results in an erroneous prediction of the sound insulation. Subsequently, the vibration behaviour of an adapted model is investigated at specific single frequencies especially within the frequency range, where also the coincidence frequency occurs. To allow a study of the physical

processes of wave transformation and the sound radiation of the CLT panels close to reality, a cavity is included and the investigated frequency range focus on 50 Hz to 630 Hz. Based on this assumption, the effect of wave transformation is studied and its presence is validated using experimental measurements on a comparable mock-up in real size. Finally, the investigations in this chapter show that this effect acts in the same frequency range as the coincidence effect. The coincidence effect or rather, its position in the frequency spectrum represents a fundamental criterion for the sound performance of a building construction. Caused by the orthotropy of the panels of cross-laminated timber, the material shows several coincidence frequencies. These frequencies are located in the mid-frequency range of about 200 Hz to 1000 Hz, depending on the composition of the panel [115]. The effect leads to an increased absorption and sound radiation and as a consequence, it leads to a decreased sound insulation. Therefore, modifications like additional linings have to be used to compensate the negative impact of this effect which is essential for direct- and flanking sound transmission. Concerning flanking sound transmission, alternative approaches can be used, since the sound energy must first pass the junction before radiating in the adjacent room. The aim is to produce a transformation of out-of-plane components to in-plane components in a junction of first order but suppress an inverse transformation in the junction of second order. As a result, the main part of the structure borne sound energy remains in the in-plane components of the wave and a radiation to the adjacent room is suppressed.

4.2.1 Numerical investigations on the relevance and impact of the effect to CLT

In this chapter, the FEM has been used to focus on numerical investigations in the low- and mid-frequency range. Figure 4.18 shows the geometry chosen. A commonly used T-shape has been extended to an H-shape of rigidly connected panels to generate a path of second order and a junction of second order. The dimensions (see Table 4.7) comply with the requirements of the standard ISO 10848-1 [90].

	Dimension (m)			Ratio (-)
	Width	Depth	Height	ISO 10848-1
Separation wall	3,6	0,12	2,3	0,31
Flanking SR	4,7	0,12	2,3	0,12
Flanking RR	4,15	0,12	2,3	0,13

Table 4.7: Dimensions and ratios of the walls

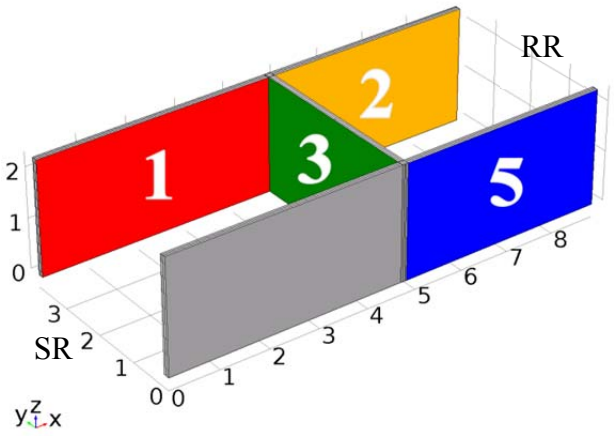

Figure 4.18: Geometry of the FEM model

These dimensions result in a base area of the receiving room (RR) of about 15 m² that is comparable to a commonly used sleeping room. The surfaces of the walls are able to vibrate freely. The constraints at the side faces have been set to zero (i.e., displacements are equal to zero) to approximate rigid floors, ceilings and rear walls (Figure 4.19), therefore, in-plane waves can occur [5]. One aim of these investigations is to evaluate the relevance of a flanking transmission path of second order. Therefore, the vibrating walls have to radiate sound energy equal to a real situation. Except the implemented walls, the sound absorption of the boundaries of the rooms has been calibrated to a reverberation time of 0.5 s, using uniform distributed wall impedances (Figure 4.19).

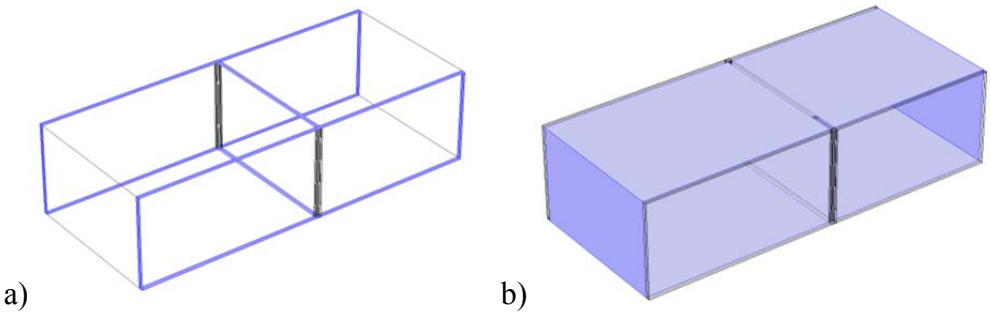

Figure 4.19: a) Fixed constraints; b) absorbing wall surfaces of the source and the receiving room

The CLT-panels have been modelled using three linear-elastic orthotropic layers. The interior layer is perpendicular to the exterior layers with respect to the fibre orientation. To compare the obtained results to concrete, the same geometry has been combined with a linear-elastic isotropic material law using common parameters (see Table 4.8).

	ρ (kg/m³)	$E_{0°}$/ $E_{90°}$ (GPa)	$\nu_{0°/90°}$ / $\nu_{90°/90°}$ (-)
CLT [14]	470	10,98 / 0,137	0,052 / 0,3
Concrete [116]	2300	25	0,33

Table 4.8: Material properties of the FEM - Model

Based on the discussion in section 2.3, hysteretic damping has been implemented using a constant value of 0.01 for spruce [88] to allow a comprehensible investigation, which is comparable with common used values.

A FEM model of two real sized rooms requires high computational power to allow comprehensive investigations within a wide frequency range. An effective meshing and frequency resolution is needed to reduce the computational costs. For this purpose, some preliminary studies have been performed to optimize the calculation procedure. The details are shown in section 4.2.1.1.

Wall 1 has been excited using an arbitrarily distributed, random force perpendicular to the surface. As a consequence, this excitation induces a high level of out-of-plane vibration and a low level of in-plane vibration. The reactions of the walls have been evaluated using the spatial averaged velocities of the whole walls. A reduction to the diffuse areas of the vibrating surface is commonly used by excluding the near fields close to the boundaries [90]. But it has to be kept in mind that different wave types show different wavelength, modal densities and modal overlapping. Therefore it is not possible to define an area of diffusivity that is valid for every type of wave. A reduction of the evaluation areas may lead to an over- or underestimation of the spatial averaged movement components and, subsequently, may cause an error during analysing the vibration behaviour of the structure.

The investigated frequency range was chosen within the range of one-third-octave-bands between 50 Hz and 1250 Hz. Frequency averaging in one-third-octave-bands have been carried out using the frequency ranges and requirements described in the standard IEC 61260-1 [117].

The aim of this study is to evaluate the in-plane displacement exclusively caused by longitudinal waves. Bending waves also cause in-plane displacements at the surfaces of the walls. The amount of these in-plane displacements increases with decreasing wavelength. In

contrast to this, bending waves do not produce in-plane displacements in the mid-surface (white area in Figure 4.20).

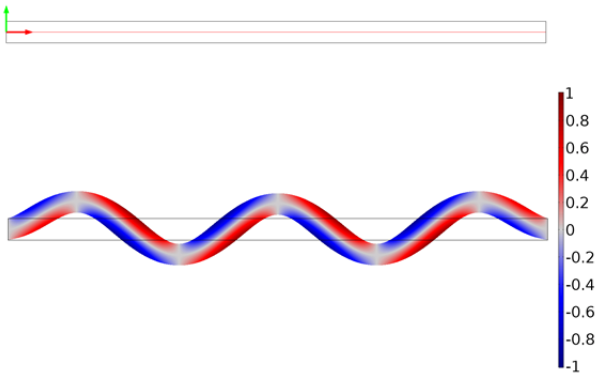

Figure 4.20: a) Mid-surface of a 2D – solid model (upper); b) normalized in-plane displacement (m) caused by a bending wave

The approach to investigate the mid-surface has been extended to full walls to reduce the influence of bending waves to the evaluated in-plane movement (Figure 4.21). To get a reliable ratio of out-of-plane components to in-plane components, the values have been spatially averaged over the mid-surface of the walls (red-coloured section in Figure 4.21).

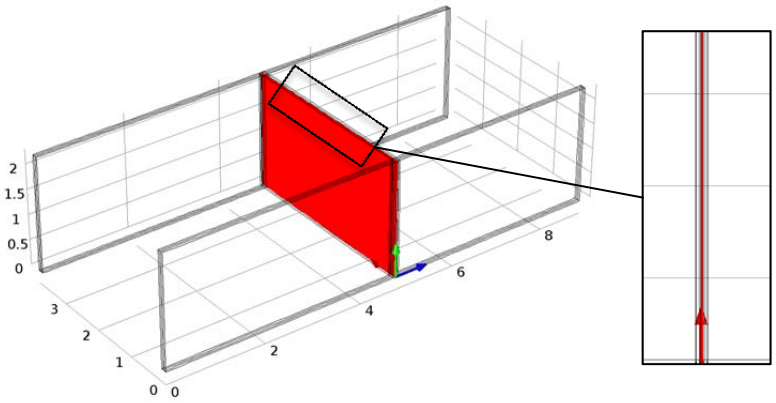

Figure 4.21: vertical cross-section of the separation wall

Based on these assumptions, the physical parameters have been evaluated for the walls, shown in Figure 4.18.

4.2.1.1 Meshing strategy using hexahedron elements

Meshing of the geometry is an essential step for a comprehensive investigation using FEM-models. In chapter 3.1, preliminary studies of the panels of cross-laminated timber have been

performed for further investigations, especially, in flanking sound transmission calculations. Here, suitable mesh sizes especially, for calculations of the out-of-plane vibration have been determined. In this chapter, the aim is to additionally investigate in-plane vibrations. Therefore a different meshing strategy has been chosen. Preliminary investigations have been performed to determine a meshing procedure that allows precise calculation of the vibration behaviour of out-of-plane and in-plane vibrations and an optimized usage of the available calculation resources. The used hexahedron elements were set to the thickness of one layer of the CLT panels of 4 cm that defines a unit thickness. The widths and heights of the elements were adjusted to the unit thickness and scaled using a factor (mesh-factor) such that they are able to represent the investigated one-third-octave-band frequency. This procedure has been performed for each one-third-octave-band separately (Figure 4.22).

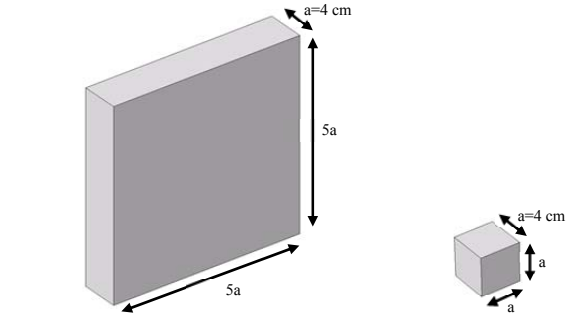

a)

Figure 4.22: Meshing of the geometry – a) element sizes for the discretization of the layers of the CLT panels: coarsest mesh (left) - mesh-factor = 5; finest mesh (right) - mesh-factor = 1;

Cube shaped elements (mesh-factor 1) have been chosen as a reference, because this mesh results in 3763011 DOF, which was within the limits of the calculation resources. Several eigenfrequencies near the upper limit of the one-third-octave-band have been determined depending on mesh-factors between 1 and 5. Quadratic shape functions have been used. For this study the level differences

$$D_{13}=10\,\lg\left[\frac{\mathrm{mean}_{b,1}(|u|)}{\mathrm{mean}_{b,3}(|u|)}\right] \quad \text{(dB)} \quad (4.6)$$

of the spatially averaged norm of the displacements u of wall 1 and wall 3 have been evaluated for each mesh-factor. The results are shown in Figure 4.23 for the lowest and highest investigated one-third-octave-band.

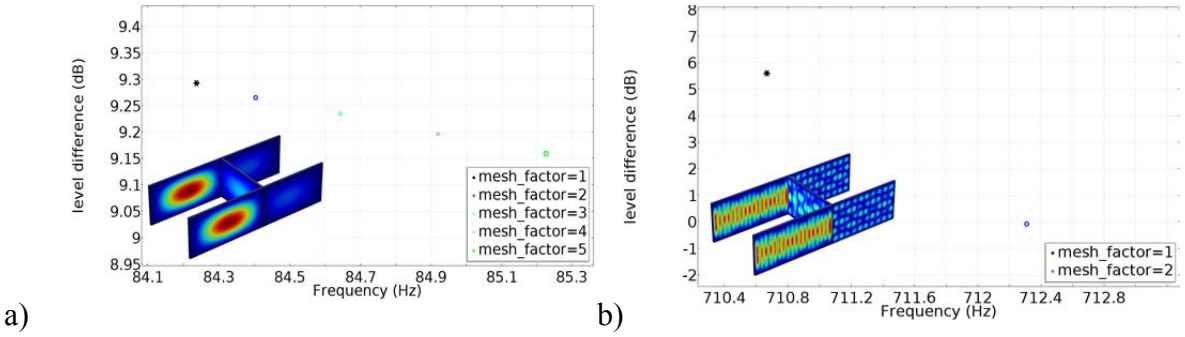

Figure 4.23: Determination of suitable mesh sizes - a) Level difference of the spatially averaged norm of the displacement of wall 1 and wall 3 for the first eigenfrequency b) Level difference of the spatially averaged norm of the displacement of wall 1 and wall 3 for the highest eigenfrequency within the one-third-octave-band of 630 Hz

A deviation of less than 0.1 dB and of 1 Hz (at lower frequencies) of the different solutions to the solution of mesh 1 has been chosen as a decision criterion for the used (reduced) mesh size. It is not possible to determine the vibration shape shown in Figure 4.23, using mesh-factor 3, 4 and 5, as these meshes are too coarse to represent this mode. This procedure has been repeated for every one-third-octave-band to get the optimal meshing-factor for the investigations. The sampling of the air borne sound field has been implemented using cube shaped hexahedron elements with a side length of 4 cm, multiplied with the corresponding mesh-factor for every edge. Quadratic shape functions have been used also for the airborne sound field. Figure 4.24 shows the mesh of the whole geometry including the airborne sound fields with a mesh-factor of 2 and the mesh sizes of the lowest and highest investigated eigenfrequencies.

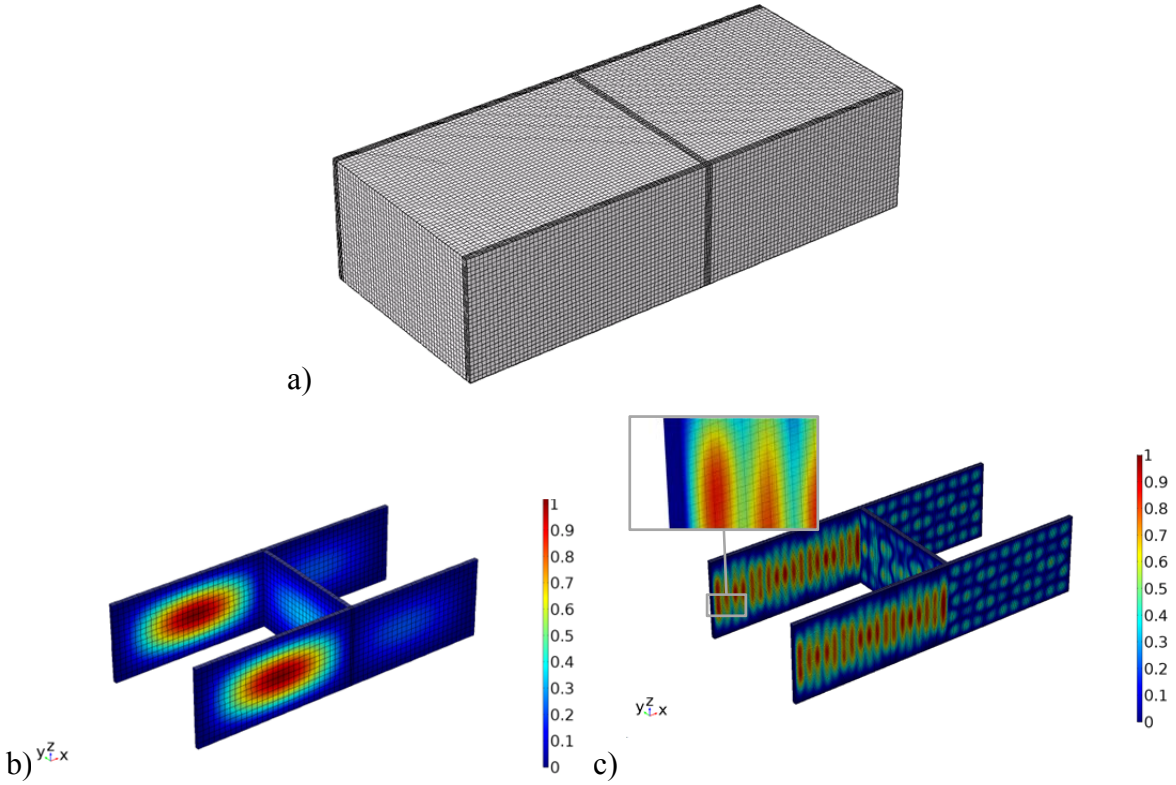

Figure 4.24: Meshing of the geometry – a) Meshing of the total geometry (mesh-factor 2); b) Mesh and results at an eigenfrequency of 84.92 Hz; mesh at an eigenfrequency of 710.64 Hz

Based on the determined mesh sizes, the frequency resolution has been optimized. Every one-third-octave-band has been separated in a fixed number of frequencies. Based on this number of frequencies, constant frequency steps were calculated for each one-third-octave-band. The resulting resolution is shown in Table 4.9.

One-third-octave-band (Hz)	Mesh factor (-)	Number of frequencies (-)	Frequency step (Hz)
50	4	27	0.44
63	4	32	0.47
80	4	37	0.51
100	3	42	0.56
125	3	47	0.63
160	3	52	0.72
200	3	57	0.82
250	3	62	0.95
315	3	67	1.11
400	2	72	1.29
500	2	77	1.52
630	1	82	1.80

Table 4.9: Mesh factors and frequency resolution for one-third-octave-band averaging

4.2.1.2 Relevance of the effect

The sound power radiated by the walls of the receiving room has been evaluated to get an impression, whether including paths of second order may influence the calculated total sound energy transmission between the adjacent rooms or not. The radiated power can be calculated using the out-of-plane velocity of the surfaces, while assuming the same radiation efficiencies for all walls. Calculations near the coincidence frequency may be sensitive to structural variations. It has to be kept in mind that usually the coincidence frequency of CLT is in the investigated mid-frequency range. Here, radiated sound power

$$P_i = \rho c \overline{v^2} S \sigma \quad \text{(W)} \quad (4.7)$$

of the single walls i was calculated depending on the density of air ρ (kg/m³) and the speed of sound in air c (m/s). The out-of-plane velocities v have been spatial averaged using the surface S of the walls, but compared to the areas defined in Figure 4.18, the areas have been reduced to the center of the panels, as shown subsequently in Figure 4.25. Same values for the radiation efficiency σ have been assumed for every wall because of the same composition and similar widths.

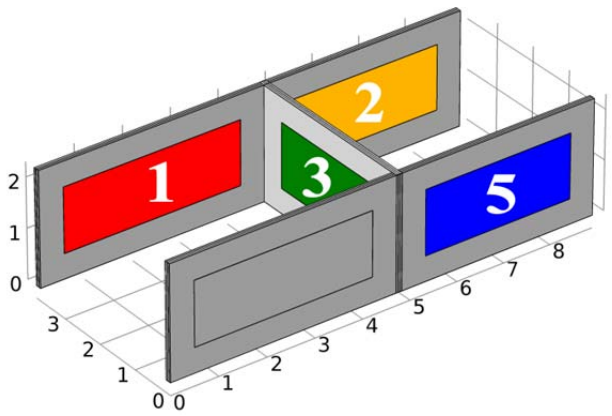

Figure 4.25: Geometry of the FEM model

The sum of the radiated sound power of walls 2 and 3 has been compared to the sum of the radiated power of walls 2, 3 and, additionally, wall 5

$$\Delta L_w = 10\,lg\left[\frac{P_2 + P_3 + P_5}{P_2 + P_3}\right] \quad , \qquad \text{(W)} \quad (4.8)$$

to shows the increasing one-third-octave based values of the air-borne sound power by including wall 5 (Figure 4.26).

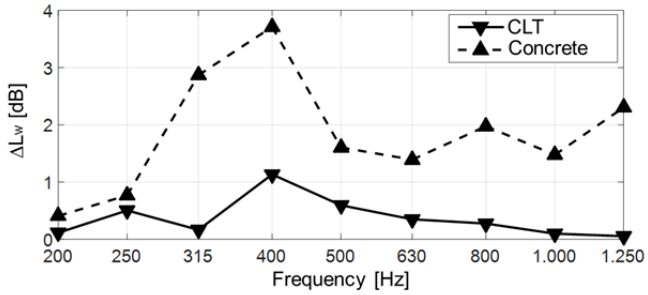

Figure 4.26: Contribution of sound radiation of wall 5 to the air-borne sound power of the receiving room

In general the reduction of the transmitted energy in the structure is depending on internal losses, radiation, flanking transmission to adjacent elements and the damping caused by the junction. The CLT model shows less influence of wall 5 caused by the high dissipation.

Depending on the required accuracy of the final prediction procedure, the additional power contribution of wall 5 may be neglected. In practice, the CLT-plates are not rigidly connected, so the resulting velocity at wall 5 as well as the sound radiation should decrease. In addition, a high radiated power caused by wall 5 seems to be evident in the concrete model. To prove, if a wave transformation occurs and if it has an effect on the transmission, the contribution of the out-of-plane component to the total movement has been evaluated.

Figure 4.27 and Figure 4.28 show the ratio of the spatial averaged squared velocities of the out-of-plane component to the sum of all velocity directions (norm of velocity) for wall 1, 2, 3 and wall 5

$$\text{ratio} = \frac{\overline{v^2_{oop}}}{\sum \overline{v^2_i}} \qquad \text{(-)} \quad (4.9)$$

A high ratio represents a high proportion of out-of-plane components and a low ratio represents a high proportion of in-plane components. Bending waves also cause in-plane displacements at the surfaces of the walls, but do not produce in-plane displacements in the mid-surface (cf. Figure 4.20). Therefore, in-plane displacements at this mid surface have

been evaluated to separate bending waves (out-of-plane components) and in-plane waves (in-plane components in the mid-surface).

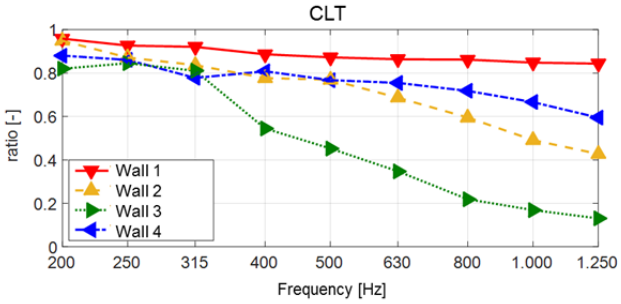

Figure 4.27: Ratio of out-of-plane components to the sum of out-of-plane and in-plane components (CLT)

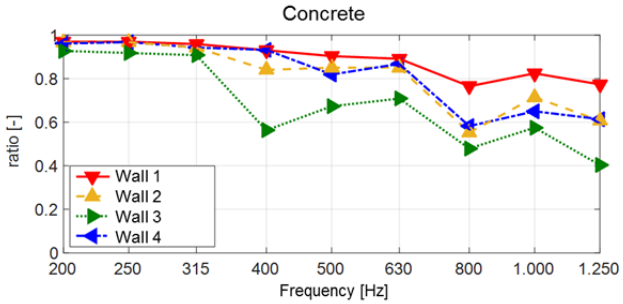

Figure 4.28: Ratio of out-of-plane components to the sum of out-of-plane and in-plane components (concrete)

As expected, the excited wall 1 shows a high level of out-of-plane velocities. More or less, a transformation process appears for both materials shown by the various ratios for the different walls. The separating wall 3 partly shows significant smaller ratio of out-of-plane velocity compared to the flanking walls 1 and 5. Therefore, this effect may be interpreted as a wave transformation from - as an example - bending-wave in wall 1 to a quasi-longitudinal wave in wall 3 and an inverse-transformation of the quasi-longitudinal wave in wall 3 to a bending wave in wall 5.

In a next step, the out-of-plane velocity level difference

$$D_{13}=10 \lg \left[\frac{\overline{v^2_1}}{\overline{v^2_3}} \right] \quad \text{(dB)} \qquad (4.10)$$

has been compared to the real reduction of the total kinetic energy density

$$E_{kin,13}=10\,\lg\left[\frac{\overline{E_{kin,1}}}{\overline{E_{kin,3}}}\right] \quad \text{(dB)} \qquad (4.11)$$

of wall 1 and wall 3 (Figure 4.29 and Figure 4.30). The total kinetic energy density includes all vibration directions and has been volume-averaged in the areas of the evaluation surfaces.

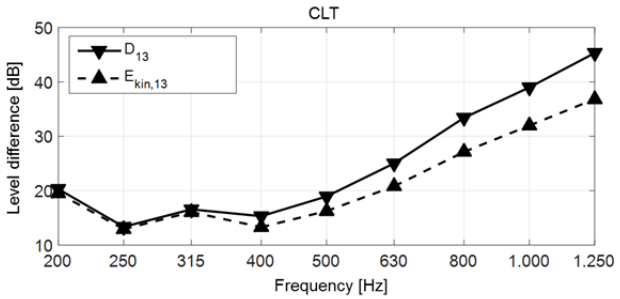

Figure 4.29: Velocity level difference compared to the level difference of the total kinetic energy density (CLT)

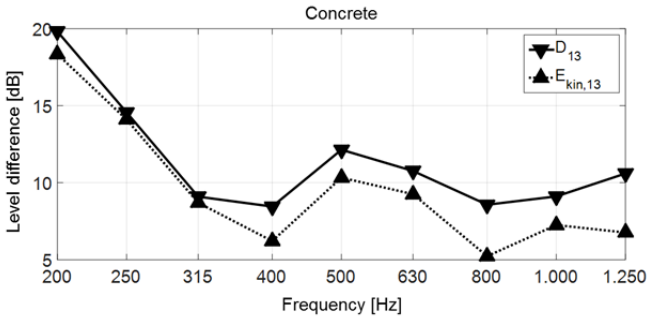

Figure 4.30: Velocity level difference compared to the level difference of the total kinetic energy density (concrete)

Figure 4.31 and Figure 4.32 allow the conclusion that the standardized out-of-plane velocity level difference does not include the total transmitted kinetic energy. It underestimates the transmission respectively, finally overestimates the flanking sound insulation, shown by the deviation of the out-of-plane velocity level difference to the transmitted kinetic energy. Furthermore, a comparison to the difference of the logarithmic ratios of the out-of-plane components is shown (see Figure 4.29 and Figure 4.30). Both graphs strongly correlate for both materials.

This high correlation is caused by the fact that, finally, the deviation between the out-of-plane velocity level difference and the difference of total kinetic energy density results in a similar calculation using the same velocity components, as shown in equations (4.12) and (4.13).

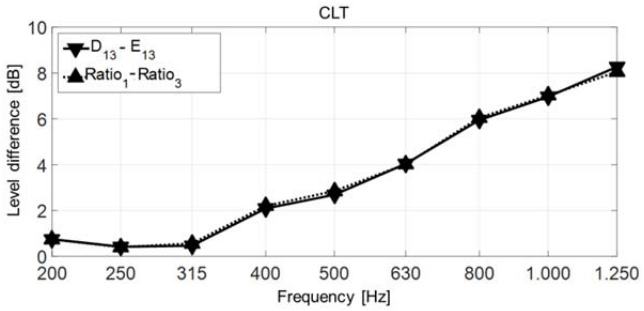

Figure 4.31: Correlation between deviation of velocity and energy based level differences and wave transformation (CLT)

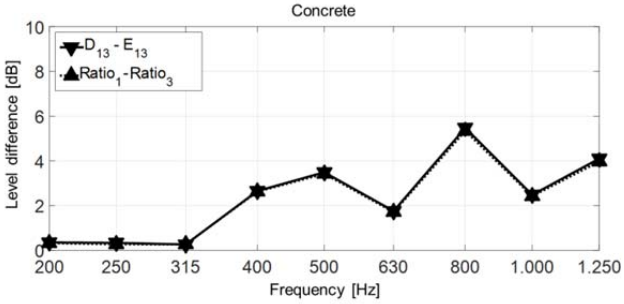

Figure 4.32: Correlation between deviation of velocity and energy based level differences and wave transformation (concrete)

$$D_{13} - E_{kin,13}$$

$$= 10 \lg \left[\frac{\overline{v^2_{1,oop}}}{\overline{v^2_{3,oop}}} \Big/ \frac{\overline{E_{kin,1}}}{\overline{E_{kin,3}}} \right]$$

$$= 10 \lg \left[\frac{\overline{v^2_{1,oop}} \; {}^1\!/_2 \, \rho \left(\overline{v^2_{3,x}} + \overline{v^2_{3,y}} + \overline{v^2_{3,z}} \right)}{\overline{v^2_{3,oop}} \; {}^1\!/_2 \, \rho \left(\overline{v^2_{1,x}} + \overline{v^2_{1,y}} + \overline{v^2_{1,z}} \right)} \right] \quad \text{(dB)} \quad (4.12)$$

$$= 10 \lg \left[\frac{\overline{v^2_{1,oop}} \left(\overline{v^2_{3,x}} + \overline{v^2_{3,y}} + \overline{v^2_{3,z}} \right)}{\overline{v^2_{3,oop}} \left(\overline{v^2_{1,x}} + \overline{v^2_{1,y}} + \overline{v^2_{1,z}} \right)} \right]$$

$$\mathrm{Ratio}_1 - \mathrm{Ratio}_3$$

$$= 10 \lg \left[\frac{\overline{v^2_{1,oop}}}{\left(\overline{v^2_{1,x}} + \overline{v^2_{1,y}} + \overline{v^2_{1,z}} \right)} \Big/ \frac{\overline{v^2_{3,oop}}}{\left(\overline{v^2_{3,x}} + \overline{v^2_{3,y}} + \overline{v^2_{3,z}} \right)} \right] \quad \text{(dB)} \quad (4.13)$$

$$= 10 \lg \left[\frac{\overline{v^2_{1,oop}} \left(\overline{v^2_{3,x}} + \overline{v^2_{3,y}} + \overline{v^2_{3,z}} \right)}{\overline{v^2_{3,oop}} \left(\overline{v^2_{1,x}} + \overline{v^2_{1,y}} + \overline{v^2_{1,z}} \right)} \right]$$

This conclusion emphasises the hypothesis that a wave transformation process in a junction leads to an underestimation of the real transmitted kinetic energy, if measurement values of common used standards ([89], [90]) are used. The small deviations between the values in Figure 4.31 and Figure 4.32 are caused by the different areas for spatial averaging: the sum of the components for the ratio calculation was averaged using the surface, whereas the kinetic energy densities were averaged using the volume.

In general, four cases of wave transformation exist during wave propagation across two independent junctions. Table 4.10 shows an interpretation of these cases, whether wave transformation may be a problem or not. If no transformation occurs, the out-of-plane velocity level difference is comparable to the reduction of total kinetic energy that finally leads to sound radiation (case A). Approximately this case is evident in Figure 4.27 at third-octave bands from 200 Hz to 315 Hz. A wave transformation in one of the two junctions transforms energy into in-plane movements that, finally, do not lead to sound radiation (case B and C). As a consequence, this effect reduces the sound transmission between two rooms. A problem occurs if the transformed components of junction 1 are inverse transformed in a second junction (case D). This case is evident in Figure 4.27 in the range of third-octave bands from 400 Hz to 1250 Hz. A part of the transmitted energy is not captured by the out-of-plane velocity level difference and this neglected energy, finally, can lead to additional sound radiation. As a consequence this effect may cause deviations between measurement and prediction of the sound transmission between two rooms based on common used standards ([89, 90]).

Case	Transformation		Problem
	Junction 1	Junction 2	
A	-	-	NO
B	+	-	NO
C	-	+	NO
D	+	+	YES

Table 4.10: Case Study

The transformation of out-of-plane components to in-plane components of a wave leads to an apparently increasing flanking sound reduction index. The influence of this effect is depending on the amount of the damping mechanism during wave propagation. Depending on the accuracy and the base problem, the effect may be neglected in most cases for materials

showing high propagation damping like cross-laminated-timber. For materials with less amount of damping mechanism - concrete, as an example - the effect of reverse transformation becomes more important, especially, during investigations in flanking sound transmission. As a consequence, a part of the transmitted energy in the structure is not captured by the measurement values. Nevertheless, this neglected energy may lead to additional sound radiation in some cases.

4.2.1.3 Detailed analysis within the frequency range of the effect of coincidence

Within this section, a detailed analysis of the effect of wave transformation is carried out. The study described in the former section has been adapted to allow a deep investigation in the relevant effect, concerning necessary effects and boundary conditions. First, the radiated sound power

$$P_i = \oiint \mathrm{abs}(I_{air,oop,i}) \quad \text{(W)} \qquad (4.14)$$

of the single walls i were calculated by integrating the sound intensity components I_{oop} (W/m²) perpendicular to the total surface of the walls, based on the assumptions in [69, 118], in difference to the procedure as described in equation (4.7).

Based on equation (4.8), the additional radiated sound power by including wall 5 has been calculated by a comparison of the sum of the radiated sound power P (W/m²) of walls 2 and 3 to the sum of the radiated sound power of walls 2, 3 and, additionally, wall 5. Figure 4.33 shows the increasing one-third-octave based values of the air-borne sound power by including wall 5.

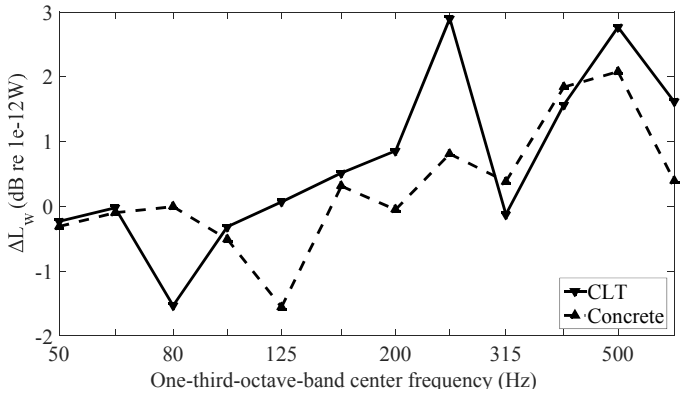

Figure 4.33: Contribution of sound radiation of wall 5 to the air-borne sound power in the receiving room

In general, the airborne sound field of the receiving room produces an acoustic coupling of the corresponding walls. At lower frequencies, a part of the resulting sound energy in the receiving room caused by the radiation of wall 2 and wall 3 is absorbed by wall 5, shown by the deceasing total energy power in the receiving room for both models. For the CLT model, above the one-third-octave-band of about 125 Hz, the radiation of wall 5 is increasing the total energy in the receiving room. A high sound radiation appears in the one-third-octave-bands of 250 Hz and 500 Hz, except 315 Hz, where again a decreasing of the total energy in the receiving room occurs. For the concrete model, the radiation of wall 5 has the largest values at the one-third-octave-bands of 400 Hz and 500 Hz. An interesting vibration behaviour was observed, especially, at 400 Hz, therefore this one-third-octave-band was chosen for further investigations. To visualize the high transmission through a path of second order, the total displacement of the model has been frequency-averaged for one-third-octave-bands between 250 Hz and 500 Hz for every single calculation point, shown in Figure 4.34 and Figure 4.35. The values have been normalized to the maximum of the excited wall 1 to achieve a clear illustration.

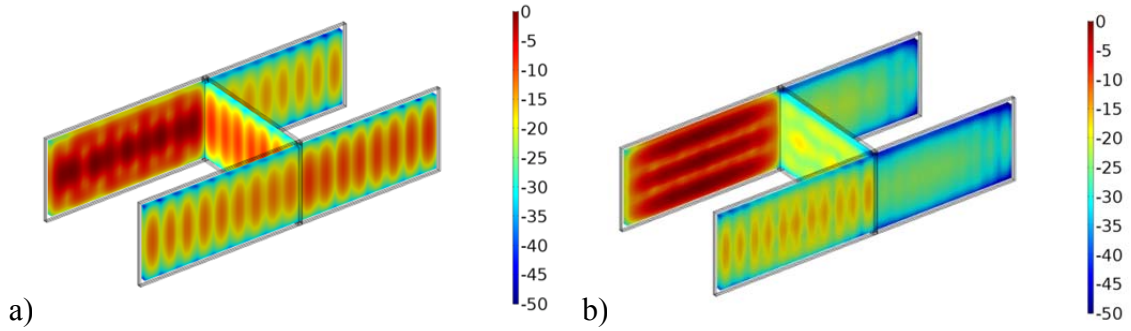

Figure 4.34: a) Normalized one-third-octave-band average of the total displacement (dB re 1e-6 m), 250 Hz; b) Normalized one-third-octave-band average of the total displacement (dB re 1e-6 m), 315 Hz

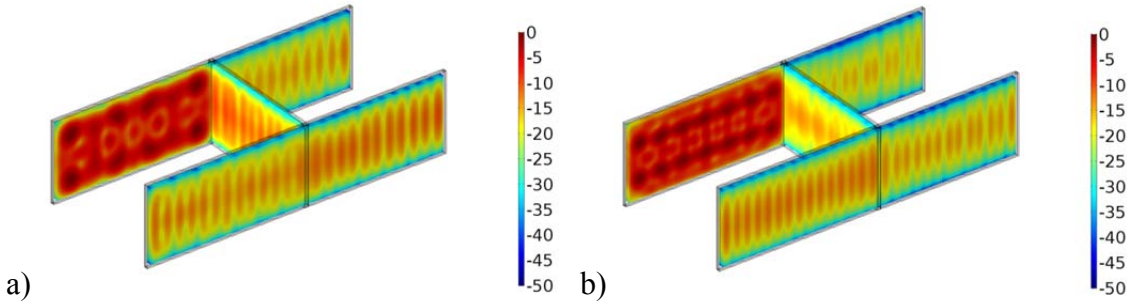

Figure 4.35: a) Normalized one-third-octave-band average of the total displacement (dB re 1e-6 m), 400 Hz; b) Normalized one-third-octave-band average of the total displacement (dB re 1e-6 m), 500 Hz

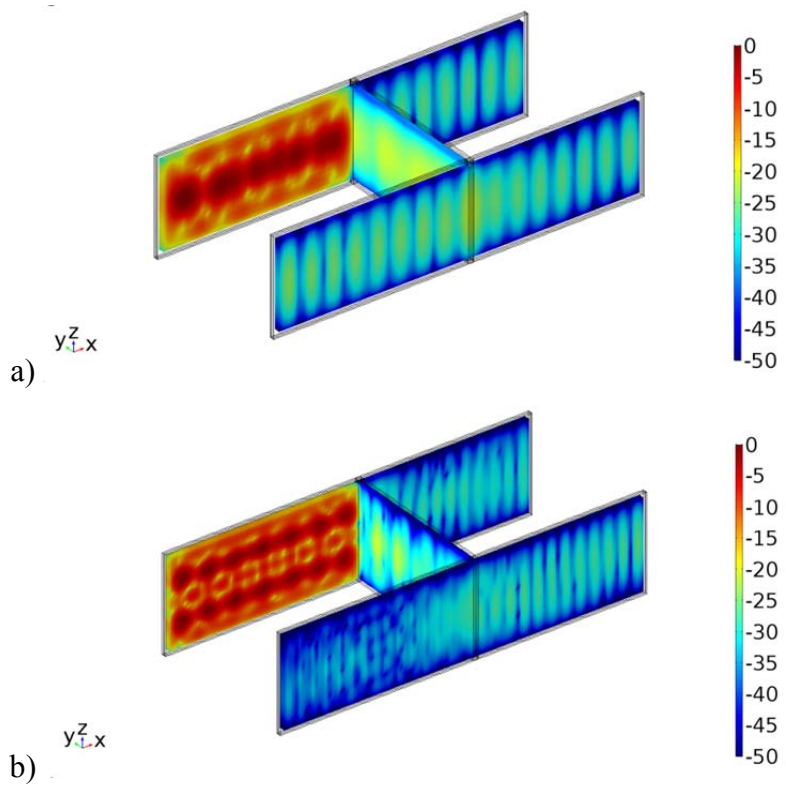

Figure 4.36: a) Normalized one-third-octave-band average of the Y-component of the displacement (dB re 1e-6 m), 250 Hz; b) Normalized one-third-octave-band average of the Y-component of the displacement (dB re 1e-6 m), 500 Hz

In general, the bending-waves contain also in-plane components at the surface of the panels. Especially at 250 Hz, the vibration characteristics of a bending wave is superposed by a high in-plane displacement over the whole separation wall. Similar levels of the in-plane displacement of the separation wall occur, compared to the out-of-plane components of the flanking walls. To identify, which vibration behaviour leads to this high transmission of a flanking path of second order, the frequency dependent values of the additional radiation of wall 5 have been evaluated. The calculated values show the frequencies, where wall 5 has most relevance to the resulting sound field within the receiving room. Figure 4.37 to Figure 4.39 show the results of calculations based on equation (4.8) for the models. The values have been normalized to the maximum of the values within the corresponding one-third-octave-bands. Double logarithmic scales allow a clear illustration. For the CLT model, a strong additional radiation occurs at frequencies of 247.62 Hz and 534.95 Hz. Also at a frequency of 242.57 Hz a high contribution of a path of second order to the total sound radiated into the receiving room within the range of this one-third-octave-band is evident. For the concrete model, a significant high additional radiation appears only at 435.5 Hz in the considered frequency range. The corresponding vibration shapes have been evaluated in order to assess,

whether a transfer (or transformation) of out-of-plane components or in-plane components causes this high transmission. Figure 4.40 to Figure 4.42 shows the normalized total displacement to illustrate the corresponding vibration shapes for the CLT and the concrete model. A horizontal cross-section at half of the height of the geometry allows a focused investigation on the Y-component (cf. axis orientation in the illustrations) of the displacement of the walls and the junction for different phase angles (surface coloured according to dB values).

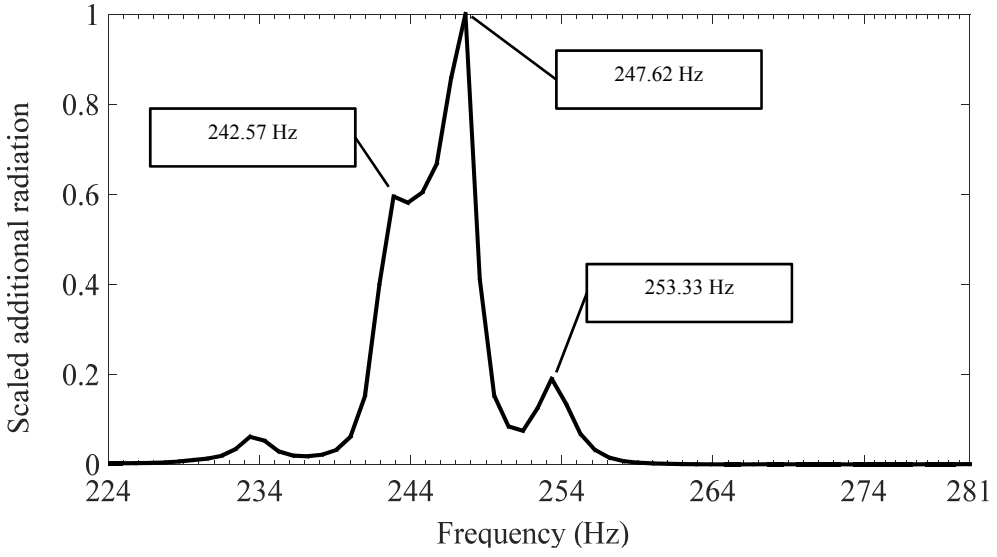

Figure 4.37: Scaled additional radiation within the one-third-octave-band of 250 Hz - CLT

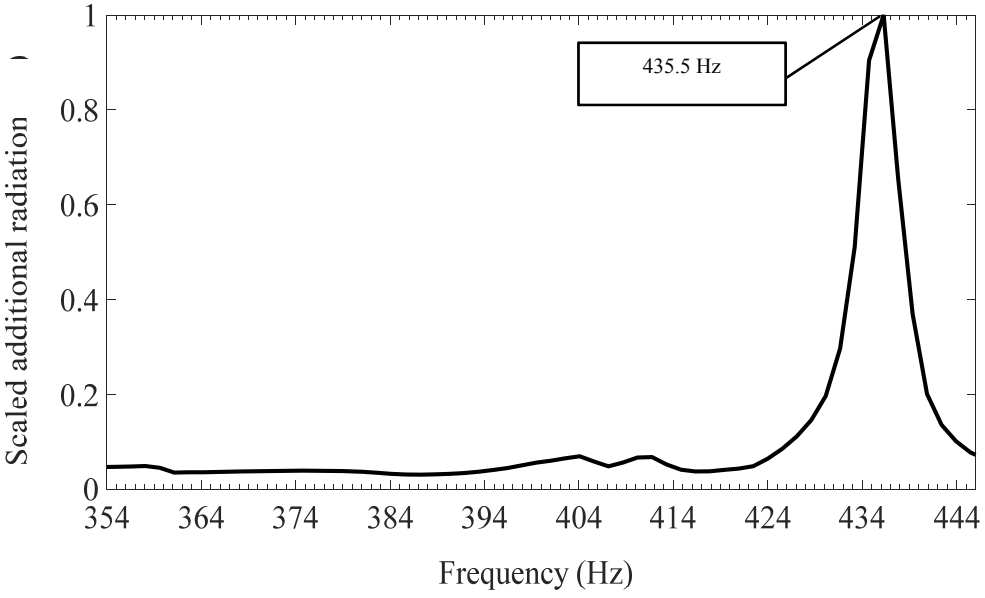

Figure 4.38: Scaled additional radiation within the one-third-octave-band of 400 Hz - Concrete

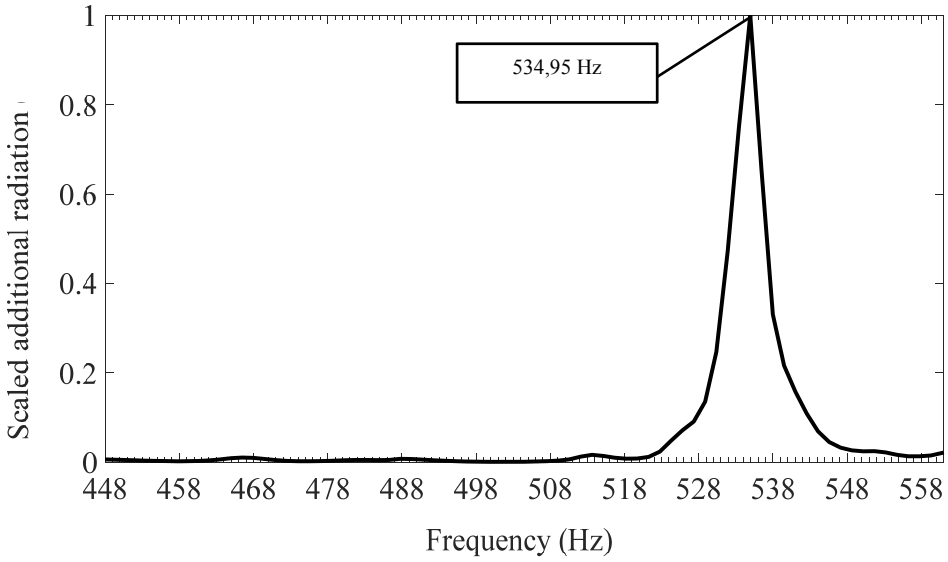

Figure 4.39: Scaled additional radiation within the one-third-octave-band of 500 Hz - CLT

Assuming that bending waves are transmitted at a junction, the junction has to act as a center of rotation. That is the case, for example, if the junction is located in the node of a global bending wave mode (cf. Figure 4.17, left). In this case, the junction should not perform a continuous displacement in a single direction. For the illustrated vibration shapes, this hypothesis is not confirmed, shown by the displacement of the junctions in the Y-direction, especially, at 435.5 Hz for the concrete model (Figure 4.38). The excitation of wall 1 induces a high level of out-of-plane components compared to the in-plane components. A transformation process appears from out-of-plane to in-plane components in the junctions. To quantify this transformation, the proportion of the out-of-plane to the in-plane movement was evaluated for the involved walls of the path of second order.

A strong additional radiation is evident at frequencies of 247.62 Hz and 534.95 Hz for the CLT model. At 242.57 Hz, a high contribution of a path of second order to the total sound radiated into the receiving room within the range of this one-third-octave-band occurs. For the concrete model, a significant high additional radiation appears only at 435.5 Hz. The corresponding vibration shapes have been evaluated in order to assess, whether a transfer (or conversion) of out-of-plane components or in-plane components causes this high transmission. Figure 4.40 to Figure 4.44 show the normalized total displacement to illustrate the corresponding vibration shapes for the CLT and the concrete model. A horizontal cross-section at half of the height of the geometry allows a focused investigation on the Y-component of the displacement of the walls and the junction for different phase angles

(surface coloured according to dB values). Assuming that bending waves are transmitted at a junction, the junction has to act as a center of rotation. In this case, the junction should not perform a continuous displacement in a single direction. For the illustrated vibration shapes, this hypothesis is not confirmed, shown by the displacement of the junctions in the Y-direction especially at 435.5 Hz for the concrete model (Figure 4.44). The excitation of wall 1 induces a high level of out-of-plane components compared to the in-plane components. A transformation process appears from out-of-plane to in-plane components in the junctions. To quantify this transformation, the proportion of the out-of-plane to the in-plane movement was evaluated for the involved walls of the path of second order.

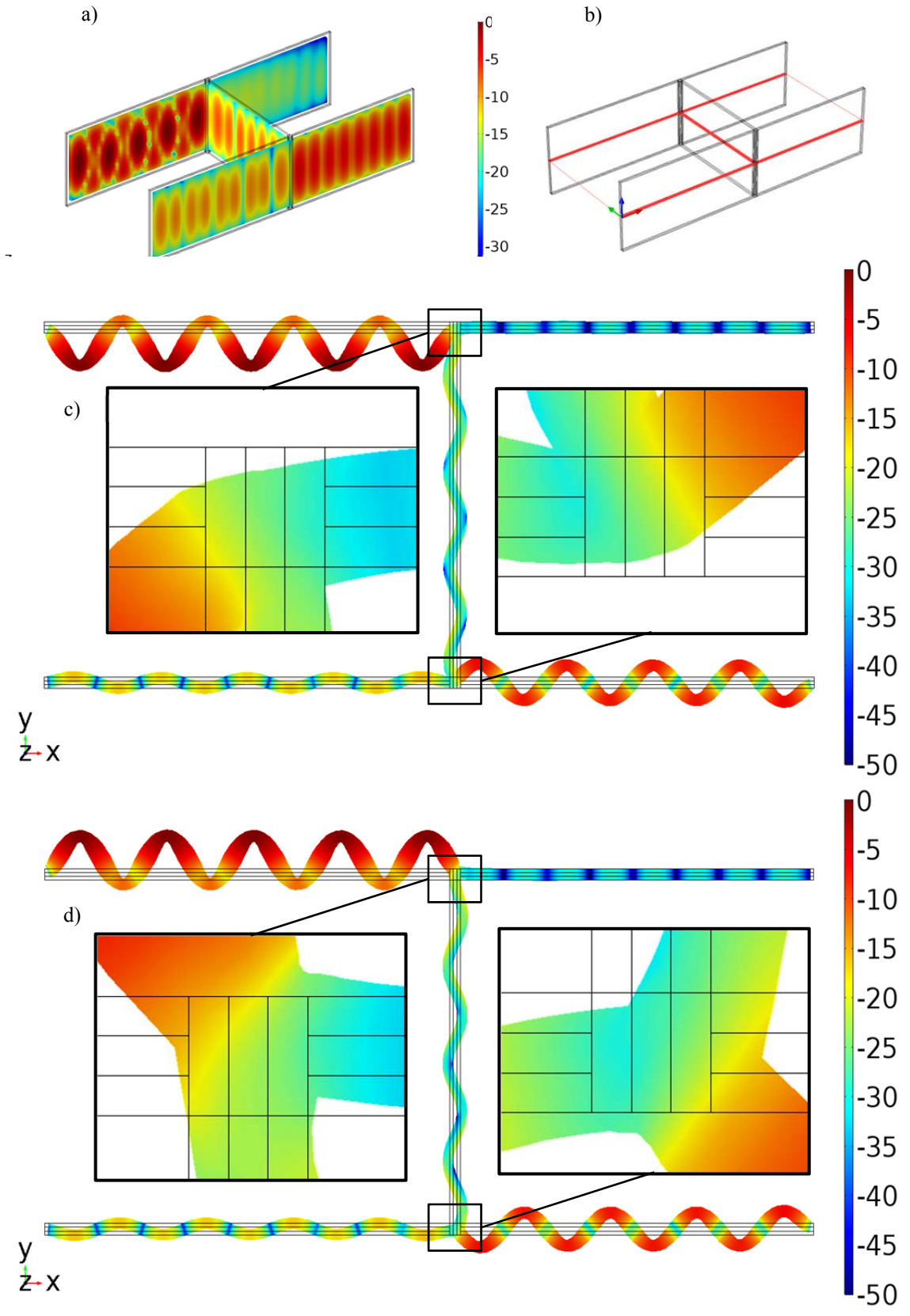

Figure 4.40: Vibration shape at 247.63 Hz – a) normalized total displacement (dB re 1e-6 m); b) horizontal cross-section of the Y-component of the displacement (dB re 1e-6 m) at a phase angle of 0° (c) and 180° (d)

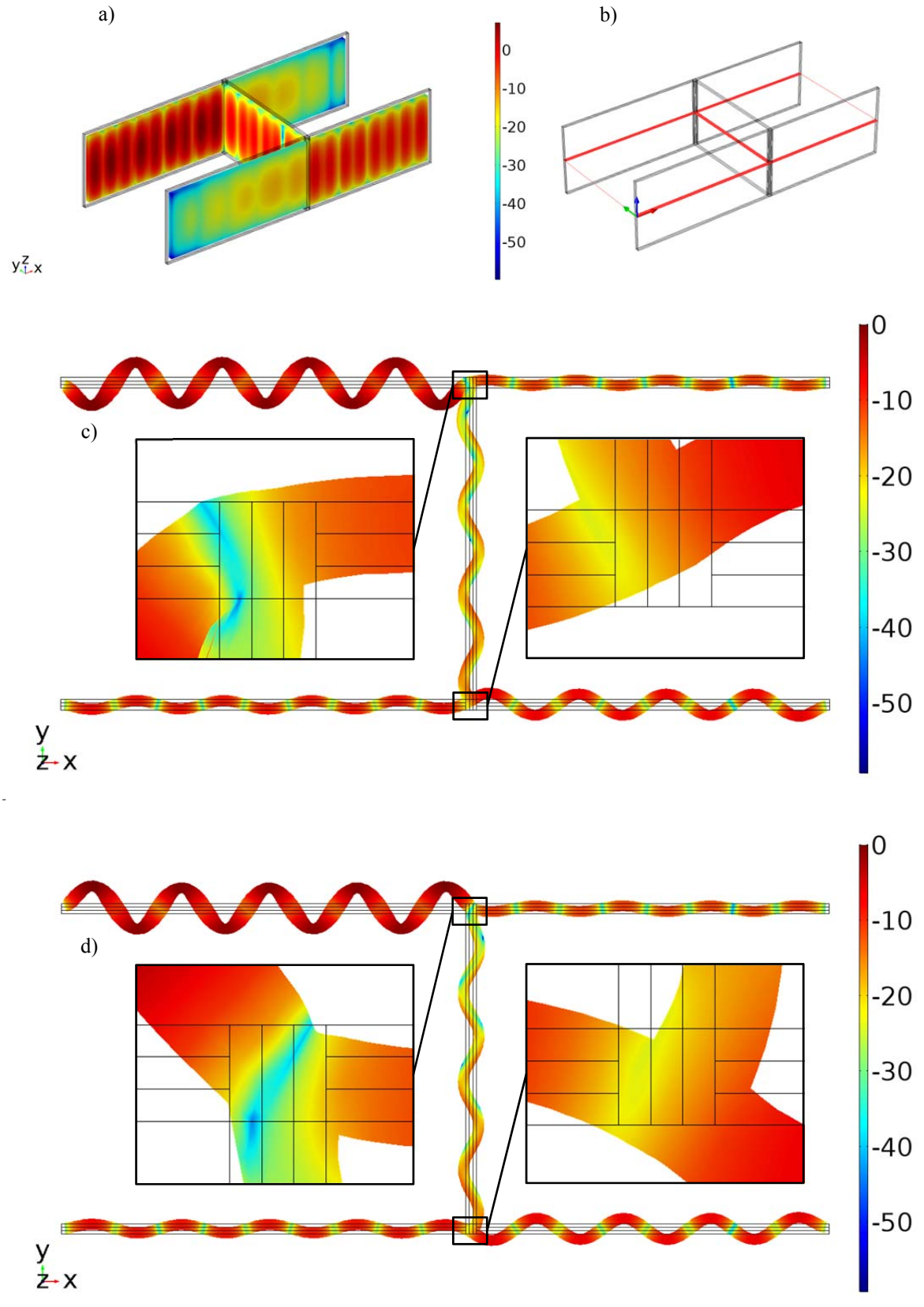

Figure 4.41: Vibration shape at 242.57 Hz – a) normalized total displacement (dB re 1e-6 m); b) horizontal cross-section of the Y-component of the displacement (dB re 1e-6 m) at a phase angle of 0° (c) and 180° (d)

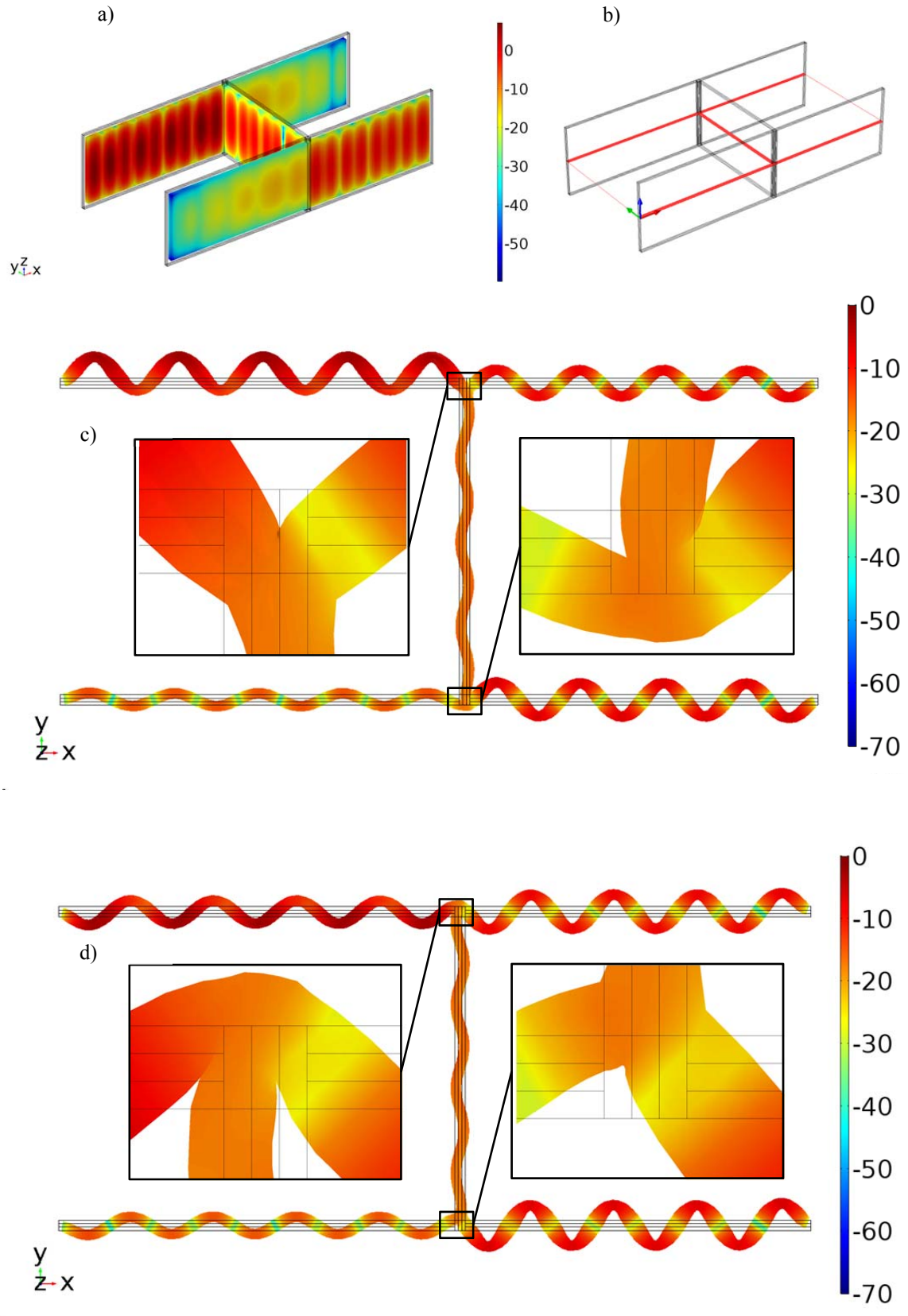

Figure 4.42: Vibration shape at 253.33 Hz – a) normalized total displacement (dB re 1e-6 m); b) horizontal cross-section of the Y-component of the displacement (dB re 1e-6 m) at a phase angle of 0° (c) and 180° (d)

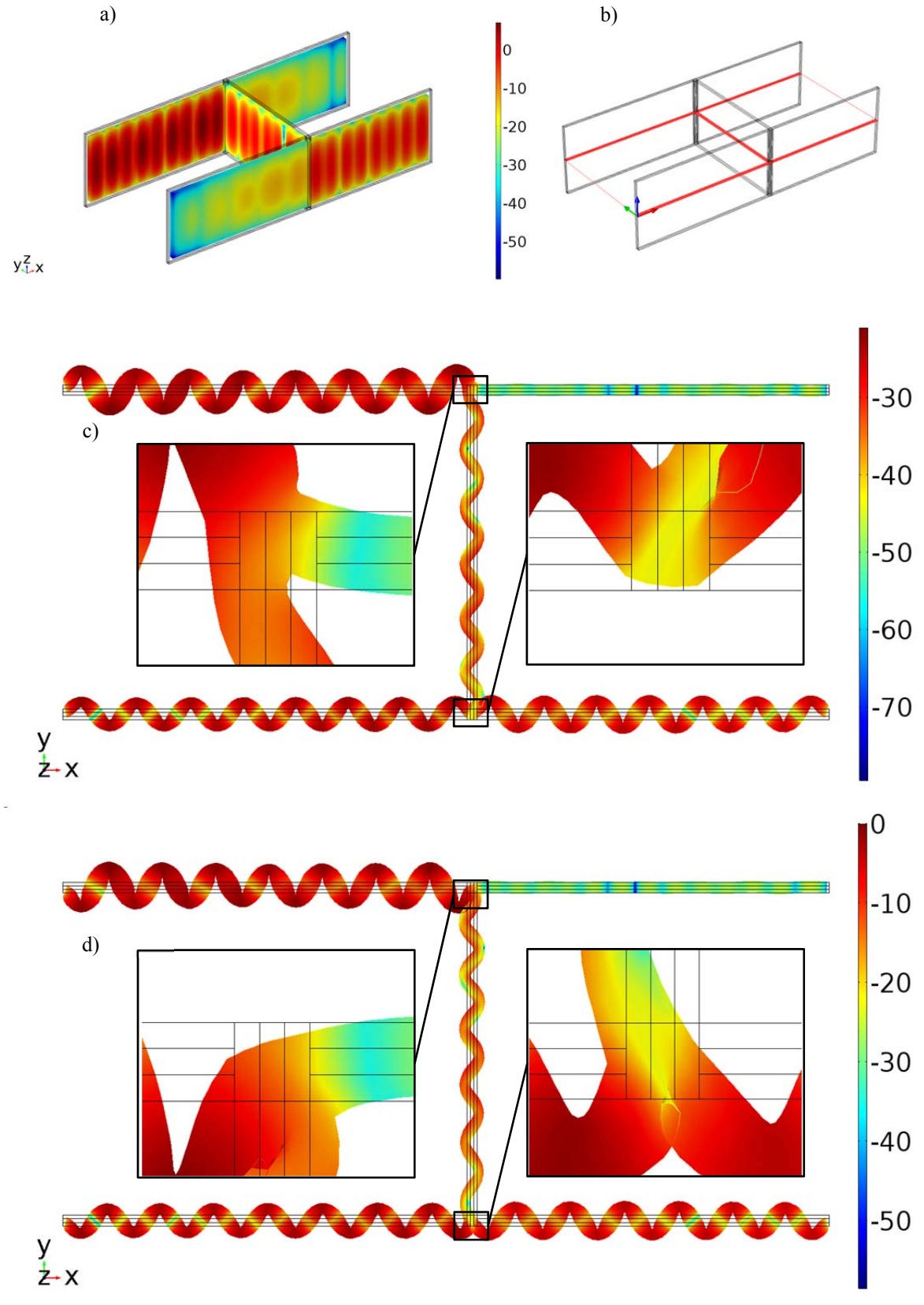

Figure 4.43: Vibration shape at 534.95 Hz – a) normalized total displacement (dB re 1e-6 m); b) horizontal cross-section of the Y-component of the displacement (dB re 1e-6 m) at a phase angle of 0° (c) and 180° (d)

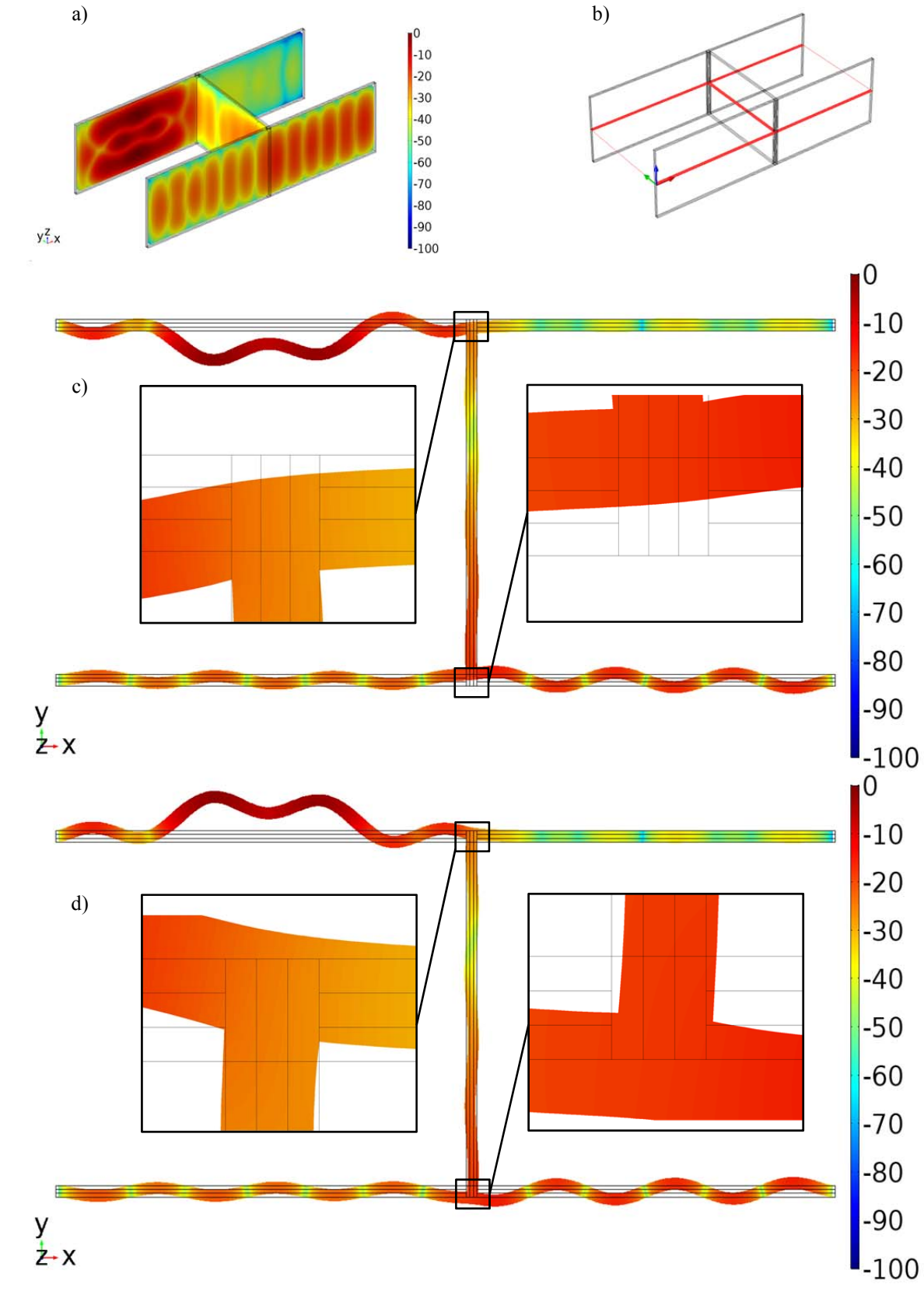

Figure 4.44: Vibration shape at 435.5 Hz – a) normalized total displacement (dB re 1e-6 m); b) horizontal cross-section of the Y-component of the displacement (dB re 1e-6 m) at a phase angle of 0° (c) and 180° (d)

Figure 4.45 and Figure 4.46 show the ratio of the spatial and frequency averaged squared velocities of the out-of-plane component to the squared norm of the velocity vector for the vertical cross-sections of walls 3 and 5, as defined in equation (4.9). A high ratio represents a high proportion of out-of-plane components, whereas a low ratio represents a high proportion of in-plane components. The additional radiation caused by wall 5 shown in equation (4.8) has been scaled to its maximum and added in absolute values.

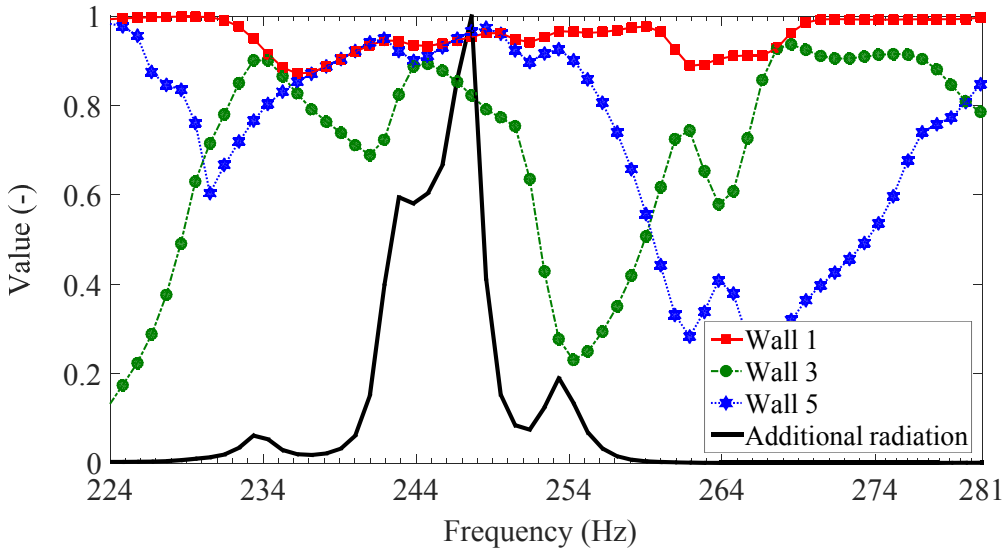

Figure 4.45: Ratio of out-of-plane components to the sum of out-of-plane and in-plane components compared to the scaled additional radiation of wall 5, 250 Hz

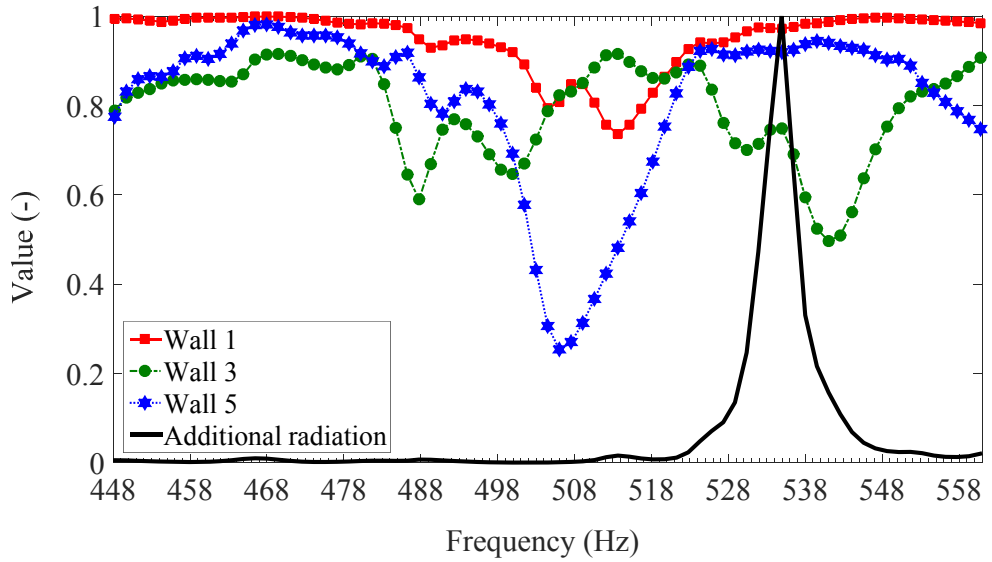

Figure 4.46: Ratio of out-of-plane components to the sum of out-of-plane and in-plane components compared to the scaled additional radiation of wall 5, 500 Hz

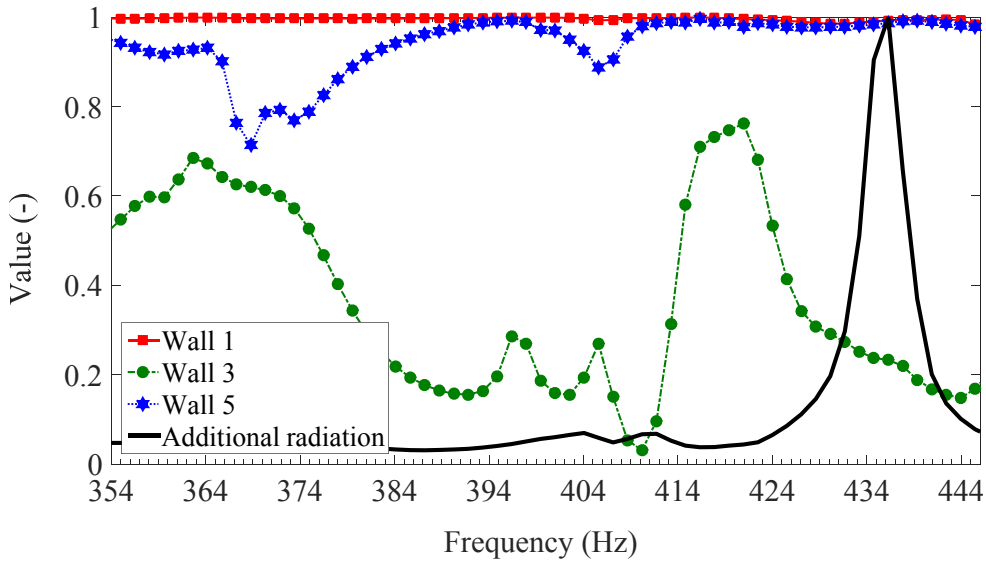

Figure 4.47: Ratio of out-of-plane components to the sum of out-of-plane and in-plane components compared to the scaled additional radiation of wall 5, 400 Hz (concrete)

For all frequencies, altering ratios of the different walls show a partly high transformation of out-of-plane to in-plane components in both junctions. At 253.33 Hz of the CLT model, out-of-plane components of wall 1 are transformed to in-plane components of wall 3 (green graph) and are transformed reverse to out-of-plane components in wall 5 (blue graph), which finally causes sound radiation. But compared to the vibration behaviour at the other frequencies, where an appreciable additional radiation of wall 5 occurs, this transmission of in-plane components may be neglected, because the main transmission is caused by bending waves (Figure 4.40 and Figure 4.41).

However, the concrete model shows a different behaviour. At the one-third-octave-band of 400 Hz, a flanking path of second order shows the greatest influence on the totally radiated sound power into the receiving room (Figure 4.33). This additional radiated power of wall 5 is mainly caused by the vibration behaviour at 435.5 Hz (Figure 4.44), where a significant wave transformation appears (Figure 4.45). It has to be noted that this part of additional acoustic energy transmission is not represented by current standardized methods [90]. This is due to the fact that the corresponding measurement procedure exclusively captures the out-of-plane components of paths of first order. Thus, this conclusion confirms the observations of previous investigations.

Summarizing the results of the present investigations, it can be stated that - more or less - a process of wave transformation occurs for both models over a wide frequency range. The

consequences for the CLT model are of secondary importance, as the main transmission is caused by bending waves that are captured using commonly used methods [90]. For the concrete model, a correlation between the impact of a transmission path of second order and a wave transformation process has been identified. Neglecting this transmission may cause an overestimation of the calculated sound insulation using standardized methods [89].

4.2.2 Measurement investigations

4.2.2.1 Test setup

In this section, experimental investigations on a suitable mock-up are discussed that confirm the existence of wave transformation in coupled CLT panels also for practical situations. Vibration measurements have been performed on a mock-up in H-shape, as shown in Figure 4.48. The size of the construction and the compositions of the panels are shown in Table 4.11. The single panels have been supported on elastomer on two points per panel to obtain a nearly free vibrating specimen, similar to the numerical models described in section 4.2.1.

Figure 4.48: Measurements on a H-Shape construction – numeration of the walls and 2-point support of single panels (circle)

Parameter (unit)	Wall 1	Wall 2	Wall 3	Wall 4	Wall 5
Width (mm)	4670	3890	3400	4670	3890
Height (mm)	2720	2720	2720	2720	2720
Layers (mm)	30/19/30/19/30	30/19/30/19/30	30/33/30	30/19/30/19/30	30/19/30/19/30
Layer – direction (-)	vertical	vertical	vertical	vertical	vertical

Table 4.11: Compositions of the panels and size of the mock-up

Figure 4.49 shows further details of the measurement setup. Wall 1, 2, 4 and 5 have been excited by an electrodynamic shaker using a swept sine excitation signal. The induced force has been measured by a force-sensor and simultaneously, the out-of-plane and in-plane components have been measured in the upper corner of the excited wall. These measurement positions in the corner have not been changed during the measurement procedure and, therefore, act as reference signals to ensure a constant vibration response of the construction during the measurement procedure. A further acceleration sensor has been used and its position has been varied to obtain the out-of-plain and in-plane components of the whole construction.

The out-of-plane components have been measured using a minimum distance of 0,5 m between the single positions and a minimum distance to the boundaries of 0,25 m. Based on these definitions, the maximum of measurement positions has been chosen for every panel which results in a minimum of 30 positions for the smallest panel. In difference to a common used regular grid of measurement positions. A distribution like a sheared rectangle has been selected to obtain different coordinates in width and height direction for every measurement position, in difference to a commonly chosen regular distribution of the measurement positions [102]. 172 measurements have been performed per excited panel.

Bending waves also cause in-plane displacements at the surfaces of the walls, but do not produce in-plane displacements in the mid-surface (cf. Figure 4.20). The in-plane components have been measured on the boundaries in the mid-surface of the plates to extract the vibration caused by quasi-longitudinal waves. These positions have been chosen because on the front surface of the panels, bending waves also result in in-plane vibration (cf. Figure 4.20) that would result in a significant error during the determination of in-plane components. Consecutive measurements on the shown positions have been performed using a variable acceleration sensor. A distance of 0,3 m has been chosen between the single measurement positions. 146 measurements have been carried out per excited panel to obtain in-plane

components. In total, 1272 measurements have been carried out for this construction. The used measurement devices are listed in appendix A 1 .

Figure 4.49: Measurements of vibration components on a construction of a H-Shape – a) Shaker excitation and measurement of the induced force; b) reference sensors for out-of-plane and in-plane components; c) measurement positions of out-of-plane components of wall 4; d) measurement positions for wall 3 (separation wall); e) f) measurement positions for in-plane components; g) measurement positions for in-plane components of the separation wall (attachment on screws);

4.2.2.2 Results and discussion

Equivalent measurements and evaluation of the vibration components have been performed as described in section 4.2.1. The ratio of the averaged out-of-plane components to the total components has been calculation in accordance with equation (4.9). Figure 4.50 to Figure 4.53 show the results of these investigations.

All results show that the proportion of out-of-plane components to the total vibration in the excited walls decreases significantly at upper mid frequencies, although an excitation exactly perpendicular to the surfaces of the walls has been chosen. The first one-third octave band that shows this behaviour seems to depend on the size of the panel rather than on its thickness respectively its composition. This observation is made during comparison of the excited panel 1 (Figure 4.50) and panel 5 (Figure 4.53) that shows a similar frequency where this effect happens. These panels differ in thickness and composition but do not differ in the size. Compared to panel 1 and panel 5, the other excited panels 2 (Figure 4.51) and panel 4 (Figure 4.52) show a significant lower frequency, where this effect occurs (630 Hz respectively 800 Hz). The difference in frequency allows us to conclude that for smaller sizes of the panels, also their composition has a slightly influence on this decreasing proportion of out-of-plane components of an excited panel.

Furthermore, a significant change in proportion of the out-of-plane components is obvious for the panels except the excited panel. Compared to the numerical investigations, as discussed in chapter 4.2.1, a similar observation can be made that in a first junction, out-of-plane components are converted to in-plane components. This wave transformation is evident, especially, for the situation shown in Figure 4.50 by a comparison between wall 1 and wall 3. Here, it seems that subsequently the components converted in the first junction are converted vice versa in the second junction, shown by a comparison of wall 3 and wall 5.

To allow a clearer investigation of this wave transformation process, the vibration responses of the panels are normalized to the excited panels.

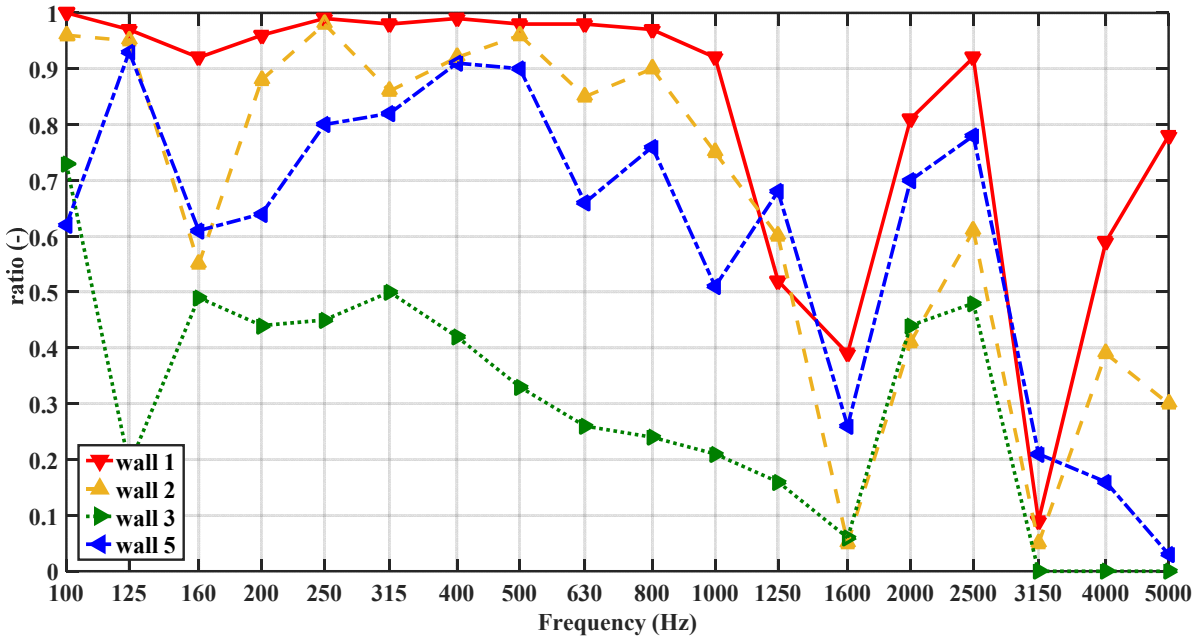

Figure 4.50: Wave transformation of measurement results –excitation of wall 1

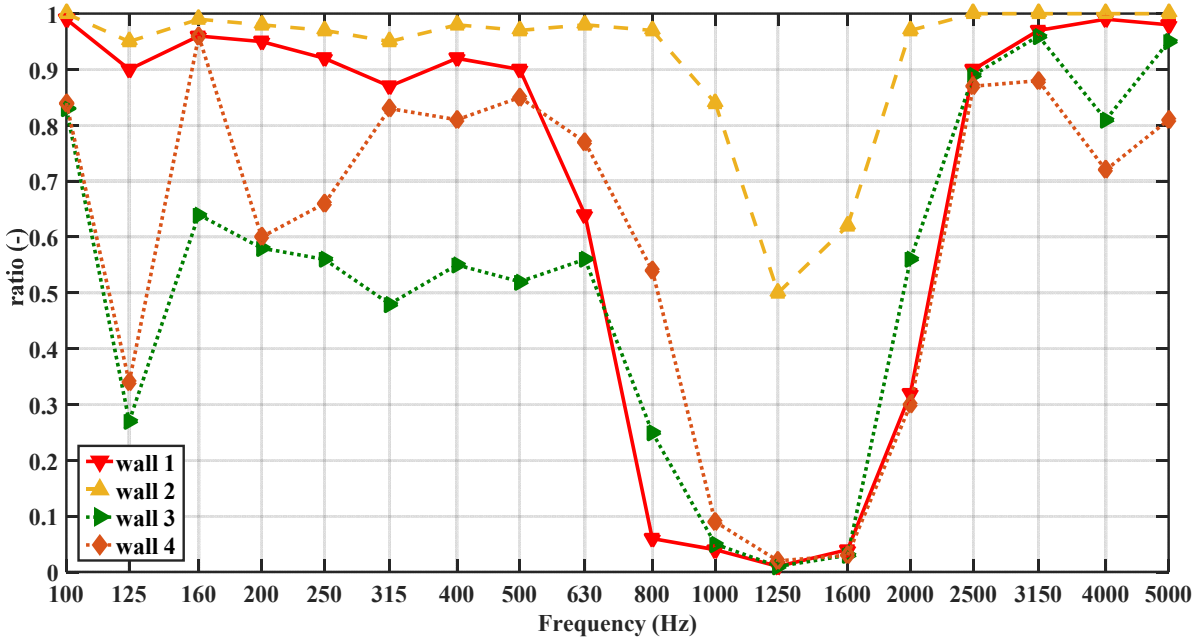

Figure 4.51: Wave transformation of measurement results –excitation of wall 2

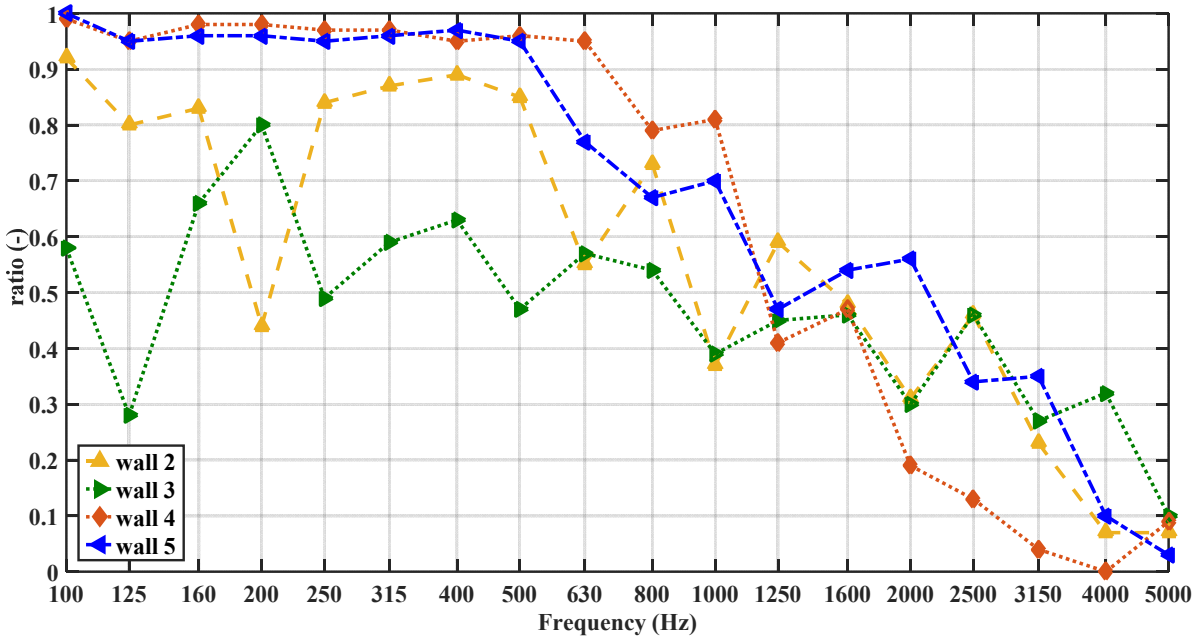

Figure 4.52: Wave transformation of measurement results –excitation of wall 4

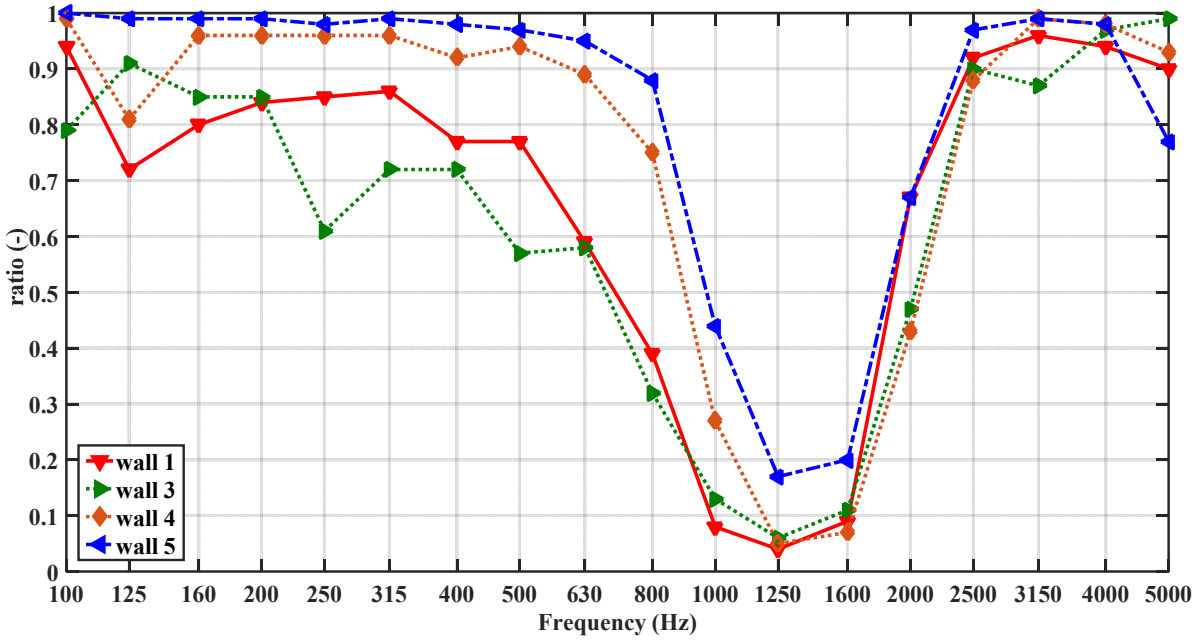

Figure 4.53: Wave transformation of measurement results –excitation of wall 5

Figure 4.54 to Figure 4.57 show the relative alteration of the ratio of out-of-plane components to the total vibration. Here, the difference between the corresponding walls and the excited wall has been calculated. Especially at mid frequencies between 200 Hz and about 800 Hz, the proportion of out-of-plane components are differing highly and, especially, in the separation wall, the in plane components partly dominate the vibration. E.g. in Figure 4.54, the high level of out-of-plane components is converted in the first junction that leads to a low proportion of out-of-plane components in the separation wall (wall 3). If we focus on a flanking path of second order, these in-plane components are converted vice versa in the second junction that leads to a higher ratio in flanking wall 5. For one-third-octave-bands of 630 Hz respectively 800 Hz, also a high ratio of in-plane components are observed in the excited walls. Figure 4.56 shows that in such a case, also in-plane components in the excited walls might be converted to out-of-plane components in a first or a second junction, shown by the increasing ratios of out-of-plane components above 1250 Hz.

These investigation shows that also for practical situations, the effect of wave transformation occurs, especially, in the mid frequency range. The effect may have a high potential to increase the flanking sound insulation for CLT, e.g. by reducing the negative impact of the coincidence effect. This hypothesis is topic of future studies and is mentioned in the outlook of this thesis.

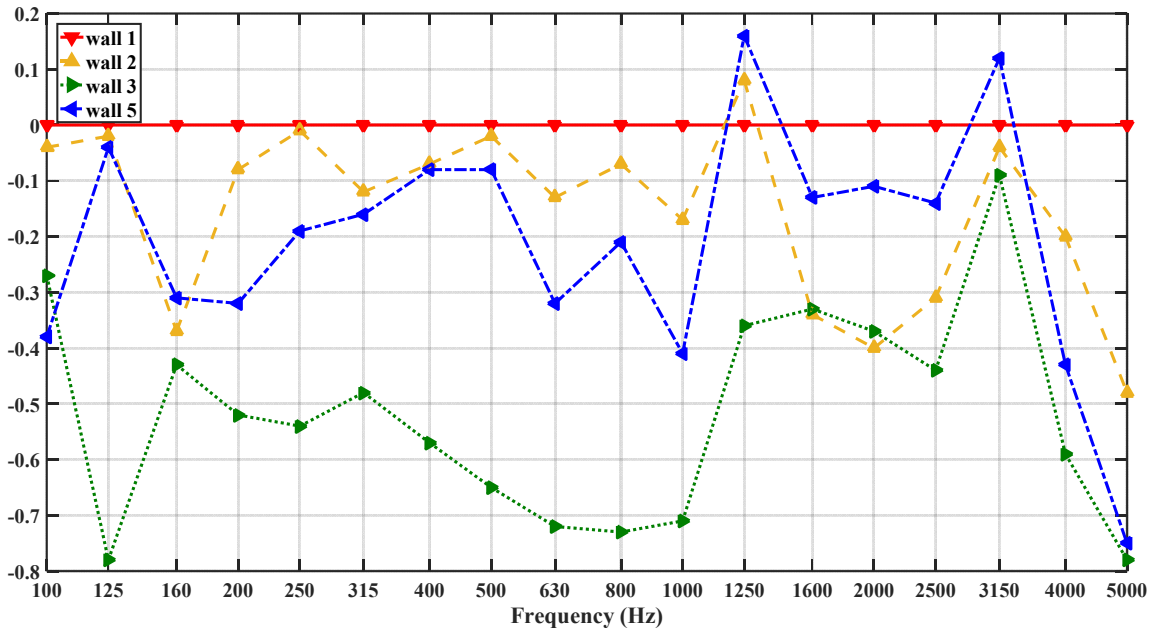

Figure 4.54: Wave transformation of measurement results – relative ratio by excitation of wall 1

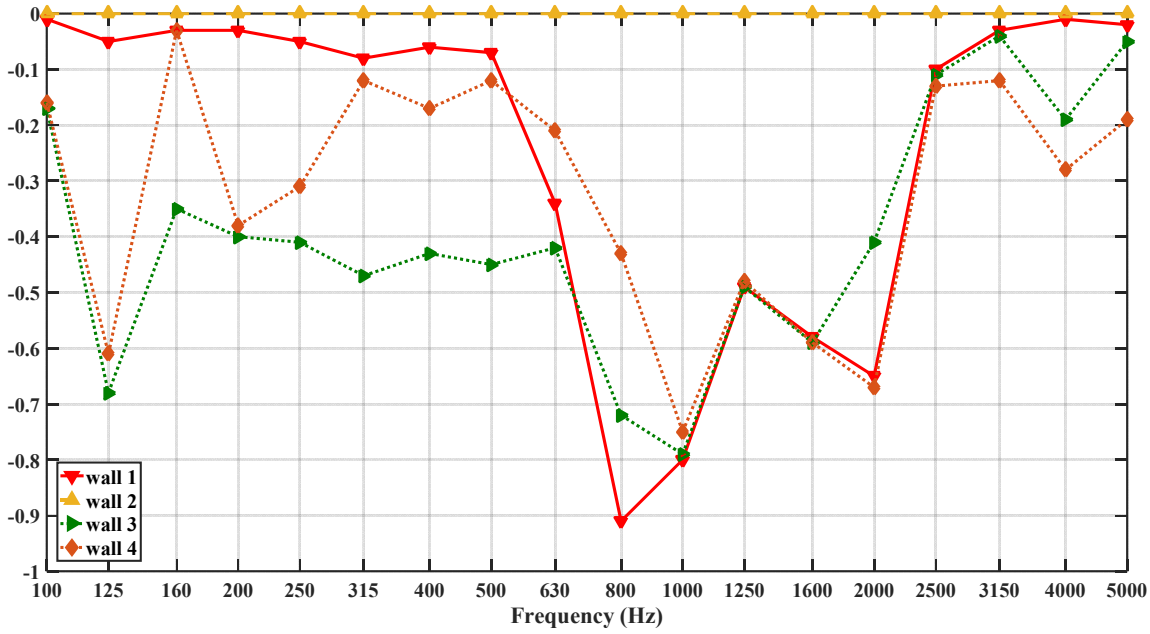

Figure 4.55: Wave transformation of measurement results – relative ratio by excitation of wall 2

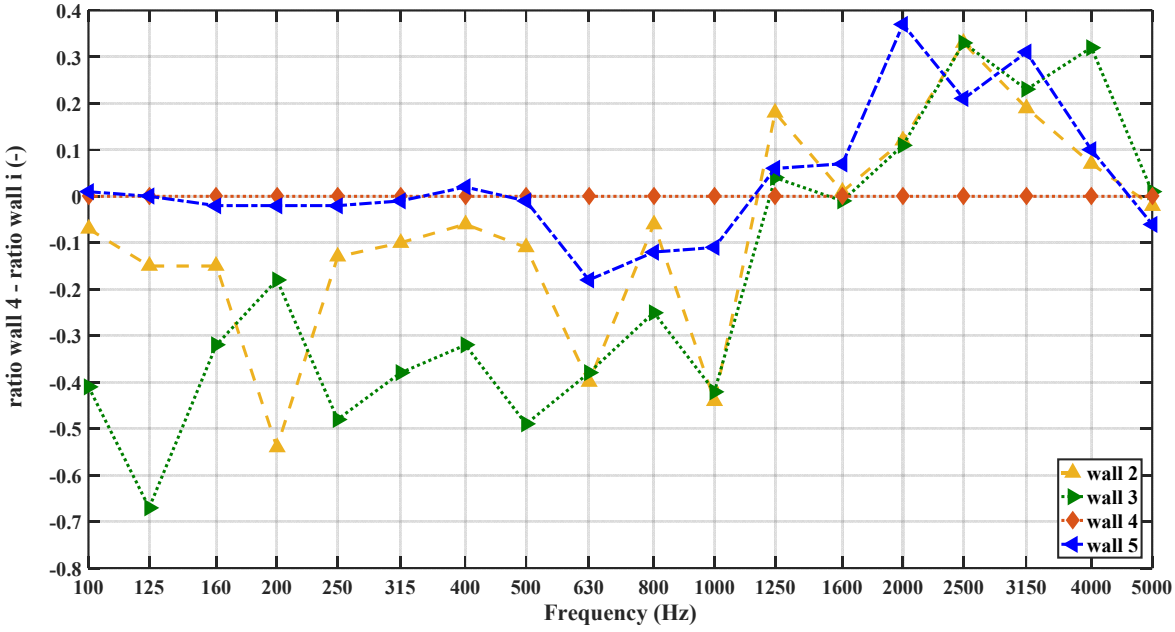

Figure 4.56: Wave transformation of measurement results – relative ratio by excitation of wall 4

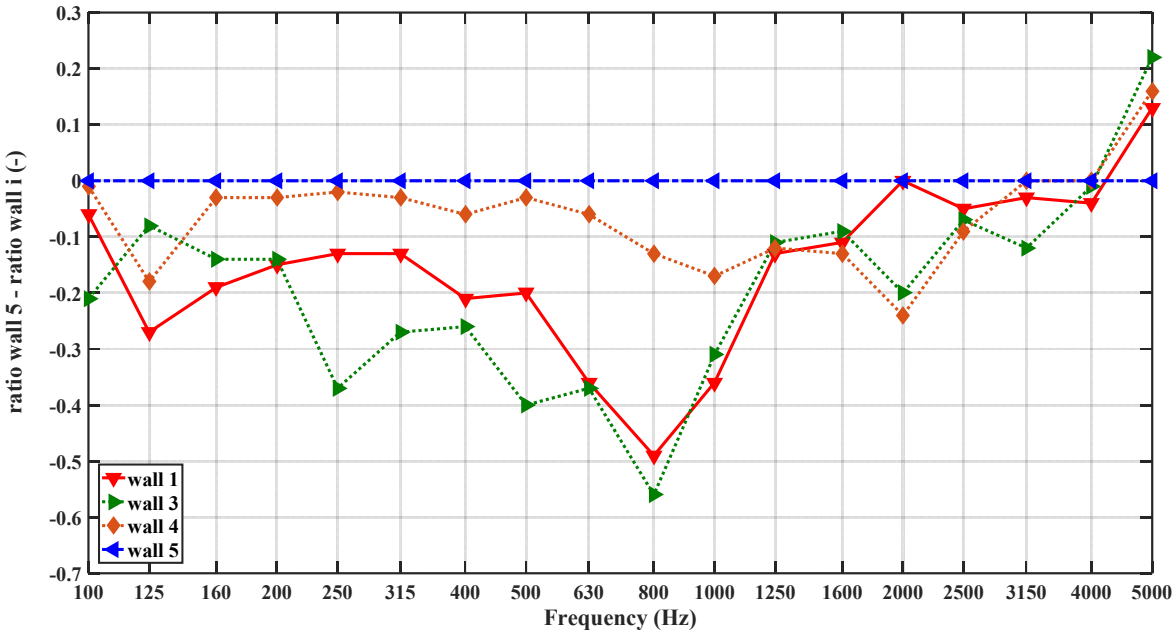

Figure 4.57: Wave transformation of measurement results – relative ratio by excitation of wall 5

4.3 Summary

In this chapter, an effect called “modal(de-)coupling” has been studied. The impact sound insulation of constructions based on panels of cross-laminated timber has been investigated at low and very low frequencies. Within this frequency range, resonances can cause a high sound transmission that can be very annoying for inhabitants caused by the tonal (sinusoidal) character of the noise. The excitation of global modes lead to a vibration response of the entire structure. An additional coupling of these global modes to the airborne sound field leads to a high sound pressure level in the room. This high level can be avoided by a suitable design of the single panels. For this purpose, the stiffness and the eigenfrequencies of panels of cross-laminated-timber are influenced by a variation of the thickness and number of the single layers of the panels. A separation of the eigenfrequencies of subsystems like single panels or cavities leads to a modal decoupling, which shows a high potential for increasing the impact sound insulation, especially, at low and very low frequencies. Improvements of the sound insulation can be reached by using less construction material. Further investigations will show, how the approach works using different room sizes and coupling stiffness’s at junctions of the CLT panels, as well as further compositions of the flanking walls and also of the floor. Measurements on the building site may show, how the effect works in a practical situation.

In addition, an effect called “wave transformation” has been investigated. The survey showed that the transformation of out-of-plane components to in-plane components of a wave leads to an apparently increasing flanking sound reduction index. The influence of this effect is depending on the amount of the damping mechanism during wave propagation. Depending on the desired accuracy of the study and the base problem, the effect may be neglected in most cases for materials showing high propagation damping like cross-laminated-timber. For materials that show a low material damping, e.g., concrete, the effect of reverse transformation becomes more important, especially, during investigations in flanking sound transmission. As a consequence, a part of the transmitted energy in the structure is not included by the measurement values. Nevertheless, this neglected energy may lead to sound radiation in some cases. As a consequence, a part of the transmitted energy in the structure is not detected by the measurement procedure. Neglecting the effect of wave transformation may lead to an error during the determination of the flanking sound transmission, especially, if paths of second order (incorporation of two junctions) are taken into account.

Then, vibration components, which are transformed in a first junction, are transformed back in a second junction and still can lead to sound radiation. Therefore, the results of these investigations showed that the effect should be considered in future revision of the EN ISO 10848 standard series for improved accuracy. Furthermore, a detailed numerical analysis of the vibroacoustic behaviour of the junctions allowed a first impression into the underlying processes during wave transformation. Experimental measurements on a real size mock-up confirmed the existence of the effect in CLT panels. In general, the investigation showed that also for practical situations, the effect of wave transformation occurs, especially, in the mid frequency range. The effect shows a high potential to reduce the negative impact of the coincidence effect on the flanking sound insulation. For this purpose, the design of the CLT panels might be chosen in a way that a significant effect of wave transformation occurs in the same frequency ranges as the so-called “coincidence effect”. As a consequence, the sound energy in these frequencies is converted into in-plane components that do not lead to sound radiation at the coincidence effect. Further investigations will show how this hypothesis works for practical use. Therefore, measurement investigations on the building site as well as further numerical investigations on the possibilities for variations of the CLT panels should be carried out in future.

5 CONCLUSION

5.1 Summary

In a first part of this thesis, numerical methods are applied to calculate the flanking sound transmission in junctions of CLT using special fastener systems. Although the general calculation effort is significantly higher than other numerical methods like the SEA, the FEM also allows deeper investigations in the physical behaviour of the structure because of the possibility to model the constructions closer to reality. Therefore, the FEM has been chosen as the main calculation method. In general, the focus was on the low and the mid frequency range. The modal behaviour and the physical behaviour in the junction during wave transformation have been investigated. Currently, investigations on panels of CLT including these effects are uncommon.

In **Chapter 3**, calculation methods for junctions of CLT panels based on the FEM have been developed. The focus was on the acoustic and mechanical behaviour of the panels, their mechanical interaction and the final calculation of the flanking sound transmission in the junction by the use of special fastener systems. A frequency range within one-third-octave-bands from 200 Hz to 1250 Hz has been investigated, because this frequency range has been used for single-number ratings of the vibration reduction index. The study is generally separated in three different steps that focus on special topics. All steps have been validated using measurement data from suitable, practical constructions. First, single CLT panels have been investigated to determine suitable calculation methods, material models and material data. The investigations showed that a linear elastic homogenous orthotropic material model can be used to calculate the vibration response of CLT, but the use of material parameters and data from investigations of side glued panels results in errors for non-side glued panels. This

is due to the reduced stiffness of the panels caused by shrinking of the topping layers. Furthermore, a simultaneous parameter fitting of several CLT panels leads to more precise solutions than using averaged material data determined from single analysis of the panels. The final results indicate a good fitting and a high reliability of the estimated values.

Then the single CLT panels have been connected to each other to form junctions using screws and angle brackets. The standardized vibration reduction index has been evaluated. The numerical calculated vibration reduction indices show a good agreement compared to measured results. At high frequencies of 1000 Hz and 1250 Hz, a tendency has been observed that the calculation underestimates the vibration reduction indices. An additional physical effect might be neglected in the numerical model that may be the topic of future studies.

Subsequently, the calculation approach has been validated using the standardized prediction methods of the EN 12354-1 during an application to a real building situation. Using a "conservative" interpretation of the standard leads to significant errors during predictions of the standardized level difference. A "progressive" approach has been developed. An individual consideration of the single components of the separation wall in the prediction method of the EN 12354-1 leads to plausible results. Using this calculation procedure, reliable results appeared. The numerically determined values of the vibration reduction index result in a minor underestimation of the total sound insulation, respectively the standardized level difference $D_{nT,w}$ of only 0,1 dB. The developed numerical calculations lead to satisfying results.

In **Chapter 4**, several acoustic effects have been investigated that have an influence on the flanking sound transmission in panels of CLT. First, an effect called "modal (de-)coupling" has been studied in the low and very low frequency range. Within this frequency range, resonances can cause a high sound transmission that can be very disturbing for inhabitants caused by the tonal (sinusoidal) character of the noise. Local modes of single components of the structure lead to global modes. An additional coupling of these global modes to the airborne sound field leads to a high sound pressure level in the room. The effect showed a high potential for an optimization of the flanking sound insulation for impact sound.

Furthermore, an effect called "wave transformation" has been investigated that occurs in the mid frequency range. The survey showed that the transformation of out-of-plane components to in-plane components of a wave leads to an apparently increasing flanking sound reduction

index. A part of the transmitted energy in the structure is not captured by a measurement procedure that only considers the out-of-plane components. Nevertheless, this excluded energy may lead to sound radiation in some cases and might lead to an error during the determination of the vibration reduction index. Furthermore, a detailed numerical analysis on the vibroacoustic behaviour of the junctions allowed a first view on the underlying processes during wave transformation. Experimental measurements on a real size mock-up confirmed the existence of the effect in CLT panels. In general, the investigation showed that also for practical situations, the effect of wave transformation is visible, especially, in the mid frequency range. The effect may have a high potential to reduce the negative impact of the coincidence effect on the flanking sound insulation.

5.2 Outlook

The numerical calculations discussed in this thesis are based on real size 3D models using the FEM. The investigations and calculations result in satisfying results but real sized models have to be used. A reduction of the size of the models, e.g., by reducing their height might lead to more efficiency, especially, for the use in parametric studies of different fastener systems or special physical effects.

Different studies of the convergence behaviour of the fitting of calculated and measured modes show a tendency that for the first modes of the panels, the Young's moduli are the determining factors to match the eigenfrequencies. Furthermore, a tendency has been observed that the shear moduli are the determining factors for fitting the eigenfrequencies at higher frequencies. By taking these findings into account, the number of the variation parameters during parameter fitting of calculated and measured eigenfrequencies can be specified more efficiently by defining the minimum with respect to the most influencing parameters. These aspects may be included in future investigations, e.g., to increase the efficiency of the fitting algorithms while the specific variation values are chosen with respect to the corresponding effects, respectively, to low or high frequent modes. In this case, also the simultaneous calculation of a high number of panels could be possible.

Several studies in the coupling of the CLT panels showed that for higher frequencies, an additional physical effect might occur during measurements that have not been included in the numerical investigations. Possible effects might be the so called "element attenuation" that

describes a damping of the wave during propagation, or the possible influence of a reduced contact area of two coupled CLT panels. These approaches might be an aspect for future investigations to increase the precision of the obtained values.

An integration of the numerical calculation methods in a practical way should be focused in the next years to allow a practical use for industry. For this purpose, promising calculation procedures that additionally include the so-called “Building Information Modelling” (BIM) are comprehensively investigated, e.g., in [119].

Two different physical effects and their impact on cross-laminated timber are discussed in this thesis, the so-called “modal(de-)coupling” and the so-called “wave transformation”. On the one hand, future investigations might focus on the consideration of these effects in standardized measurement or calculation procedures. On the other hand, these effects might be used to allow advancements of CLT panels and their connection in order to increase the competitiveness with other building materials. For this purpose, e.g., measurement investigations on the building site should be the next step to obtain an insight into the impact of the effects for a practical situation. Nevertheless, during such measurements several aspects have to be considered, e.g., a suitable number and distribution of measurement positions, especially, for determining local and global modes. Additionally, a correct positioning of the sensor for determining in-plane components has to be found because in contrast to the studies on a free vibrating H-shaped mock-up as described in this thesis, the mid-surface of the panels is not directly accessible on the building site. Appart from the EMA, alternative calibration methods allow the determination of mechanical properties. For example, Santoni et al. [33] determined the elastic constants of CLT panels using measurements of flexural wave velocity. The results of the experiments were fitted with Mindlin’s dispersion relation for thick plates. The main advantage of this procedure is the possibility to neglect the panel sizes and boundary conditions. This procedure shows a high potential, especially, for reduction of the implementation of the panel by single layers to a single Mindlin plate for future investigations. Mecking [120] currently continues Santonis work to allow an identification of frequency dependent elastic material parameters using this promising approach.

APPENDIX

A 1 Measurement devices and examples

Figure 5.1: Test stand

Figure 5.2: Measurement procedure for an EMA

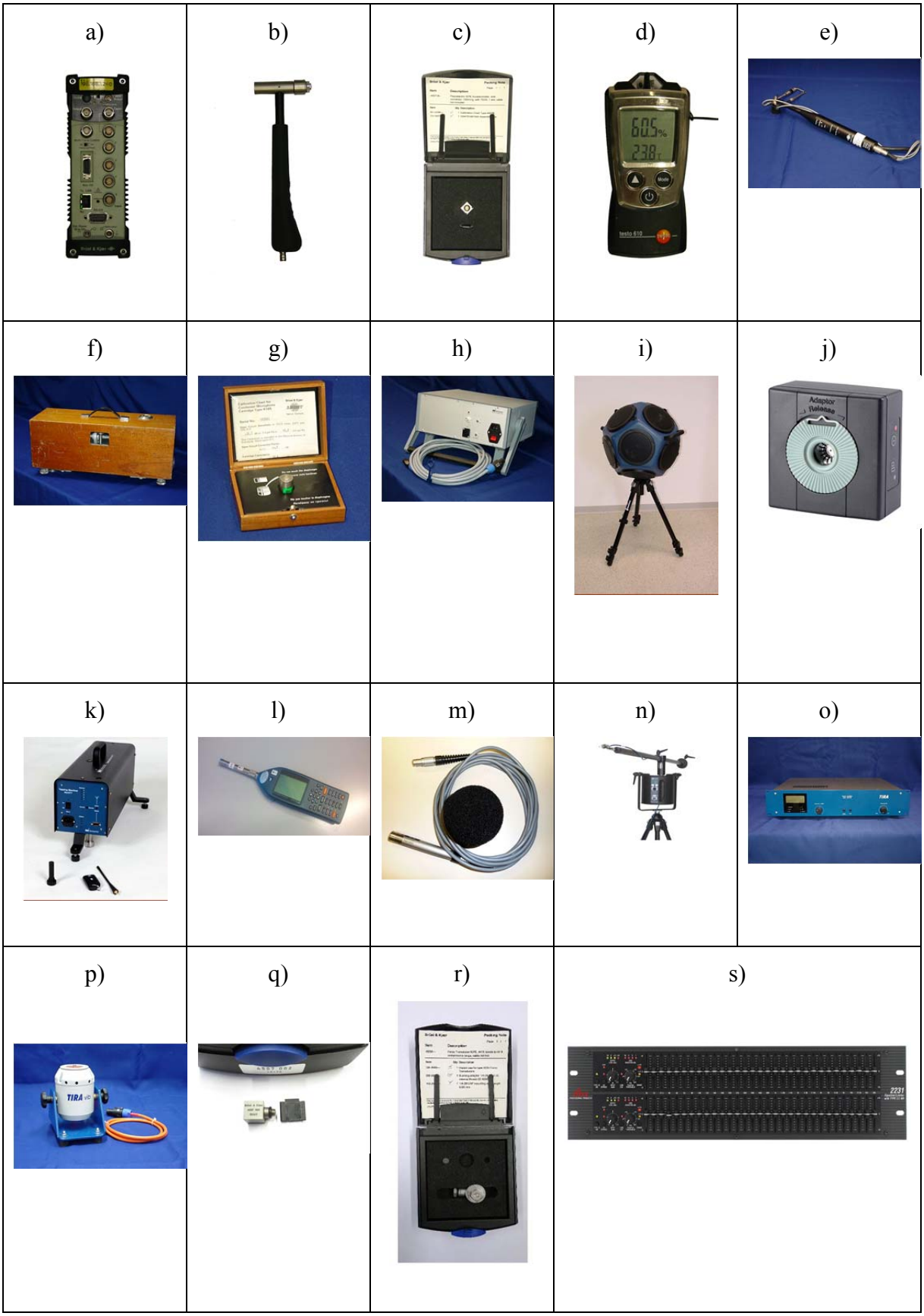

Figure 5.3: Measurement equipment – illustration

Label	Manufacturer	Type	Description
a)	Brüel & Kjaer	Type 3560-B-X06	Pulse - multi-analyser system
b)	Brüel & Kjaer	Type 8206	impact hammer
c)	Brüel & Kjaer	Type 4507-B	DeltaTron accelerometer
d)	Testo	610	temperature and humidity
e)	Brüel & Kjaer	Type 3547	sound intensity probe
f)	Brüel & Kjaer	Type 3204	tapping machine
g)	Brüel & Kjaer	Type 4165	condenser microphone
h)	Norsonic AS	260H	power amplifier
i)	Norsonic AS	270H	dodecahedron loudspeaker
j)	Brüel & Kjaer	Type 4231	sound calibrator
k)	Norsonic AS	NC-277	tapping machine
l)	Norsonic AS	Nor140	precision sound analyser
m)	Brüel & Kjaer	4190-L-001	condenser microphone
n)	Norsonic AS	Nor265	microphone boom
o)	TIRA GmbH	Type BAA 60 / TV 50018	power amplifier
p)	TIRA GmbH	TIRAvib S502 / TV 50018	shaker
q)	Brüel & Kjaer	Type 4507-002	deltaTron accelerometer
r)	Brüel & Kjaer	Type 8230	force transducer
s)	dbx	Type 2231	graphical equalizer

Table 5.1: Measurement equipment - details

A 2 Single CLT panels

Figure 5.4: Single CLT - specimen and test setup – 3s CLT wall

Figure 5.5: Single CLT - specimen and test setup – 5s CLT wall

Figure 5.6: Single CLT 5s floor – specimen and test setup

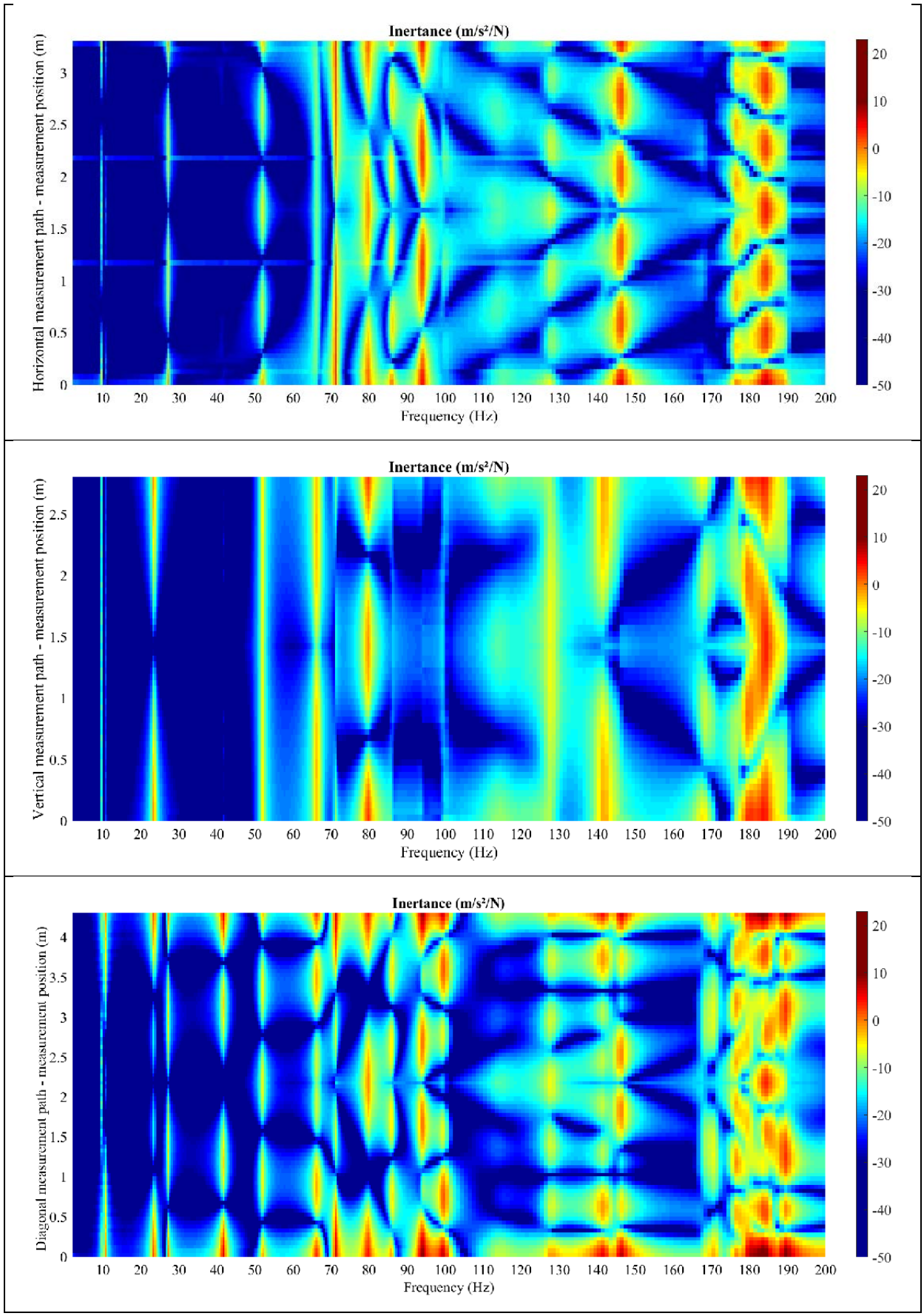

Figure 5.7: Results of the experimental modal analysis – CLT 3s wall

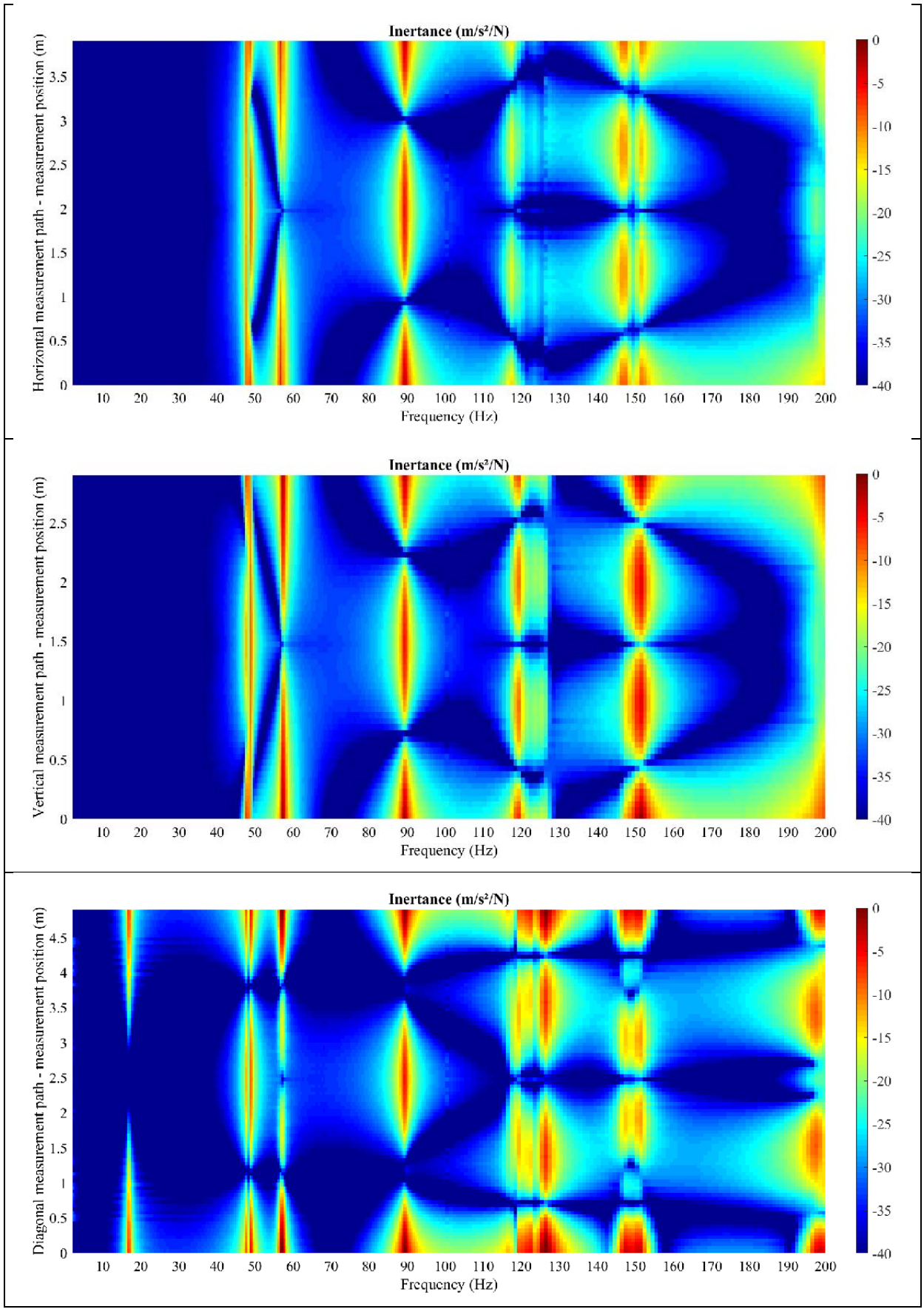

Figure 5.8: Results of the experimental modal analysis – CLT 5s floor

	Structural reverberation time (s)		Total loss factor (-)		
Frequency	3s Wall	5s Floor	3s Wall	5s Floor	AVG
20	5,28	5,52	0.021	0,020	0.020
25	6,71	4,11	0.013	0,021	0.017
32	6,47	3,88	0.011	0,018	0.014
40	3,68	4,81	0.015	0,011	0.013
50	3,45	4,66	0.013	0,009	0.011
63	3,50	3,54	0.010	0,010	0.010
80	3,09	2,47	0.009	0,011	0.010
100	1,97	1,73	0.011	0,013	0.012
125	1,02	1,52	0.017	0,012	0.014
160	1,05	1,07	0.013	0,013	0.013
200	0,94	0,68	0.012	0,016	0.014
250	0,70	0,50	0.012	0,018	0.015
315	0,56	0,40	0.013	0,018	0.015
400	0,45	0,30	0.012	0,019	0.015
500	0,34	0,24	0.013	0,018	0.016
630	0,23	0,21	0.015	0,017	0.016
800	0,19	0,17	0.014	0,016	0.015
1 000	0,16	0,14	0.014	0,016	0.015
1 250	0,13	0,13	0.014	0,014	0.014
1 600	0,12	0,12	0.012	0,012	0.012
2 000	0,11	0,11	0.010	0,010	0.010
2 500	0,11	0,11	0.008	0,008	0.008
3 150	0,12	0,11	0.006	0,006	0.006
4 000	0,13	0,11	0.004	0,005	0.005
5 000	0,14	0,11	0.003	0,004	0.004
6 300	0,29	0,11	0.001	0,003	0.002
8 000	0,40	0,12	0.001	0,002	0.002
10 000	3,37	0,12	0.000	0,002	0.001

Table 5.2: Single CLT - Structural reverberation time and total loss factor

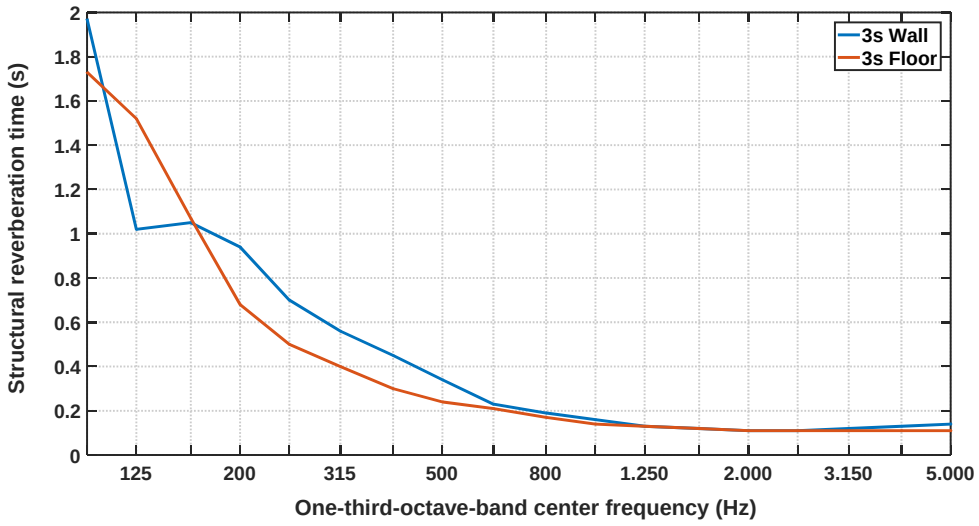

Figure 5.9: Single CLT 5s wall – structural reverberation time

A 3 T-shaped mock-up

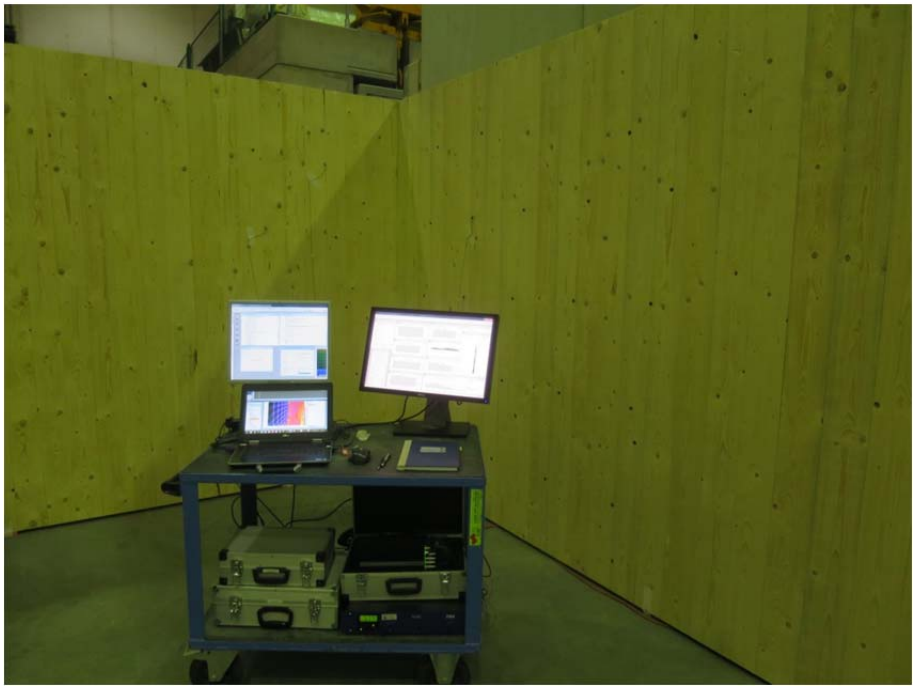

Figure 5.10: Test setup and measurement devices

Figure 5.11: mounting of the acceleration sensors during measurements

A 4 H-Shaped mock-up

Figure 5.12: Measurement positions of out-of-plane components of wall 1

Figure 5.13: Measurement positions of out-of-plane components of wall 2

Figure 5.14: Connection of wall 4 and wall 3

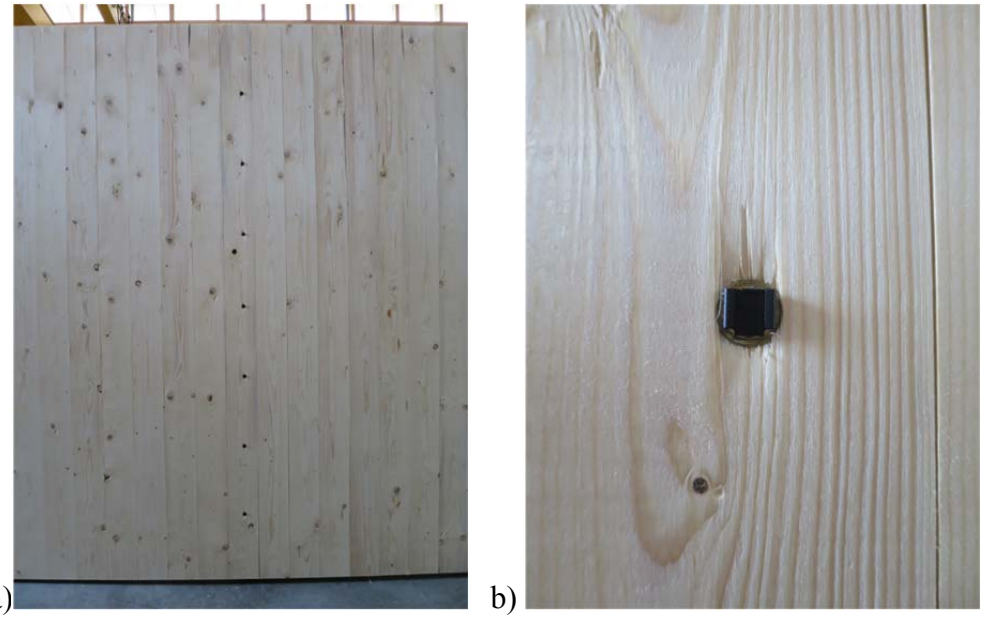

Figure 5.15: Measurement positions for determination of horizontal in-plane components for the separation wall – a) overall view; b) detailed view

A 5 Measurements on the building site

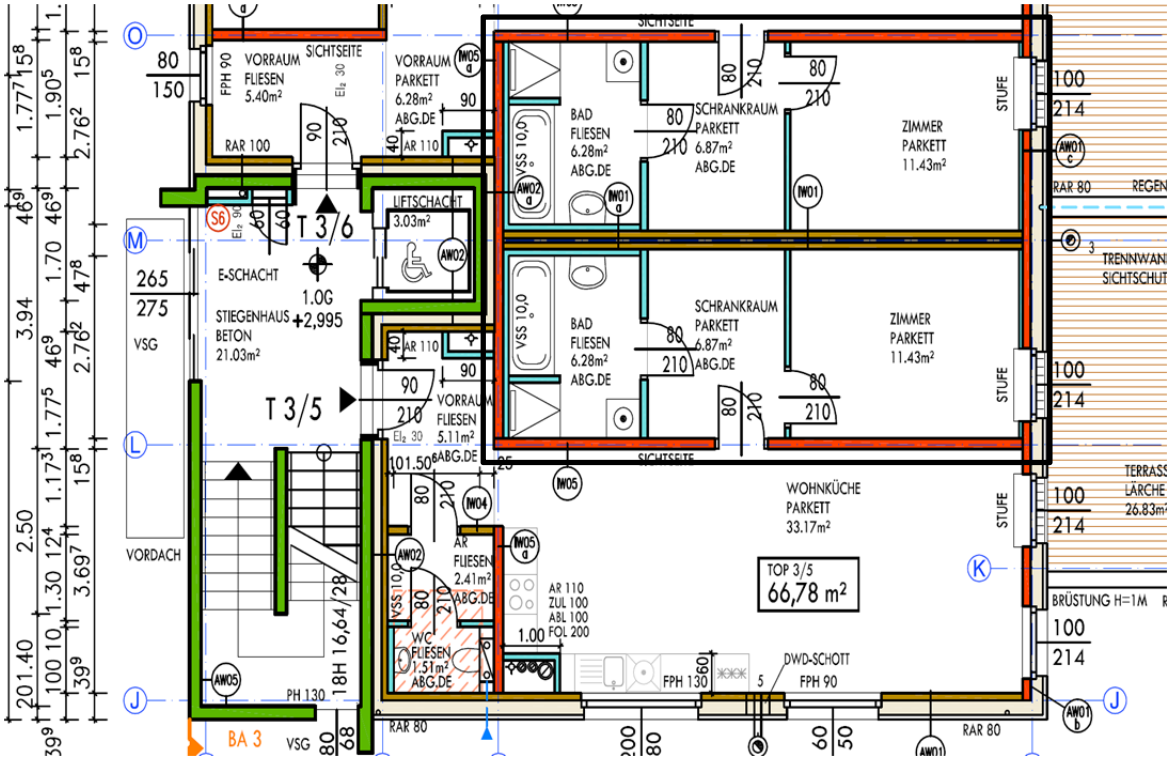

Figure 5.16: Horizontal cross-section of the investigated situation; 2nd floor

Figure 5.17: Building situation

Figure 5.18: Mounting of the ceilings using screws

REFERENCES

[1] R. Brandner, G. Flatscher, A. Ringhofer, G. Schickhofer, and A. Thiel, "Cross laminated timber (CLT): overview and development," *European Journal of Wood and Wood Products,* vol. 74, pp. 331-351, 2016.

[2] D. Bard, J. Negreira, C. Guigou Carter, G. Borello, J.-L. Kouyoumji, A. Speranza*, et al.*, "Modelling prerequisites – FEM/SEA - Impact and Airborne Sound," RISE Research Institutes of Sweden AB Report no STB01, RISE Report 2017:56, 2017.

[3] J. Negreira, "Vibroacoustic performance of wooden buildings: Prediction and Perception," PhD Thesis, Engineering Acoustics, Lund University, Lund, Sweden, 2016.

[4] S. Mecking, T. Kruse, C. Winter, and U. Schanda, "Schlussbericht: Vibroakustik im Planungsprozess für Holzbauten – Modellierung, numerische Simulation, Validierung - Teilprojekt 3: Parameterentwicklung und SEA-Modellierung," University of Applied Sciences, Rosenheim, Germany IGF-Vorhaben Nr. 18724 N und 17328 N, 2017.

[5] C. Hopkins, *Sound insulation*: Butterworth-Heinemann, 2007.

[6] C. Hopkins, "Structure-borne sound transmission between coupled plates," PhD, Heriot-Watt University, 2000.

[7] A. Timpte, "Vibration Reduction Indices of Cross Laminated Timber Structures," Master Thesis, TU München / HS Rosenheim, Rosenheim, 2017.

[8] A. Homb, "Measurements of junction vibration level differences of timber framed constructions," in *INTER-NOISE and NOISE-CON Congress and Conference Proceedings*, 2014, pp. 2305-2312.

[9] L. De Geetere, B. Ingelaere, and M. Rychtarikova, "Flanking sound transmission measurements on a timber frame mock-up. Project AH+, part 4," in *Inter-noise 2013*, Innsbruck, Austria, 2013.

[10] I. B. De Geetere Lieven and R. Monika, "Vibration level difference measurements on a timber frame mock-up. Project AH+, part 3," in *Inter-noise 2013*, Innsbruck, Austria, 2013.

[11] K. Persson, "Micromechanical modelling of wood and fibre properties," PhD Thesis, Department of Mechanics and Materials, Lund University, Lund, Sweden, 2000.

[12] O. Floden, "Vibrations in Lightweight Structures - Efficiency and Reduction of Numerical Models," PhD Thesis, Department of Construction Sciences, University of Lund, 2014.

[13] N.-G. Vardaxis, "Finite Element Modeling for Cross Laminated Timber Constructions," Master Thesis, Department of Civil and Environmental Engineering, Chalmers University of Technology, Göteborg, Sweden, 2014.

[14] M. Kohrmann, R. Völtl, G. Müller, U. Schanda, and M. Buchschmid, "Abschlussbericht zum AiF Forschungsvorhaben „VibWood“," TU Munich / HS Rosenheim,2014.

[15] J. Ramis, E. Segovia, J. Alba, J. Carbajo, and L. Godinho, "Numerical evaluation of the vibration reduction index for structural joints," *Archives of acoustics,* vol. 37, pp. 189-197, 2012.

[16] O. Flodén, K. Persson, and G. Sandberg, "Numerical methods for predicting vibrations in multi-storey wood buildings," presented at the World Conference on Timber Engineering, Vienna, Austria, 2016.

[17] M. Kohrmann, M. Buchschmid, G. Muller, R. Voltl, and U. Schanda, "Numerical models for the prediction of vibro-acoustical characteristics of light-weighted ceilings," in *INTER-NOISE and NOISE-CON Congress and Conference Proceedings*, 2013, pp. 3387-3397.

[18] A. Bolmsvik, A. Linderholt, A. Brandt, and T. Ekevid, "FE modelling of light weight wooden assemblies - Parameter study and comparison between analyses and experiments," *Engineering Structures,* vol. 73, pp. 125-142, Aug 15 2014.

[19] D. Clasen and S. Langer, "Finite element approach for flanking transmission in building acoustics," *Building Acoustics,* vol. 14, pp. 1-14, 2007.

[20] S. Reinhold, C. Hopkins, and B. Zeitler, "Numerical simulation of a laboratory reception plate using finite elements," in *DAGA*, Kiel, Germany, 2017.

[21] J. A. Steel and R. J. M. Craik, "Statistical Energy Analysis of Structure-borne Sound Transmission by Finite Element Methods," *Journal of Sound and Vibration,* vol. 178, pp. 553-561, Dec 1994.

[22] D. Gsell, G. Feltrin, S. Schubert, R. Steiger, and M. Motavalli, "Cross-laminated timber plates: Evaluation and verification of homogenized elastic properties," *Journal of Structural Engineering,* vol. 133, pp. 132-138, 2007.

[23] A. Guelzow, "Zerstörungsfreie Bestimmung der Biegesteifigkeiten von Brettsperrholzplatten," PhD Thesis Nr. 17944, Eidgenössische Technische Hochschule ETH Zürich, 2008.

[24] B. Van Damme, S. Schoenwald, M. A. Blanco, and A. Zemp, "Limitations to the Use of Homogenized Material Parameters of Cross Laminated Timber Plates for Vibration and Sound Transmission Modelling," in *The 22nd International Congress on Sound and Vibration*, Florence, Italy, 2015.

[25] A. Greim, "Identikation der Materialparameter einer Brettsperrholzdecke durch Kalibrierung eines numerischen Modells mit gemessenen Eigenfrequenzen," Master Thesis, Department of Civil, Geo and Environmental Engineering, Technical University of Munich, 2012.

[26] M. Filippoupolitis, C. Hopkins, R. Völtl, U. Schanda, J. Mahn, and L. Krajci, "Experimentally Validated Finite Element Models for the Modal Response of a Solid Timber Floor Formed from Dowel–Connected Joists," in *Proceedings of Forum Acusticum, Krakow, Poland*, 2014.

[27] B. Van Damme, S. Schoenwald, and A. Zemp, "Modeling the bending vibration of cross-laminated timber beams," *European Journal of Wood and Wood Products,* pp. 1-10, 2017.

[28] A. Paolini, F. Frischmann, S. Kollmannsberger, E. Rank, S. Mecking, C. Winter*, et al.*, "Parameteridentifikation von Brettsperrholz-Elementen mittels Bayesscher Optimierung," in *Fortschritte der Akustik, DAGA 2016*, 2016.

[29] M. Kohrmann, "Numerical Methods for the Vibro-Acoustic Assessment of Timber Floor Constructions," PhD Thesis, Department of Civil, Geo and Environmental Engineering, Munich, Germany, 2017.

[30] Å. Bolmsvik, "Structural-acoustic vibrations in wooden assemblies: Experimental modal analysis and finite element modelling," PhD Thesis, School of Engineering, Linnaeus University, Växjö, Sweden, 2013.

[31] O. Perret, A. Lebée, C. Douthe, and K. Sab, "The Bending–Gradient theory for the linear buckling of thick plates: Application to Cross Laminated Timber panels," *International Journal of Solids and Structures,* vol. 87, pp. 139-152, 6/1/ 2016.

[32] D. Keunecke, S. Hering, and P. Niemz, "Three-dimensional elastic behaviour of common yew and Norway spruce," *Wood science and technology,* vol. 42, pp. 633-647, 2008.

[33] A. Santoni, S. Schoenwald, B. Van Damme, and P. Fausti, "Determination of the elastic and stiffness characteristics of cross-laminated timber plates from flexural wave velocity measurements," *Journal of Sound and Vibration,* vol. 400, pp. 387-401, Jul 2017.

[34] D. Clasen, "Numerische Untersuchung der akustischen Eigenschaften von trennenden und flankierenden Bauteilen," PhD Thesis, Institute of applied mechanics, Technische Universität Braunschweig, Braunschweig, Germany, 2008.

[35] A. Rabold, "Anwendung der Finite-Element-Methode auf die Trittschallberechnung," PhD Thesis, Chair for Computation in Engineering, Technical University of Munich, Munich, Germany, 2010.

[36] R. H. Lyon and R. G. DeJong, "Theory and Application of Statistical Energy Analysis," ed Boston: Newnes, 1995, p. x.

[37] M. Crocker and A. Price, "Sound transmission using statistical energy analysis," *Journal of Sound and Vibration,* vol. 9, pp. 469-486, 1969.

[38] E. Wester and B. Mace, "Statistical energy analysis of two edge-coupled rectangular plates: ensemble averages," *Journal of Sound and Vibration,* vol. 193, pp. 793-822, 1996.

[39] C. Hopkins, "Statistical energy analysis of coupled plate systems with low modal density and low modal overlap," *Journal of sound and vibration,* vol. 251, pp. 193-214, 2002.

[40] S. Schoenwald, "Flanking Sound transmission through lightweight framed double leaf walls - Prediction using statistical energy analysis," PhD Thesis, Department of Architecture, Building and Planning, Technische Universiteit Eindhoven, Eindhoven, The Netherlands, 2008.

[41] L. Galbrun, "The prediction of airborne sound transmission between two rooms using first-order flanking paths," *Applied Acoustics,* vol. 69, pp. 1332-1342, 12// 2008.

[42] F. Fahy and A. Mohammed, "A study of uncertainty in applications of SEA to coupled beam and plate systems, part I: computational experiments," *Journal of Sound and Vibration,* vol. 158, pp. 45-67, 1992.

[43] T. W. Wu and A. Dandapani, "A Boundary Element Solution for Sound Transmission Through Thin Panels," *Journal of Sound and Vibration,* vol. 171, pp. 145-157, 1994/03/24/ 1994.

[44] M. Messner, *Fast boundary element methods in acoustics* vol. Computation in Engineering and Science: Monographic Series TU Graz, 2012.

[45] J. T. Katsikadelis, *The boundary element method for plate analysis*. Athens, Greece: Elsevier, 2014.

[46] F. G. Kollmann, T. F. Schösser, and R. Angert, *Praktische Maschinenakustik*. Berlin: Springer Berlin Heidelberg, 2006.

[47] J. Dong, K. K. Choi, N. Vlahopoulos, A. Wang, and W. Zhang, "Sensitivity Analysis and Optimization Using Energy Finite Element and Boundary Element Methods," *AIAA Journal,* vol. 45, pp. 1187-1198, 2007.

[48] G. Müller, *Numerische Methoden der Technischen Akustik*. Berlin, Heidelberg, Germany: Springer-Verlag Berlin Heidelberg, 2017.

[49] D. Zhu, H. Chen, X. Kong, and W. Zhang, "A hybrid finite element–energy finite element method for mid-frequency vibrations of built-up structures under multi-distributed loadings," *Journal of Sound and Vibration,* vol. 333, pp. 5723-5745, 2014.

[50] R. J. Craik and R. Wilson, "Sound transmission through parallel plates coupled along a line," *Applied Acoustics,* vol. 49, pp. 353-372, 1996.

[51] L. Gagliardini, L. Houillon, G. Borello, and L. Petrinelli, "Virtual SEA-FEA-based modeling of mid-frequency structure-borne noise," *Sound and vibration,* vol. 39, p. 22, 2005.

[52] G. Müller and M. Buchschmid, "Hybrid approaches for vibroacoustical problems based on the finite element method and statistical energy analysis," *Wave Motion,* vol. 51, pp. 622-634, Jun 2014.

[53] M. Buchschmid, G. Müller, and A. Kropp, "Closing the mid-frequency-gap: acoustic biw design using a hybrid sea-fea approach," in *The 16th International Congress on Sound and Vibration. Krakow, Poland, ICSV16*, 2009.

[54] M. Wachulec, "Power Flow and Structure-borne Noise in Medium Frequency Range," Structural Dynamics Group, Department of Civil Engineering, Aalborg University, 2002.

[55] P. J. Shorter and R. S. Langley, "Vibro-acoustic analysis of complex systems," *Journal of sound and vibration,* vol. 288, pp. 669-699, 2005.

[56] R. S. Langley and P. Bremner, "A hybrid method for the vibration analysis of complex structural-acoustic systems," *The Journal of the Acoustical Society of America,* vol. 105, pp. 1657-1671, 1999.

[57] P. J. Shorter and R. S. Langley, "On the reciprocity relationship between direct field radiation and diffuse reverberant loading," *The Journal of the Acoustical Society of America,* vol. 117, pp. 85-95, 2005.

[58] V. Cotoni, P. Shorter, and R. Langley, "Numerical and experimental validation of a hybrid finite element-statistical energy analysis method," *The Journal of the Acoustical Society of America,* vol. 122, pp. 259-270, 2007.

[59] X. Wang and C. Hopkins, "Application of SEA and Advanced SEA to Structure-borne Sound Transmission on a Rectangular Beam Framework," presented at the The 21st International Congress on Sound and Vibration, Beijing, China, 2014.

[60] L. Cremer, M. Heckl, and E. Ungar, *Structure-borne sound*: Springer, 1973.

[61] B. Gibbs and P. Craven, "Sound transmission and mode coupling at junctions of thin plates, part II: Parametric survey," *Journal of Sound and Vibration,* vol. 77, pp. 429-435, 1981.

[62] S. Hambric and P. Taylor, "Comparison of experimental and finite element structure-borne flexural power measurements for a straight beam," *Journal of sound and vibration,* vol. 170, pp. 595-605, 1994.

[63] N. J. Kessissoglou, "Power transmission in L-shaped plates including flexural and in-plane vibration," *Journal of the Acoustical Society of America,* vol. 115, pp. 1157-1169, 2004.

[64] C. Hopkins, "Experimental statistical energy analysis of coupled plates with wave conversion at the junction," *Journal of Sound and Vibration,* vol. 322, pp. 155-166, 2009.

[65] T. Hering, "Strukturintensitätsanalyse als Werkzeug der Maschinenakustik," PhD Thesis, Department of Mechanical Engineering, Technische Universität Darmstadt, Darmstadt, Germany, 2012.

[66] R. P. Szwerc, C. B. Burroughs, S. A. Hambric, and T. E. McDevitt, "Power flow in coupled bending and longitudinal waves in beams," *Journal of the Acoustical Society of America,* vol. 107, pp. 3186-3195, Jun 2000.

[67] Z. Wang, J. Xing, and W. Price, "An investigation of power flow characteristics of L-shaped plates adopting a substructure approach," *Journal of Sound and vibration,* vol. 250, pp. 627-648, 2002.

[68] N. Kessissoglou, "Effects of in-plane modes on the power flow characteristics in ship structures," in *Proceedings of the Acoustics*, 2002, pp. 433-442.

[69] M. Möser, *Messtechnik der Akustik*: Springer-Verlag Berlin Heidelberg, 2010.

[70] M. Möser and W. Kropp, *Körperschall: physikalische Grundlagen und technische Anwendungen*: Springer-Verlag Berlin Heidelberg, 2009.

[71] H. Hiebel, "Analytische Berechnung der Schallabstrahlung des ebenen Biegewellenwandlers," Master Thesis, Graz Unversity of Technology, 2005.

[72] H. Kuttruff, *Akustik: Eine Einführung*: Hirzel Verlag, 2004.

[73] N. Labonnote, "Damping in timber structures," PhD Thesis, Department of Structural Engineering, Norwegian University of Science and Technology, Trondheim, Norway, 2012.

[74] S. Kuhl, "Gezielte Leitung von Körperschall unter Zuhilfenahme der Strukturintensitätsrechnung," PhD Thesis, Technische Universität Darmstadt, Darmstadt, Germany, 2010.

[75] D. Clasen and S. Langer, "Consideration of flanking transmission within numerical simulation of sound insulation," *Acta Acustica United With Acustica,* vol. 92, p. S47, 2006.

[76] D. Clasen and S. Langer, "Numerical investigation of the influence of joints on airborne sound insulation," *Proc. ICSV,* vol. 12, 2005.

[77] F. Rieg, R. Hackenschmidt, and B. Alber-Laukant, *Finite Elemente Analyse für Ingenieure*, 4th Edition ed. Munich, Germany: Hanser, 2012.

[78] O. C. Zienkiewicz, R. L. Taylor, R. L. Taylor, and J. Zhu, *Finite Element Method: Its Basis and Fundamentals, The: Its Basis and Fundamentals*: Elsevier, Incorporated, 2013.

[79] A. Jäger, T. Bader, K. Hofstetter, and J. Eberhardsteiner, "The relation between indentation modulus, microfibril angle, and elastic properties of wood cell walls," *Composites Part A: Applied Science and Manufacturing,* vol. 42, pp. 677-685, 2011.

[80] K. Hofstetter, C. Hellmich, and J. Eberhardsteiner, "Development and experimental validation of a continuum micromechanics model for the elasticity of wood," *European Journal of Mechanics-A/Solids,* vol. 24, pp. 1030-1053, 2005.

[81] R. Stürzenbecher and K. Hofstetter, "Bending of cross-ply laminated composites: An accurate and efficient plate theory based upon models of Lekhnitskii and Ren," *Composite Structures,* vol. 93, pp. 1078-1088, 2011.

[82] S. Mecking, T. Kruse, and U. Schanda, "Messung und Berechnung der Körperschallübertragung am Bauteilstoß von Massivholzelementen," Technical University of Applied Sciences Rosenheim, Rosenheim, Germany2014.

[83] H. Hörig, "Zur Elastizität des Fichtenholzes," *Zeitschrift für technische Physik,* vol. 12, pp. 369-379, 1931.

[84] E. Krabbe, *Messungen von Gleit-und Dehnungszahlen an Holzstäbchen mit rechtechigen Querschnitten*. Hannover, Germany: Technische Hochschule Hannover, 1960.

[85] F. H. Neuhaus, "Elastizitätszahlen von Fichtenholz in Abhängigkeit von der Holzfeuchtigkeit," PhD Thesis, Department of Civil and Environmental Engineering, Ruhr-Universität Bochum, Bochum, Germany, 1981.

[86] O. Wommelsdorff, "Dehnungs-und querdehnungszahlen von Hölzern," PhD Thesis, University of Applied Sciences and Arts Hannover, Hannover, Germany, 1966.

[87] C. Foster, "Damping and Poisson factor behaviour in timber considered as an orthotropic material, part 1; the loss factor," *Journal of sound and vibration,* vol. 158, pp. 405-425, 1992.

[88] M. Möser, *Technische Akustik* vol. 10. Germany: Springer-Verlag Berlin Heidelberg, 2015.

[89] ISO, "ISO 12354-1:2017 - Estimation of acoustic performance of buildings from the performance of elements — Part 1: Airborne sound insulation between rooms," ed, 2017.

[90] ISO, "EN ISO 10848-1: 2006: Acoustics-Laboratory measurement of the flanking transmission of airborne and impact sound between adjoining rooms. Part 1: Frame document," *International Organization for Standardization,* 2006.

[91] R. Oqvist, F. Ljunggren, and A. Agren, "On the uncertainty of building acoustic measurements - Case study of a cross-laminated timber construction," *Applied Acoustics,* vol. 73, pp. 904-912, Sep 2012.

[92] C. Simmons, "Managing uncertainty in building acoustics: comparisons of predictions with the 12354 standards to measurements," Luleå tekniska universitet, 2009.

[93] J. Mahn, "Prediction of flanking noise transmission in lightweight building constructions: A theoretical and experimental evaluation of the application of EN12354-1," 2009.

[94] IEC, "IEC 61260-1:2014 - Electroacoustics - Octave-band and fractional-octave-band filters - Part 1: Specifications," ed, 2014.

[95] J. Rösler, H. Harders, and M. Baeker, *Mechanisches Verhalten der Werkstoffe*, 5 ed. Wiesbaden, Germany: Springer Vieweg, 2016.

[96] D. J. Ewins, "Model validation: Correlation for updating," *Sadhana,* vol. 25, pp. 221-234, June 01 2000.

[97] M. Pastor, M. Binda, and T. Harčarik, "Modal assurance criterion," *Procedia Engineering,* vol. 48, pp. 543-548, 2012.

[98] R. J. Allemang, "The modal assurance criterion–twenty years of use and abuse," *Sound and vibration,* vol. 37, pp. 14-23, 2003.

[99] A. Paolini, F. Frischmann, S. Kollmannsberger, E. Rank, S. Mecking, C. Winter*, et al.*, "Parameteridentifikation von Brettsperrholz-Elementen mittels Bayesscher Optimierung," presented at the Fortschritte der Akustik, DAGA 2016, Aachen, Germany, 2016.

[100] COMSOL, "Default Material Library," Comsol Multiphyics GmbH, Göttingen, Germany2018.

[101] J.-G. Richter, B. Zeitler, I. Sabourin, and S. Schoenwald, "Comparison of different methods to measure structural damping," presented at the Proceedings of Acoustics Week in Canada 2011, Quebec City, Canada, 2011.

[102] C. Winter, M. Buchschmid, S. Mecking, G. Müller, and U. Schanda, "Ein hybrider FEM/SEA Ansatz zur Prognose der Schallübertragung an Bauteilstößen," presented at the DAGA 2014, Oldenburg, 2014.

[103] ISO, "ISO 16283-1:2014: Acoustics - Field measurements of sound insulation in buildings and of building elements - Part 1: Airborne sound insulation," ed, 2014.

[104] C. Crispin, L. De Geetere, and B. Ingelaere, "Some considerations about the «element attenuation»(Project AH+, Part 1)," in *Inter-noise 2013*, Innsbruck, Austria, 2013.

[105] I. O. f. Standardization, "ISO 10140-3:2015: Acoustics - Laboratory measurement of sound insulation of building elements - Part 3: Measurement of impact sound insulation," ed, 2015.

[106] G. Müller, "Beurteilung von Schallimmissionen: Gesetze – Vorschriften – Normen – Richtlinien," ed. Berlin, Heidelberg: Springer, 2017.

[107] C. Hopkins, "Vibration transmission between coupled plates using finite element methods and statistical energy analysis. Part 1: Comparison of measured and predicted data for masonry walls with and without apertures," *Applied Acoustics,* vol. 64, pp. 955-973, 2003/10/01/ 2003.

[108] L. Maxit and J. L. Guyader, "Extension of SEA model to subsystems with non-uniform modal energy distribution," *Journal of Sound and Vibration,* vol. 265, pp. 337-358, 8/7/ 2003.

[109] L. Maxit and J. L. Guyader, "Estimation of SEA Coupling Loss Factors using a Dual Formulation and FEM Modal Information, Part I: Theory," *Journal of Sound and Vibration,* vol. 239, pp. 907-930, 2001/02/01 2001.

[110] L. Maxit and J. L. Guyader, "Estimation of SEA Coupling Loss Factors using a Dual Formulation and FEM Modal Information, Part II: Numerical Applications," *Journal of Sound and Vibration,* vol. 239, pp. 931-948, 2001/02/01 2001.

[111] À. Aragonès, L. Maxit, and O. Guasch, "A graph theory approach to identify resonant and non-resonant transmission paths in statistical modal energy distribution analysis," *Journal of Sound and Vibration,* vol. 350, pp. 91-110, 2015.

[112] N. Totaro and J. L. Guyader, "MODal ENergy analysis," *Journal of Sound and Vibration,* vol. 332, pp. 3735-3749, 8/5/ 2013.

[113] K. Larsson and N. Amiryarahmadi, "Influence of excitation position and floor-room modal coupling on low frequency impact noise," presented at the Internoise 2015, 2015.

[114] H. Petritsch, "FEM - Simulationen mit COMSOL Multiphysics im Anwendungsbereich der Technischen Akustik," Master Thesis, Institute of Signal Processing and Speech Communication, Graz University of Technology, Graz, Austria, 2011.

[115] A. Santoni, P. Fausti, S. Schoenwald, and H.-M. Tröbs, "Sound radiation efficiency measurements on cross-laminated timber plates," in *INTER-NOISE and NOISE-CON Congress and Conference Proceedings*, 2016, pp. 5979-5989.

[116] COMSOL, "COMSOL Multiphysics Version 5.2 – Default material database," C. M. GmbH, Ed., ed. Göttingen, Germany, 2016.

[117] IEC, "IEC 61260-1:2014: Electroacoustics -Octave-band and fractional-octave-band filters," in *Part 1: Specifications*, ed: IEC, 2014.

[118] ISO, "ISO 15186-2:2003: Acoustics - Measurement of sound insulation in buildings and of building elements using sound intensity – Part 2: Field measurements," ed, 2003.

[119] A. Paolini, E. Frischmann, S. Kollmannsberger, A. Rabold, T. Horger, B. Wohlmuth*, et al.*, "BIM gestützte strukturdynamische Analyse mit Volumenelementen höherer Ordnung," *Bauingenieur,* vol. 93, pp. 160-166.

[120] S. Mecking, U. Schanda, and S. Schoenwald, "Material characterisation of Cross Laminated Timber using experimental wave velocities," presented at the Euronoise 2018, Crete, Greece, 2018.